CHALMERS
UNIVERSITY OF TECHNOLOGY

Parametric Study of Traffic Induced Ground Vibrations due to Heavy Vehicles

Master's thesis in Sound and Vibration

ADAM MARCZAK and MARTIN ZETTERLUND

Department of Architecture and Civil Engineering
CHALMERS UNIVERSITY OF TECHNOLOGY
Gothenburg, Sweden 2019

Master's thesis 2019:06

Parametric Study of Traffic Induced Ground Vibrations due to Heavy Vehicles

ADAM MARCZAK
and
MARTIN ZETTERLUND

CHALMERS
UNIVERSITY OF TECHNOLOGY

Department of Architecture and Civil Engineering
Division of Applied Acoustics
Chalmers University of Technology
Gothenburg, Sweden 2019

Parametric Study of Traffic Induced Ground Vibrations due to Heavy Vehicles
ADAM MARCZAK and MARTIN ZETTERLUND

Supervisor: Patrik Höstmad, Professor in Applied Acoustics at the Department of Architecture and Civil Engineering at Chalmers University of Technology
Second Supervisor: Andreas Sigfridsson, Consultant Sound & Vibration, Norconsult
Third Supervisor: Ginko Georgiev, Structural Engineer, Norconsult
Fourth Supervisor: Gunnar Widén

Examiner: Patrik Höstmad

Master's Thesis 2019:06
Department of Architecture and Civil Engineering
Division of Applied Acoustics
Chalmers University of Technology
SE-412 96 Gothenburg
Telephone +46 31 772 1000

Cover: Overview Picture of a Heavy Vehicle passing a speed-bump during conducted measurements.

Typeset in LaTeX
Printed by Chalmers Reproservice
Gothenburg, Sweden 2019

Parametric Study of Traffic Induced Ground Vibrations due to Heavy Vehicles
ADAM MARCZAK and MARTIN ZETTERLUND
Department of Architecture and Civil Engineering
Chalmers University of Technology

Abstract

Due to recently imposed building regulations the demands of sound exposure levels to buildings have changed, allowing urban planners to design residential areas in direct proximity to roads and railways. While the Swedish building code requires for a risk evaluation regarding comfort vibrations when a railway is in adjacency to the area under consideration it neglects the contribution from heavy vehicles such as trucks and buses. Nevertheless, when a building stands finish a certain vibration level may not be exceeded, independent of the source of vibrations. This issue is presently approached by using doubtful reference values for transfer factors from ground to building which are based on personal experience and measurements conducted with trains as the source of excitation.

This thesis examines the induced vibration levels from heavy vehicles by modelling ground and buildings together in finite element models. Using an experimental and numerical approach, ground induced vibrations are measured from an arbitrary heavy vehicle and then used for validation of the finite element model which acts as the base of the parametric study. Investigated parameters are diverse types of foundations i.e. frame foundations, basement foundation and piling foundation with varying static loads, sizes and thicknesses.

The results show that presently used reference values overestimate the impact of some structural measures for vibration transfer reduction while neglecting important factors such as the static load on the foundation and the size of the building. The most effective structural counter-measure proved to be a piling foundation however its efficiency is highly dependent on the density of the piling-grid. Further, the parametric study showed no significant difference between a basement foundation and a slab on grade foundation.

Keywords: Ground-Borne Vibrations, Heavy Vehicles, Transfer Factor, Residential Vibration Exposure.

Acknowledgements

We want to begin by thanking Patrik Höstmad who has been advising, tutoring and supporting us through out this thesis. We thank you for your help and the patience that you showed us throughout this term.

This thesis would not have been possible without the support of the Acoustics department at Norconsult AB in Gothenburg. Thus, we would like to sincerely thank our primary supervisor at the department, Andreas Sigfridsson, for all of his time, support and ability to help us organize this project. We would also like to extend this gratitude to Ginko Georgiev and Gunnar Widén for their participation, advises and support of this thesis. We also thank the entire Acoustics Department at Norconsult for welcoming us into their workplace and creating a great atmosphere full of encouragement which was needed when we were struggling.

We would also like express our gratitude to our families, girlfriends and friends who listened and supported us, regardless of the lack of interest they had in our thesis.

Adam Marczak & Martin Zetterlund, Gothenburg, June 2019

Contents

List of Figures

List of Tables

1
Introduction

1.1 Background

It is currently not required to investigate the impact of ground vibrations induced by heavy vehicles in the detailed development planning phase, with ground vibration risk analysis only being a requirement when a railway is in the proximity of the area of interest. However, investigations and measurements made in affiliation to the detailed development planning have shown that in some cases the vibration levels induced by heavy vehicles have been proven to be much higher than those induced by the railway.

Even though it is not a legislated requirement to investigate how vibrations from heavy vehicles affect the buildings in the detailed development planning stage, it can create problems in later stages. The requirement of comfort vibrations when the building stands finished does not consider the source of the vibrations but clearly specifies maximum levels that cannot be exceeded in accordance to the regulating standard, *SS 460 48 61*. Thus, all the possible ground vibrations must be considered in the planning phase by the designing teams.

Presently civil engineering consultancy firms have different prediction-tools based on similar projects where the forecast is based on personal experience combined with doubtful reference values of transfer functions between ground and building. Furthermore, these values often consider line sources such as trains, neglecting point-sources such as the vibrations induced by heavy vehicles. It is therefore of interest to investigate the risks of ground vibrations spreading from heavy traffic, especially in areas where the ground is composed of loose soils and/or clay, as the case often is in the city of Gothenburg.

1.2 Purpose and Goal

The general purpose of this thesis is to investigate and assess the different transfer functions for ground vibrations between the ground and the building structure depending on varying construction parameters where the source of excitation is a heavy vehicle. Parameters of interest are different construction framings (light or heavy), different foundation types and the difference between pile foundation and slab foundations.

The specific goal is to find which construction methods and measures can result in standard values for reduction of ground vibration transfer between ground and building with heavy vehicles as the source of excitation and to what extent they could be considered valid for future use.

The thesis is centered around heavy vehicles, such as trucks and how these induce ground vibrations.

1.3 Limitations

Because the work involves many different parameters that may vary, some limitations will be made. The first limitation is to focus on concrete buildings only as it is built to a greater extent than timber structures. This limitation will be implemented to be able to compare buildings with each other without having too many unknown error sources.

Another limitation that will be implemented is to model only bearing structural elements in buildings when using the finite element method software Solvia. This is done to reduce the workload but also because the supporting elements in the building will be at focus when looking at vibrations.

The ground is a linear elastic media with constant damping, so a linear behavior is assumed with constant dynamic properties. Non-linear behaviours and analysises will not be included in the scope of this thesis.

Limitations that may become relevant later in the work are to simplify different types of heavy vehicle impact in frequency to a range based on different weight and spring systems.

1.4 Collaboration

This thesis is written in collaboration with the acoustics department of Norconsult AB in Gothenburg.

1.5 Thesis outline

The outline of the thesis is highly correlated with the work process implemented. The adjacent chapter describes the **Theoretical** insight into the field of ground vibrations along with point-source modelling approaches and previously conducted studies. Other treated areas included reigning legislations, currently used amplification factors and a brief introduction to soil properties.

The **Method** chapter describes the conducted field measurement in detail, presents the FEM modelling and implementation of the analytical source model.

The consequent chapter presents the **Results**, beginning with the outcome of the measurement and how well it correlates with the FEM and Source models. The subsequent sections of the results chapter present the found amplification factors from the FEM modelling in the Parametric study. The results are commented and discussed in the results section for easier interpretation.

The **discussion** chapter treats, interprets and includes interpretation of the results presented in the previous chapter, leading to a **Conclusion** which is included in the last chapter of the thesis.

Finally, the report will be finished with a **Future work** section, outlining suggestions made by the authors on how the content of this thesis could be used for eventual projects or theses.

The thesis report ends with the **Bibliography**, presenting the references and along with the **Appendices** for more detailed information.

2

Theory

This section presents the relevant theory regarding ground vibrations, different wave types, source models and legislations in order for the reader to understand the fundamental elements included in the thesis.

2.1 Causes and Effects of Ground Vibrations

2.1.1 Waves in Continuous Medium

Defining the equation of motion for physical systems that is subjected to vibrations can be done using the wave equation, as presented below:

$$\frac{\partial^2 u}{\partial t^2} = v^2 \frac{\partial^2 u}{\partial x^2} \tag{2.1}$$

In this formulation it is typically assumed that there is only one space dimension, here denoted by x, however, the dependent variable denoted as u can be used to describe a second space parameter such as displacement. The variable v is the velocity of the wave which varies depending on the wave type. The wave equation is the fundamental equation used when describing the behaviour of systems subjected to longitudinal and torsional vibration as well as pressure waves, however the equation is also bound by its dimensional limitation [1].

As this thesis treats the propagation of waves in the earth a contrasting approach must be used. In order to treat the complex problem of waves in continuous mediums, such as the earth, an equilibrium of an infinitely small element must be studied to derive the equations of motion. In this case the infinite elastic medium represents the endless character of earth. As the ground is subjected to forces, stress starts acting inside of the continuum [2]. The most elementary object to consider is an infinitely small cubic volume aligned with axes of a orthonormal Cartesian coordinate system such as the one presented below:

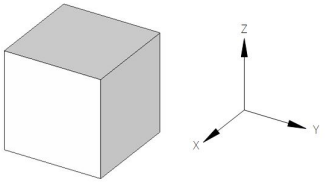

Figure 2.1: Simple cube-object with the axes of an orthonormal Cartesian coordinate system

However, when describing stress acting on a medium the isolation of a certain element of a whole volume is imprecise. The stresses are not uniform and vary from point to point. Thus, studying the forces acting on the sides of arbitrary many sub-volumes of the continuum must be considered to properly scale the forces that arise [3]. Nonetheless, it can be assumed that if the element is small enough the stresses can be treated as constant with variation of tension between them as linear and defined as:

$$\Delta\sigma_{ij} = \frac{\partial\sigma_{ij}}{\partial x_k}\Delta x_k \tag{2.2}$$

Such a presentation of the above-mentioned element is presented in the figure below [2][4]. On each infinitely small cube surface there is a normal component of stress as well as two tangential stress components and where τ_{ij} denotes the shear stress and σ_i is the total normal stress in the i-direction:

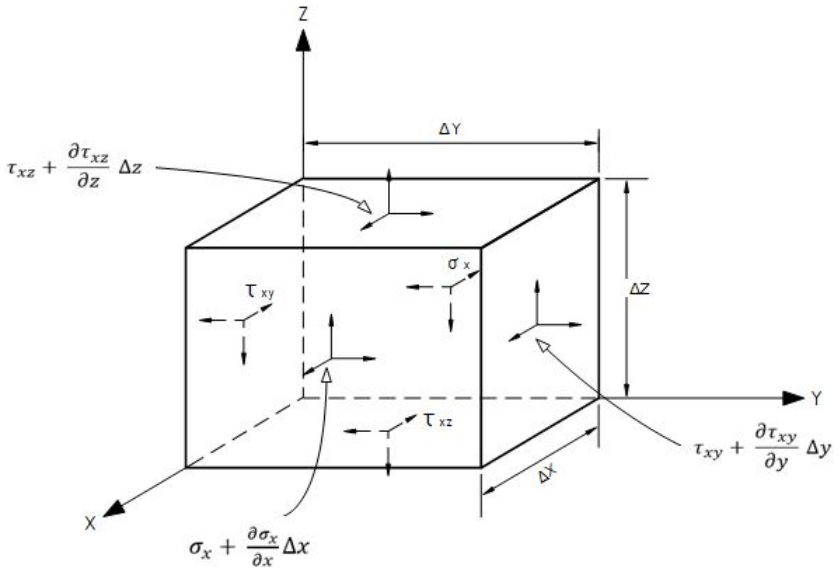

Figure 2.2: The 3 dimensional stress state on a small object within an infinite elastic medium, adapted from Reference [1].

Here the dotted vectors are the stressed acting on the hidden faces from the point of the reader while the solid faces are acting on the frontal elements. By assuming

the translational equilibrium of this infinitely small element a sum of forces can be expressed for every axis:

$$\begin{aligned}\left(\sigma_x + \frac{\partial\sigma_x}{\partial_x}\Delta_x\right)\Delta_y\Delta_z - \sigma_x\Delta_y\Delta_z + \left(\tau_{xy} + \frac{\partial\tau_{xy}}{\partial_y}\Delta_y\right)\Delta_x\Delta_z \\ -\tau_{xy}\Delta_x\Delta_z + \left(\tau_{xz} + \frac{\partial\tau_{xz}}{\partial_z}\Delta_z\right)\Delta_x\Delta_y - \tau_{xz}\Delta_x\Delta_y = 0\end{aligned} \tag{2.3}$$

after applying Newtons second law as well as omitting the body forces the following can be derived for the respective directions:

$$\left(\frac{\partial\sigma_x}{\partial_x} + \frac{\partial\tau_{xy}}{\partial_y} + \frac{\partial\tau_{xz}}{\partial_z}\right)\Delta_x\Delta_y\Delta_z = \rho(\Delta_x\Delta_y\Delta_z)\frac{\partial^y u}{\partial t^y} \tag{2.4}$$

The notations 1, 2 and 3 represent the different directions that vary depending on which axis is being treated however the presented relation remains [1]. With this the equilibrium of equations for the stresses can be formed for every direction each:

$$\rho\frac{\partial^2 u}{\partial t^2} = \frac{\partial\sigma_x}{\partial x} + \frac{\partial\tau_{xy}}{\partial y} + \frac{\partial\tau_{xz}}{\partial z} \tag{2.5}$$

$$\rho\frac{\partial^2 v}{\partial t^2} = \frac{\partial\tau_{yx}}{\partial x} + \frac{\partial\sigma_y}{\partial y} + \frac{\partial\tau_{yz}}{\partial z} \tag{2.6}$$

$$\rho\frac{\partial^2 w}{\partial t^2} = \frac{\partial\tau_{zx}}{\partial x} + \frac{\partial\tau_{zy}}{\partial y} + \frac{\partial\sigma_z}{\partial z} \tag{2.7}$$

where u, v and w represent the second derivatives of the displacement field of respective direction with respect to time. Since the components of the stresses within the cubical volume are all positive, they can be defined by the 9 stress components (3 normal stresses and 6 shear stresses) [1]. However, if the moments of the forces are taken about the central axes of the cube at the equilibrium state it is possible to assume:

$$\sigma_{xy} = \sigma_{yx} \qquad \sigma_{xz} = \sigma_{zx} \qquad \sigma_{yz} = \sigma_{zy} \tag{2.8}$$

Therefore, allowing to define the state of stress at any point by knowledge of six stress components only. The relation for an elastic medium allows to express the normal stresses relationships from the terms of the Lamé's constants (G and λ) and the cubical dilation (ϵ):

$$\begin{aligned}\sigma_x &= \lambda\bar{\epsilon} + 2G\epsilon_x \\ \sigma_y &= \lambda\bar{\epsilon} + 2G\epsilon_y \\ \sigma_z &= \lambda\bar{\epsilon} + 2G\epsilon_z\end{aligned} \tag{2.9}$$

where the shear stresses are expressed similarly per Equation 2.8:

$$\begin{aligned}\sigma_{xy} &= G\gamma_{xy} \\ \sigma_{yz} &= G\gamma_{yz} \\ \sigma_{xz} &= G\gamma_{xz}\end{aligned} \tag{2.10}$$

here γ is the shear strain variables (Calculated in Equation 2.13) for given directions and $\overline{\epsilon}$ denotes the volume expansion of the cube in the direction given by the prefix, calculated as:

$$\epsilon_1 = \frac{\partial \zeta_1}{\partial_1} \tag{2.11}$$

where ζ denotes the displacement for the different directions. Further, G is the shear modulus and λ is the Lamé's constant (As seen in Equations 2.9 and 2.10) defined as:

$$G = \frac{E}{2(1+v)} \qquad \lambda = \frac{vE}{(1+v)(1-2v)} \tag{2.12}$$

with E denoting the Young's modulus and v being the Poisson's ratio of the material. The previously mentioned strain relation is then obtained by:

$$\gamma_{12} = \frac{\partial \zeta_2}{\partial_1} + \frac{\partial \zeta_1}{\partial_2} \tag{2.13}$$

and as it is now known only the rotation relationship must be formulated:

$$\begin{aligned} 2\overline{\omega}_x &= \tfrac{\partial w}{\partial y} - \tfrac{\partial v}{\partial z} \\ 2\overline{\omega}_y &= \tfrac{\partial u}{\partial z} - \tfrac{\partial w}{\partial x} \\ 2\overline{\omega}_z &= \tfrac{\partial v}{\partial x} - \tfrac{\partial u}{\partial y} \end{aligned} \tag{2.14}$$

where $\overline{\omega}$ represents the rotation about each axis. By combining the above equations, the formulation of motion for an infinite homogeneous, isotropic, elastic medium is found which corresponds to what the ground model in this thesis represents:

$$\rho \frac{\partial^2 \zeta_1}{\partial t^2} = (\lambda + G)\frac{\partial \overline{\epsilon}}{\partial_1} + G\nabla^2 \zeta_1 \tag{2.15}$$

here ∇^2 is the Laplacian operator in the Cartesian coordinates and defined as shown below [1]:

$$\nabla^2 = \frac{\partial^2}{\partial x^2} + \frac{\partial^2}{\partial y^2} + \frac{\partial^2}{\partial z^2} \tag{2.16}$$

2.1.1.1 P-waves & S-waves

In Section 2.1.1 the introduction of how wave propagation in structures is approximated based on the wave equation and the state of equilibrium of a infinitely small object is presented. The equation of motion conferred in Section 2.1.1 as Equation 2.15 could be rewritten in the following form as:

$$\rho \frac{\partial^2 \overline{\epsilon}}{\partial t^2} = (\lambda + 2G)\nabla^2 \overline{\epsilon} \tag{2.17}$$

when Equation 2.15 is differentiated for each direction (x, y and z) and then summed up. The propagation velocity of the wave can now be extracted using the previously presented relations in Equation 2.12, as following:

$$c_P = \sqrt{\frac{\lambda + 2G}{\rho}} \longleftrightarrow c_P = \sqrt{\frac{E(1-v)}{\rho(1-2v)(1+v)}} \tag{2.18}$$

where the right-hand equation is the more known formula for the wave propagation of a P-wave in a solid. To express this in the exact form of the wave equation the following expression is formulated:

$$\frac{\partial^2 \overline{\epsilon}}{\partial t^2} = c_P^2 \nabla^2 \overline{\epsilon} \tag{2.19}$$

this shows that the volume expansion, $\overline{\epsilon}$ of the cubical volume in question is propagating at the velocity of c_P [1].

Thus, the expression above presents the wave equation of the Primary wave. Often referred to as P-waves, Compression waves or Dilatational waves, these waves are volume waves which move with a longitudinal motion, similar to how sound waves move in air. The motion is a combination of compression and dilatations within the medium as presented in the figure below [5]:

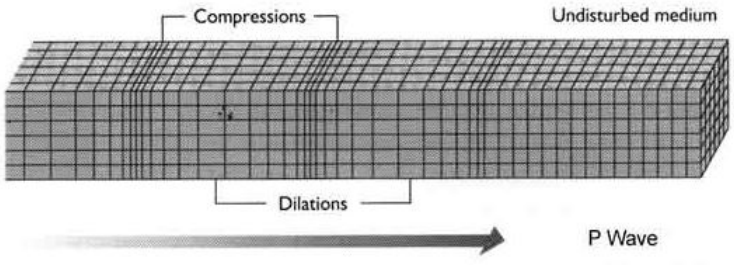

Figure 2.3: The Motion of a Primary wave in a solid [5].

The second solution for the equation of motion (Equation 2.15) can be found by differentiating the equations of y- and z-direction with respect to their respective directions and eliminate the volume expansion coefficient $\overline{\epsilon}$ by subtracting the two equations ending up with:

$$\rho \frac{\partial^2}{\partial t^2}\left(\frac{\partial w}{\partial y} - \frac{\partial v}{\partial z}\right) = G\nabla^2\left(\frac{\partial w}{\partial y} - \frac{\partial v}{\partial z}\right) \tag{2.20}$$

then by using the expression for rotation, presented in Equation 2.14, the following relation is given:

$$\rho \frac{\partial^2 \overline{\omega}_x}{\partial t^2} = G \nabla^2 \overline{\omega} \tag{2.21}$$

Similarly to the Equation 2.17, this expression is also valid in the y- and z-direction, which indicate that the rotation is dependent on the velocity of the wave and by solving the equation for ρ while considering the relations given in Equation 2.12 we get:

$$c_{\mathrm{S}} = \sqrt{\frac{G}{p}} \longleftrightarrow c_S = \sqrt{\frac{E}{\rho 2(1+v)}} \tag{2.22}$$

which inserted back in Equation 2.21 will give the wave equation form for the propagation of a secondary wave, as per the following expression:

$$\frac{\partial^2 \tilde{\omega}_x}{\partial t^2} = c_S^2 \nabla^2 \overline{\omega}_x \tag{2.23}$$

The S-waves are also volume waves that move in a shear or transverse motion [1]. The S-wave is also known as a shear wave or distortional wave and is characterized by a shearing motion, mowing its medium sideways at a right angle to the direction of travel. The motion of a Secondary wave is presented in the figure below [5]:

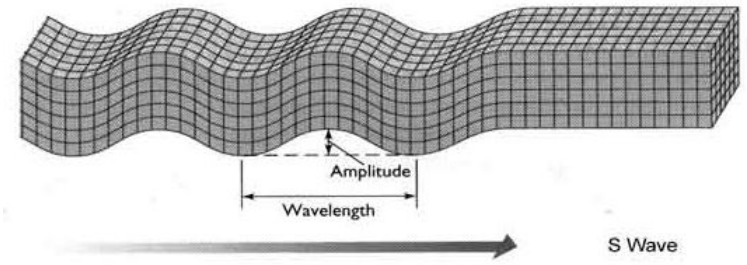

Figure 2.4: The Motion of a Secondary wave in a solid [5].

The reason of why P-wave is short for primary wave and S-wave for secondary wave is because P-waves arrives faster than S-waves when conducting a seismologic experiment. Another important difference between the S- and P-waves is that P-waves can move through both liquid mediums and solid rock where the S-waves only can move through solid rock [6]. This is due to the character of the S-wave which shears/twists its medium sideways. A liquid that is sheared will not spring back to its original position, hence not allowing the wave to continue propagating [5].

2.1.1.2 Rayleigh waves & Love waves

A third solution of the equation of motion is possible if correct boundary conditions are applied. For this solution a free surface is required with the wave running along a solid boundary, in this case the x-axis as shown in the figure included below:

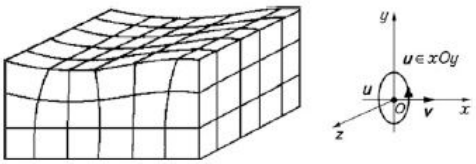

Figure 2.5: Schematic presentation of the Rayleigh wave propagation on the free surface of a solid [7].

This means that the analyzed volume cannot be arbitrary placed within the medium, but is required to have one free side to the surface while simultaneously the assumption is made that the wave is running along that solid boundary (x in Figure 2.6).

This wave is called the Rayleigh wave and consists of a combination of longitudinal and transversal waves for which the amplitude is directly dependent on the depth (the y-dimension in Figure 2.6) of the propagating wave. The closer the wave is to the surface the higher the amplitude. As the combination between the longitudinal and transversal motions should be linear the transversal propagation velocity must be equal to c_S calculated as in Equation 2.22. Thus, a wave number can be calculated as:

$$k_S = \frac{\omega}{c_S} \qquad\qquad k_P = \frac{\omega}{c_P} \tag{2.24}$$

Where $\omega = 2\pi f$ with f being the frequency [7]. Reformulation of the equation of motion then yields:

$$\frac{\partial^2 \zeta}{\partial z^2} = (k^2 - \frac{\omega^2}{c^2})\zeta \tag{2.25}$$

where ζ is extracted from the component vector from the Equations of motion 2.23/2.19 as shown below:

$$\overline{\epsilon} = e^{i(kx-\omega t)}\zeta(z)$$

ζ represents the expression of a periodic function. In order for Expression 2.25 to result in a solution which does not constitute a undamped plane wave the right hand expression must yield $k^2 - \omega^2/c^2 > 0$ giving the solution for function $\zeta(z)$ as:

$$\zeta(z) = A\, e^{(\pm\sqrt{[k^2 - \frac{\omega^2}{c^2}]z})} \tag{2.26}$$

Where A represents an arbitrary constant. The negative solution would correspond to a deformation for $z \to -\infty$ yielding an impossible solution. Hence the positive answer must be used and the previously formulated wave equations for the P- and S-wave in Equation 2.19 and 2.23 must be considered [7]. Assuming the previously stated boundary conditions along with the assumption that the velocities within this wave are equal to c_p and c_s respectively, the predicted displacement can be formulated as:

$$\zeta_{index} = A\, e^{j(kx-\omega t)} e^{(\kappa_{P/S} z)} \tag{2.27}$$

with ζ depending on the constant κ:

$$\kappa_P = \sqrt{(k_P^2 - \omega^2/c_P^2)} \qquad \kappa_S = \sqrt{(k_S^2 - \omega^2/c_S^2)} \tag{2.28}$$

for respective type of motion. In these expressions the amplitude changes along the y-axis. The true displacement is the sum between the longitudinal displacement (denoted as ζ_P) and the transversal displacement (denoted as ζ_S). However, the boundary conditions of the free surface yield:

$$\sigma_{yy} = 0 \qquad \sigma_{yx} = 0 \qquad \sigma_{yz} = 0 \tag{2.29}$$

meaning no normal or tangential stress components on the surface [7]. This yields the following expressions for the true displacement [8]:

$$\zeta_{yy} = 0 \qquad \zeta_{yx} = 0 \qquad \sigma(\zeta_{xx} + \zeta_{yy}) + (1-\sigma)\zeta_{zz} = 0 \tag{2.30}$$

as the displacements are independent of the coordinate y, the conditions for the tangential displacement can be defined as:

$$\zeta_{yz} = \frac{1}{2}\left(\frac{\partial \zeta_y}{\partial z} + \frac{\partial \zeta_z}{\partial y}\right) = \frac{1}{2}\partial\zeta_y/\partial z = 0 \tag{2.31}$$

considering Equation 2.27 would yield $\zeta_y = 0$ meaning that there is no displacement at the surface perpendicular to the propagation direction of the wave. This means that the displacement caused by the S-wave in x- and z-direction must be 0 as per $\frac{\partial \zeta_{tx}}{\partial x} + \frac{\partial \zeta_{tz}}{\partial z} = 0$ [8].

Now considering the right-hand equation included in Equations 2.28 for the S-waves a following ratio can be formulated between the two displacements:

$$\zeta_{Sx}/\zeta_{Sz} = \frac{-\kappa_S}{jk} \longrightarrow \quad \zeta_{Sz} = -jkae^{jkx+\kappa_S z - j\omega t} \tag{2.32}$$

$$\zeta_{Sx} = \kappa_S a e^{Jkx+\kappa_s z - j\omega t} \tag{2.33}$$

where a is a constant. This gives the expression for true displacement for the S-wave contribution. As for the P-wave, or the longitudinal contribution the condition can be formulated as:

$$\frac{\partial \zeta_{Px}}{\partial z} - \frac{\partial \zeta_{Pz}}{\partial x} = 0 \tag{2.34}$$

The process is similar to the S-wave, where we consider the left-hand expression in Equation 2.28 and formulate a expression for the true displacement for the longitudinal motion for x- and z-directions:

$$\zeta_{Px} = kbe^{jkx+\kappa_P z - j\omega t} \qquad \zeta_{Pz} = -j\kappa_P b e^{jkx+\kappa_P z - j\omega t} \tag{2.35}$$

where b is a constant. Using the previously defined expressions for true displacement at the surface the conditions can be rewritten as:

$$\frac{\partial \zeta_x}{\partial x} + \frac{\partial \zeta_z}{\partial x} = 0 \tag{2.36}$$

and with the third expression being rewritten as:

$$c_P^2 \frac{\partial \zeta_z}{\partial z} + \left(c_P^2 - 2c_S^2\right) \frac{\partial \zeta_x}{\partial x} = 0 \tag{2.37}$$

by combining the S- and P-wave contributions and rewriting the true displacement as a sum ($\zeta_x = \zeta_{Px} + \zeta_{Sx}$ and $\zeta_z = \zeta_{Pz} + \zeta_{Sz}$) the conditions included in Equation 2.30 can be rewritten as:

$$a\left(k^2 + \kappa_S^2\right) + 2bk\kappa_P = 0 \tag{2.38}$$

$$2ac_S^2\kappa_S k + b\left[c_P^2\left(\kappa_P^2 - k^2\right) + 2c_S^2 k^2\right] = 0 \tag{2.39}$$

dividing this expression by c_S^2 and replacing

$$\kappa_P^2 - k^2 = -\omega^2/c_P^2 = -\left(k^2 - \kappa_t^2\right) c_S^2/c_P^2 \tag{2.40}$$

gives:

$$2a\kappa_S k + b\left(k^2 + \kappa_S^2\right) = 0 \tag{2.41}$$

by squaring, substituting κ_S^2 and κ_P^2 as well as combining the two conditions formulated as Equation 2.38 with 2.41 we end up with the following equation:

$$\left(2k^2 - \frac{\omega^2}{c_S^2}\right)^4 = 16k^4\left(k^2 - \frac{\omega^2}{c_S^2}\right)\left(k^2 - \frac{\omega^2}{c_P^2}\right) \tag{2.42}$$

Which proves the relation between ω and k, by expressing ω as:

$$\omega = c_S k\xi \tag{2.43}$$

by inputting this into Equation 2.42 and solving for ξ as well as dividing by k^8 on both sides we obtain:

$$\xi^6 - 8\xi^4 + 8\xi^2\left(3 - 2\frac{c_S^2}{c_P^2}\right) - 16\left(1 - \frac{c_S^2}{c_P^2}\right) = 0 \tag{2.44}$$

which is the expression for Rayleigh wave propagation speed. This shows that the surface wave speed is independent of frequency and is non-dispersive. It also shows that ξ is dependent on the ratio between the propagation velocity of P- and S-waves, which in turn depends on the Poisson's ratio, v, and can also be expressed as:

$$c_S/c_P = \sqrt{\{(1-2\nu)/2(1-\nu)\}} \tag{2.45}$$

where ξ must be real, $\xi < 1$ and positive in order for the constants κ to be real. This is only satisfied for one solution for Equation 2.44 meaning a single ξ value is

obtained for any ratio of c_S/c_L. Hence, for a Rayleigh wave the frequency must be proportional to the wave number.

It can further be mathematically proven that for a real material the relationship $c_R < c_S < c_P$ between the different wave velocities is true which leaves the wave equation of the Rayleigh wave with only one solution, which is dependent on the Poisson's ratio, ν:

$$c_R = \frac{0,87\nu + 1,12\nu}{1+\nu} c_S \tag{2.46}$$

The described propagation characteristics of the Rayleigh wave are presented in the figure below:

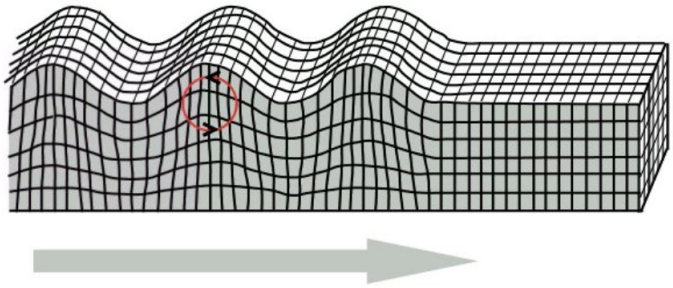

Figure 2.6: The Motion of a Rayleigh wave in a solid [35]

Rayleigh waves are the type of surface waves that move with an elliptical kind of motion in a similar characteristic to rolling ocean waves [9][5]. The velocity, as previously stated, is highly dependent on the medium and its material properties, however the Rayleigh wave has a velocity lower than P- or S-waves in general.

In a scenario where an arbitrary infinite volume is excited causing all three types of waves to propagate within it, a receiving point on the surface and at a distance from the source will first be excited by the early arriving P-wave. After the arrival of the P-wave a period of relatively low or no oscillation occurs followed by the arrival of the S-wave. The period of arrival of P and S-waves is referred to as *minor tremor* and is followed up by another period referred to as *major tremor* which indicates the arrival of the Rayleigh wave. This period is characterised by a much higher magnitude oscillation as Rayleigh waves are responsible for most of the vibrational energy transfer at the surface.

The greater the distance between the source and receiver the bigger time interval between the two *tremor*-periods. At a longer distances the Rayleigh wave might be the only distinguishable wave on the surface [10][1].

Another type of surface waves are the Love waves, named after the English mathematician A.E.H. Love. The Love wave moves from side to side meaning its motion only consists of horizontal components, as shown in the figure below:

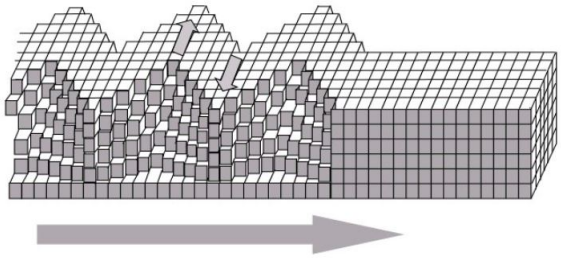

Figure 2.7: The Motion of a Love wave in a solid [36].

The Love wave can be described as a S-wave with no vertical displacement, moving only in the horizontal plane with a generally higher velocity than the Rayleigh wave [5]. Love waves cannot propagate over water for similar reasons to those previously stated for the S-wave.

The Love wave can only be confined if the surface layer of the medium has a higher velocity than the lower layer, as it travels at a velocity that is between the shear wave velocity of the top layer and the shear wave velocity of the lower one. The propagation is due to reflections of the wave between the layers as when a wave is reflected due to the change in impedance between either two different layers or between the solid and a void, such as air or water [1]. Due to these properties the influence of Love-waves can often be neglected when dealing with uniform soils [21].

2.1.2 Ground Vibrations induced by Heavy Vehicles

Ground vibrations from heavy vehicles that are treated in this thesis are the vibrations induced due to road irregularities such as potholes or speed bumps. Nevertheless, when a vehicle is moving on an even surface it still creates stress fields in the ground as the mass is moving along, producing waves. However, the amplitude of these waves is generally low, making it frivolous from a comfort-vibration standpoint. Unlike the ground vibrations induced by rail-borne traffic, the excitation from a heavy vehicle is modelled as a point source instead of a line source [11].

The frequency spectrum of the induced ground vibrations varies between different type of vehicles mostly in relation to the stiffness of the suspension system. A stiff suspension system gives a broader frequency spectrum while a soft suspension system coincidence all the energy into a narrow frequency range. Generally, busses have softer suspension than trucks and therefore buses often causes higher vibration levels than trucks. The amplitude of the induced vibrations is highly dependent on the velocity of the vehicle as well as the roughness of the irregularity that causes it. Nevertheless, the vibration of the un-damped mass (vehicle axis) as well as the damped mass (all weight on the suspension system) have a bigger impact on the frequency response than it has on the amplitude [11].

When considering the propagation of vibrations induced by a heavy vehicle it is advantageous to consider both the near and far field. The contribution of the near-

field is only of significance at a distance approximately of one wavelength where the main contribution of energy is transported by the body waves (P- and S-waves). As the distance from the point source increases the surface waves (Rayleigh waves) are mainly responsible for the energy transport [21].

2.1.2.1 Vehicle Source Modelling

A simplified method of modelling the impact of a vehicle is known as the Quarter Car Model (referred to as QCM). The model is shown in a graphical representation below:

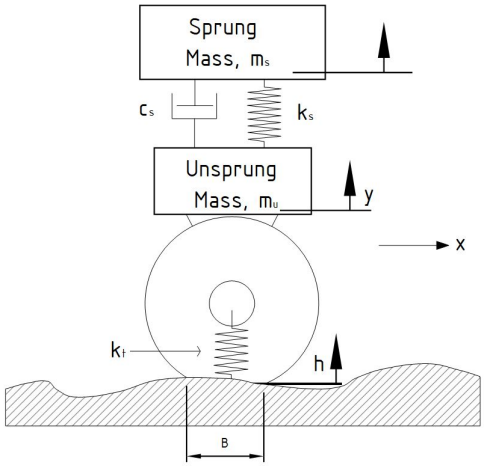

Figure 2.8: Quarter Vehicle Model, Adapted after reference [29]

In this model the vehicles wheel axis and the accompanying structure is simplified as a system with two degrees of freedom. The lower mass is the unsprung mass which represents the tire and components surrounding it while the upper mass is the sprung mass which is the weight of the truck on top of the suspension system. The unsprung mass includes the mass of the different components such as the wheel axles, wheel bearings, wheel hubs, tires and some of the weight of the driveshaft, springs, shock absorbers and suspension links [30]. In some cases, the mass of the brakes can be seen as a part of the unsprung mass if its mounted within the wheel. The sprung mass includes the rest of the vehicles weight which in the most cases is heavier than the unsprung mass.

A mass spring damper system with two degrees of freedom has two resonance frequencies. These resonance frequencies are dependent on the stiffness of the two springs, the two masses and the dampers. The impact of the damper does not affect the resonance frequencies significantly and the undamped natural frequency is close to the frequency of the maximum response for cases with light damping. Therefore, it is possible to predict the resonance frequency of the mass spring damper system by calculating the undamped natural frequencies [31].

The mass spring damper system presented below can be described by the subsequent Equation 2.47:

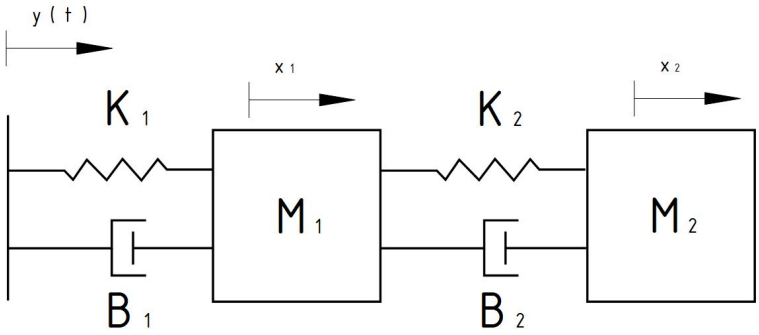

Figure 2.9: A Mass-Spring system consisting of 2 Degrees of Freedom, Adapted after reference [31]

$$\begin{bmatrix} M_1 & 0 \\ 0 & M_2 \end{bmatrix} \begin{pmatrix} \ddot{x}_1 \\ \ddot{x}_2 \end{pmatrix} + \begin{bmatrix} B_1 + B_2 & -B_2 \\ -B_2 & B_2 \end{bmatrix} \begin{pmatrix} \dot{x}_1 \\ \dot{x}_2 \end{pmatrix} \cdots + \begin{bmatrix} K_1 + K_2 & -K_2 \\ -K_2 & K_2 \end{bmatrix} \begin{pmatrix} x_1 \\ x_2 \end{pmatrix} = \begin{pmatrix} K_1 y(t) + B_1 \dot{y}(t) \\ 0 \end{pmatrix} \tag{2.47}$$

Since the undamped case is needed, the equation can be simplified to:

$$\begin{bmatrix} M_1 & 0 \\ 0 & M_2 \end{bmatrix} \begin{pmatrix} \ddot{x}_1 \\ \ddot{x}_2 \end{pmatrix} + \begin{bmatrix} K_1 + K_2 & -K_2 \\ -K_2 & K_2 \end{bmatrix} \begin{pmatrix} x_1 \\ x_2 \end{pmatrix} = \begin{pmatrix} K_1 y(t) \\ 0 \end{pmatrix} \tag{2.48}$$

The undamped mass spring system will create a harmonic oscillation which can described by the follow equation:

$$\begin{pmatrix} x_1 \\ x_2 \end{pmatrix} = \begin{pmatrix} A_1 \\ A_2 \end{pmatrix} e^{j\omega t} \tag{2.49}$$

Where A_1 and A_2 are constants, yielding the following:

$$\begin{bmatrix} K_1 + K_2 - M_1\omega^2 & -K_2 \\ -K_2 & K_2 - M_2\omega^2 \end{bmatrix} \begin{pmatrix} A_1 \\ A_2 \end{pmatrix} = \begin{pmatrix} 0 \\ 0 \end{pmatrix} \tag{2.50}$$

Solving A_1 and A_2 non-trivially is only possible if the determinant of the coefficient matrix is equal to zero which gives the following equation:

$$M_1 M_2 \omega^4 - (M_1 K_2 + M_2 (K_1 + K_2))\, \omega^2 + K_1 K_2 = 0 \tag{2.51}$$

The solution to Equation 2.51 becomes:

$$\omega_{1,2} = \sqrt{\frac{(M_1 K_2 + M_2 (K_1 + K_2)) \pm \sqrt{(M_1 K_2 + M_2 (K_1 + K_2))^2 - 4 M_1 M_2 K_1 K_2}}{2 M_1 M_2}} \tag{2.52}$$

Where the first resonance frequency is found when the right hand set of the numerator in the equation is negative and the second resonance frequency is found when the same set remains positive [31].

When modelling the vehicle of interest these resonance frequencies are presented as the suspended mass resonance and the axle hop resonance [32]. The suspended mass resonance should be within the interval of 0,8 - 3 Hz with the axle hope resonance at 8-15 Hz [32][33].

When viewing the impulse of a vehicle in time domain with force as the y-axis quantity the response can have the characteristics as shown in the figure below:

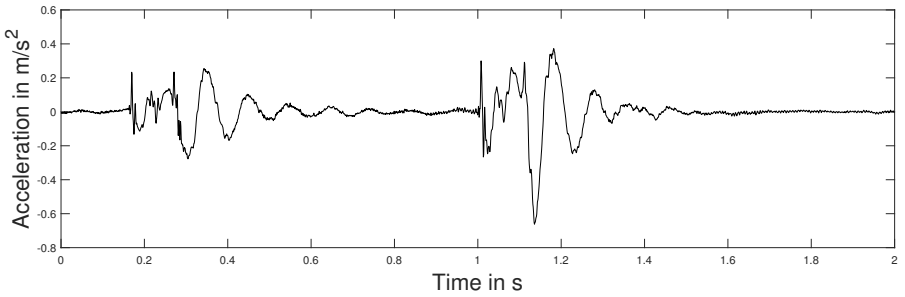

Figure 2.10: Measured Time Signal of a loaded Two-axis truck (Scania P280L) passage over a speed bump at 20 km/h

In this example it is possible to see the two different resonance frequencies of the mass spring damper system. The suspended mass resonance is at 1 Hz which can be seen in the oscillation time between 1.6 - 2 seconds where approximately half of an oscillation occurs. Between 0,4 - 0,6 seconds it is possible to see that the axle hop resonance is approximately 10 Hz since approximately two oscillations occurs.

2.1.2.2 Road unevenness

The characteristics of the road unevenness changes the impact to the ground from the heavy vehicle. Road unevenness can be defined as a set of different criteria, such as potholes, catch-basins or speed bumps but also cobblestone roads. Since the road unevenness can occur in so many different forms, ground vibrations induced by heavy vehicles cannot be simplified to a single or a general case. As previously stated, a flat pavement will in general have an insignificant impact on the vibration generation, however adding a depressed catch-basin could drastically increase the broadband amplitude of the vibrations [11].

Considering the frequency spectrum in the figures below it is further possible to distinguish that the velocity influences the amplitude of the responses. The most distinct difference is for $v = 30$ km/h at 16 Hz and for $v = 50$ km/h at 20 - 25 Hz. **BB2** and **BB3** are passages over the catch basin, while **BB6** and **BB8** are passages over a flat surface [11]:

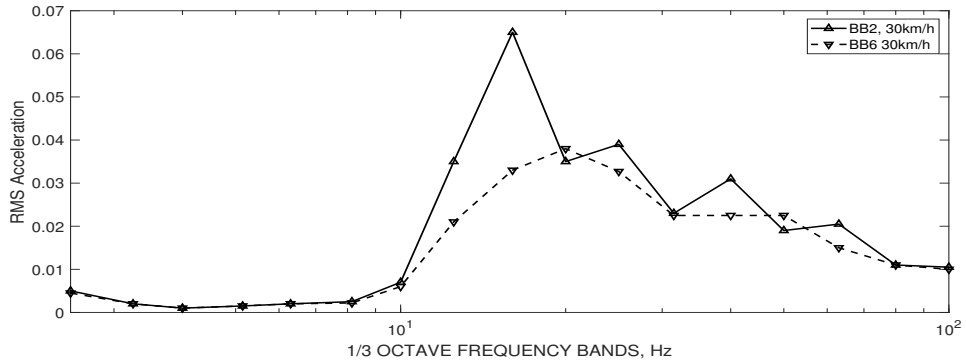

(a) Catch-basin passage vs. flat surface passage v=30km/h, Adapted after reference [11]

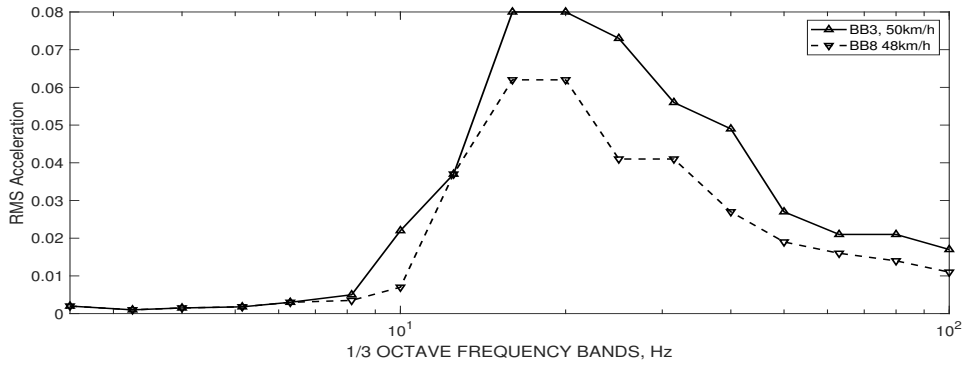

(b) Catch-basin passage vs. flat surface passage v=50km/h, Adapted after reference [11]

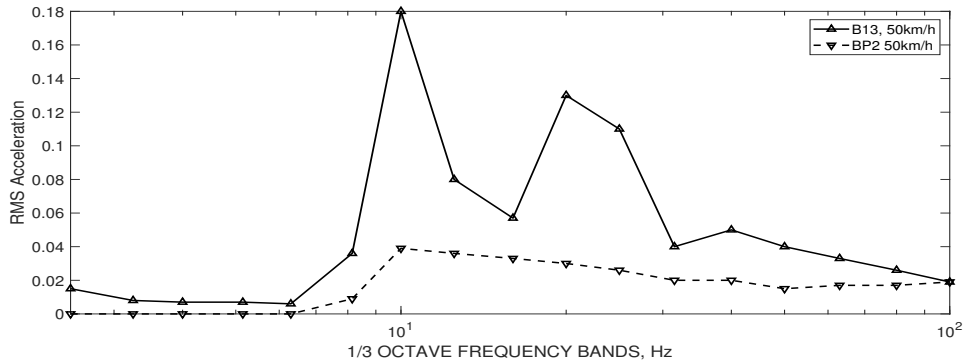

(c) Wooden plank passage vs. flat surface passage v=30km/h, Adapted after reference [11]

Figure 2.11: Variation of acceleration levels depending on the velocity and unevenness, Adapted after reference [11]

For the case of a bus passing over a wooden plank rather than a flat surface the change of amplitude is much higher than the catch-basin scenario. This can be seen in Figure (c) of 2.11, where the increase of amplitude is significant for frequencies between 10 - 25 Hz. **B13** is the passage over a flat road while **BP2** is a passage over the wooden plank.

It has been established that the geometry and depth of the unevenness or obstacle will have a high impact on the frequency spectrum and amplitude levels of the excitation caused. Commonly used speed-bumps such as Speed Cushions, Short humps or Trapezoidals were implemented in a numerical model where a vehicle model passed over them at the velocity of 36 km/h. Per the results, the bump with the sharpest edges and highest slope was assumed to be responsible for generating the highest vibration levels [12].

2.1.2.3 Vehicle speed

As previously stated, the vehicle velocity is highly correlated with the received amplitude levels for ground vibrations. This is presented in the table below [11]:

Table 2.1: Broadband acceleration amplitudes ($\times 10^{-4} g$ RMS) [11]

Vel. Range (km/h)	20-30		46-50		66-70	
Measurement Direction	Transv.	Vert.	Transv.	Vert.	Transv.	Vertical
Bus	1.6	4.2	2.9	6.1	3.7	7.8
Loaded truck	0.91	1.0	1.1	1.8	1.6	2.4
Empty truck	0.86	1.1	1.1	1.9	1.3	2.7

Nevertheless, the vehicle velocity can also affect the frequency characteristics of the impact force and resulting vibrations. The induced ground vibrations due to the increasing vehicle speed of buses show effect in a narrow band of frequencies (10 - 15 Hz) meanwhile trucks have influence in a broader frequency range (between 10 - 40 Hz) due to the suspension stiffness of the different vehicle types. The effect for the bus which had an air-bag suspension system had a greater increase between 25km/h to 50 km/h than the truck which has a multi-leaf steel spring suspension system [11]. A detailed comparison between the vibration level induction for bus vs. truck is presented in the table below:

Table 2.2: Comparison of vibration levels ($mm/s^2, RMS$) induced by a bus and a truck on a premise [11]

Location	25 km/h		50km/h	
	Bus	Truck	Bus	Truck
Ground in front of house	20.5	19.9	64.5	33.2
External foundation wall	11.2	10.1	30.9	15.7
Mid-point of floor 1st storey	20.3	20.8	62.9	30.1
Mid-point of floor in 2nd storey	35.0	37.3	96.2	46.7

Both Table 2.1 and 2.2 present the results as Root-Mean-Square (RMS) values which are the most commonly used descriptor of an average vibration. RMS is the square root of the mean squared value of the vibrations and is in this case calculated for each one-third octave band within the frequency range 1.6 - 25 Hz using an 8-second integration time which captures the entire signal [11].

2.1.2.4 The vehicle mass

The impact of the mass of the vehicle on the induced ground vibrations is presented in the figures below where a comparison is made between a truck filled with water (Total weight of 11070 kg) and the same truck empty (Total weight of 8700 kg) where **TL2** and **TL6** describe the loaded trucks and **T3** and **T5** are empty [11]:

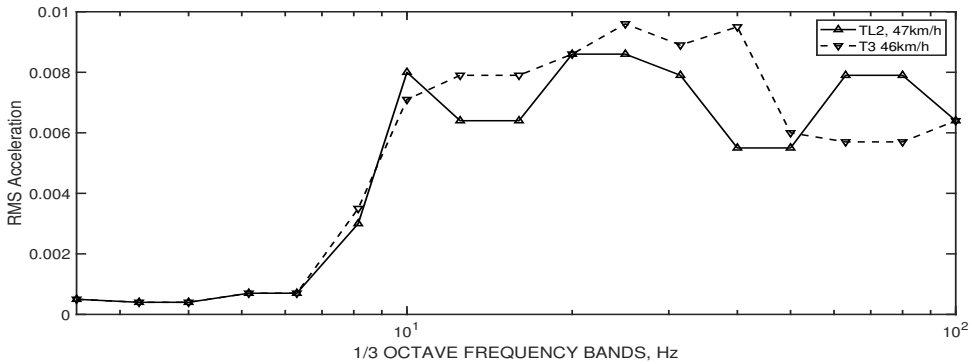

(a) Loaded and un-loaded truck at approx. v=50km/h, Adapted after reference [11]

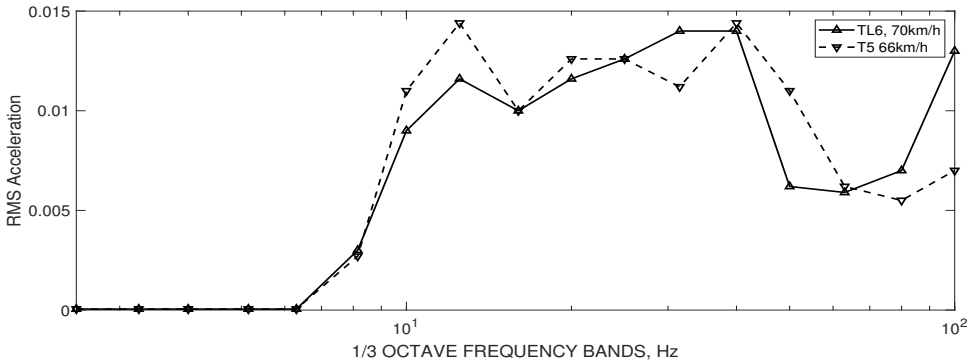

(b) Loaded and un-loaded truck at approx. v=70km/h, Adapted after reference [11]

Figure 2.12: Loaded/Unloaded Vehicle at different vehicle speeds [11]

The difference is minor and does not follow a strict pattern as the lower Figure of 2.12 shows that at some times a lower weight can result in a higher level of acceleration, meaning that the weight of the vehicle is of secondary importance when approximating the excitation induced by a heavy vehicle [11][13].

2.1.3 Effects of Ground Vibrations

2.1.3.1 Legislation regarding Ground Vibrations

The standard regulating the method of measurements of comfort vibration in Sweden is denoted as *SS 460 48 61 "Vibration and Shock" - Measurement and guidelines for the evaluation of comfort in buildings*. The standard defines the measurement technique and includes target values in form of an appendix [14]. In accordance to the human response to vibrations, following values are given as recommendations in the range of 1 - 80 Hz:

Table 2.3: The human response to vibration levels in accordance to *SS 460 48 61* [14]

	Weighted velocity	Weighted Acceleration
Moderate Annoyance	0,4 - 1,00 mm/s	14,4 - 36,0 mm/s^2
Feasible Annoyance	>1 mm/s	>36 mm/s^2

The previously mentioned standard is profoundly based on *SS-EN ISO 8041-1:2017* named *"Human response to vibration - Measuring instrumentation - Part 1: General purpose vibration meters"* which describes the terms, methodology and different values that are to be considered when dealing with comfort vibrations [15].

These standards are used as the base for legislations that are currently in use within Sweden when it comes to measurement and foundation for evaluation of the vibrations. Further standards and relevant methods include Nordtest Method *NT ACOU 082* (1991). The standard, titled *"Vibration and Shock, Evaluation of Annoyance"* describes in detail the measurement procedure for measuring of ground vibrations in and outside of buildings as well as the measurement positions and the general methodology [16].

2.1.3.2 Transmission of vibrations from ground to building and its effect on the comfort vibration level

The previously described Nordtest method also presents a prediction of transfer-functions of vibration levels from ground to buildings in form of an appendix. In the same standard a frequency weighting-curve is presented as it should be applied for the results evaluation to include the vibration tolerances, this table is included in [16] as Table 1. The standard states: *"At time it is more appropriate to measure vibration in the ground than in a building"* and hence have developed reference values that can be applied as an approximation of vibrational energy transfer from ground to building [16]. This could be used when measurement inside the buildings are impossible or if the measurements are to be done before the actual building has been erected. These reference values for the transfer functions are used by some consultancy firms today [1] and are given as shown in following table:

[1]NORCONSULT AB - Various reports regarding ground vibration (2019-04-16)

Table 2.4: Comfort weighted vibrational transfer from ground to building in accordance to Annex 3 of Nordtest Method NT ACOU 082 [16]

Transfer from ground into buildings	ΔL_A **in dB** (Approx. Amp. Factor)
From a position in the ground outside the building to a point on the foundation, vertical direction:	
- Building without basement (frame-type foundation)	- 2 dB (0,8)
- Building with basement (1,5 - 3m below surface)	- 8 dB (0,4)
From foundation (vertical) to a point on the floor in the building, vertical direction:	
- 1-storey house or ground floor of 2-storey house with timber deck:	+12 dB (4)
- Upper floor of 2-storey house with a timber deck:	+ 20 dB (10)
- Multi-storey building with/without wooden floors:	+ 9 dB (2,5)
From foundation (vertical) to a point on the floor (or the wall) of the building, horizontal direction:	
- 1-storey house or ground floor of 2-storey house, with timber deck:	+ 5 dB (1,8)
- Upper floor of 2-storey building with a timber deck:	+ 20 dB (10)
- Multi-storey building with concrete deck	+ 1 dB (1,1)

These values have been found in a set of measurements performed on a small number of single family houses where the source of vibrations was passing trains with a frequency range of 1 - 80 Hz. The transfer functions were found by the difference of the weighted acceleration levels between the ground and structure [16].

Another table of approximated amplification between ground vibrations and structure commonly used by consultancy firms in Sweden is presented below. This table applies a similar frequency weighting (Included as Appendix B in [14]) as the Nordtest and considers RMS SLOW values:

Table 2.5: Weighted amplification factors of Ground-Vibrations into structures [23]

Transmission ground to foundation with	**Amplification factor**
Pile foundation	0.3
Basement constructed as a slab on grade	0.4
Slab on grade	0.6

Floor structure	**Amplification factor**
Concrete, short spans	1
Concrete, wide spans	3
Stiff wooden floor structure	3
Weak wooden floor structure	6

Generally, the governing factors which define the level and frequency content of vibrations in the structure induced by ground-borne vibrations is the excitation source, transmission path and the structure itself. As slabs and walls in structures have their typical natural frequency in the range of 10 - 30 Hz with the entire structure often falling in between 5 - 10 Hz it is possible to excite the resonances, thus amplifying the vibration levels and altering the measured frequency content of the initial excitation [21].

2.1.3.3 Health Issues

Health issues circumferential with ground-borne vibrations and bad soundscapes have been given increased attention as connections have been made to physical and psychical illness. In its 2014 report, the European Environment Agency estimated that within the European Economic Area (EU countries with Switzerland and Norway) there are 10 000 premature deaths annually that could be attributed to noise exposure [17].

Long term exposures to negative soundscapes have been proven to cause different cardiovascular problems such as increased chance of heart attack and high blood pressure. Other known health issues connected to noise exposure are anxiety and depression among other stress-related disorders [18]. It has also been proven that physical abnormalities connected to child- and birth development that have lasting effects even after leaving the hazardous area can be traced to long term noise exposure. The World Health Organization concluded that even one million healthy life years are lost every year due to environmental noise from traffic related sources in the western parts of Europe [19].

However, the main health issue to be considered is the sleep deprivation associated with nocturnal vibrations and noise [18][34]. Humans are most sensitive to vibrations when in a recumbent posture with the highest sensitivity to vertical vibrations around 4 - 10 Hz, corresponding to the typical range of train and heavy vehicle frequency spectra. Studies show that vibration levels that are slightly above the wakeful perceptual detection threshold cause an increased cardiac activity for a sleeping person while other effects such as awakening and alterations of sleep structure occur after a slightly higher vibration level is reached [34].

2.1.3.4 Property Damages

Vibrations induced by heavy vehicles have sometimes been believed to cause fatigue damage on real estate such as cracks in the facade. It has since then been proven that the levels that are reached from heavy vehicles are not sufficient enough to cause property damage. However, the additional energy that is transferred to a building from the ground vibrations could be a factor that deepen the already existing issues due to the aging of the building and result in cracks that are not wholly due to the effects of the vehicles passing by [11][22].

2.2 Soil and Foundation types

2.2.1 Soil types

The vibrational amplitudes of ground vibrations depend on both the soil type as the soil types natural frequency. While the first one does not change over time, the second could, depending on the amount of ground water, temperature and its stress history. In general, the lower the stiffness and damping the soil type has the higher the vibrations will be [20].

The mechanical properties of soils depend directly on the interaction between the three different phases of soil, which are the solid, liquid and gas phases. In clay, which is the soil of special interest in this thesis the solid phase consists mainly of mineral and clay particles which are responsible for the load-bearing structure of the soil. The cavities of the soil are usually filled with air (if the soil is above ground-water level) and the relationship between the volume of solid mass, pore water and pore-gas make up the geotechnical properties of the soil [24].

A soil type with a fine structure and a grain size that is below 0,002 mm is classified as clay, which has the smallest particle size of any soil type. Clay in the liquid phase (containing ground water) is highly compressible due to its open structure and has a low strength allowing high volumetric changes. Its strength and behavior will be dependant on the stress-strain relation, consolidation of the soil and the shear stiffness. A consolidated clay experiences a slowly dissipating pore pressure due to its low permeability [25]. The clay in the Gothenburg region which is of special interest in this thesis exhibits the characteristics of a slightly over-consolidated and highly saturated soft clay, meaning that the clay in its current state has been unloaded from a previous loading (glacial ice for the Scandinavian region) [26].

2.2.2 Foundation types

The type of foundation plays an important role when it comes to ground vibration transfer. A foundation can either amplify or attenuate vibrations from the ground and transfer them into the building which makes it an important parameter to consider when studying the transfer functions from ground to building [20].

This section presents a brief theory regarding foundation types that will be considered in this thesis.

2.2.2.1 Shallow foundations

Shallow foundations are usually located less than 1,8 meter under the lowest floor of the building and are implemented when the soil is assumed to have sufficient bearing capacity. These types of foundations are assumed to be the most economically effective. Shallow foundations are often found to be supported by other structural elements such as footings which assist with the load transfer into the ground and prevent the foundation from overturning or sliding [41].

The Shallow Foundation will in this thesis be referred to as a Slab-on-Grade Foundation.

2.2.2.2 Basement foundations

Basement foundations are also known as Foundation Walls where the enclosed space makes up the basement. Basement foundations are popular in buildings due to their functionality as extra house space as well as a structural component that supports the load and resists horizontal forces near the ground surface keeping the building from over-turning [42].

2.2.2.3 Piling foundations

Piling foundations are columnar elements in the foundation of the building that have the function of transferring the static load when the soil is assumed to be insufficient to bear it by itself. The piles are led through the soil to the solid rock foundation or down to soil with higher stiffness and transfers the load to the more suitable ground [40]. Another significant effect of applying piling foundation is the load distribution along the mantle of all piles. As the load is being distributed over a larger surface the tensions become lower in the clay itself, lowering the risk of momentous movements or collapse.

Piling foundations have also been known from experience to cause a reduction to vibration amplification from ground to foundation [23] as presented in Section 2.1.3.2.

3
Methods

3.1 Measurement

This section describes in detail the measurement session that was carried out with the goal and purpose of validating the results generated by the analytical models that have been implemented in this thesis. The measurement was executed in cooperation with Norconsult AB that provided all the necessary equipment and resources.

3.1.1 Site

The chosen measurement site was located in a smaller community in the proximity of Gothenburg. As it was part of an ongoing Norconsult project the exact location will remain undisclosed. A site map is presented in the figures below along with a further description of the site:

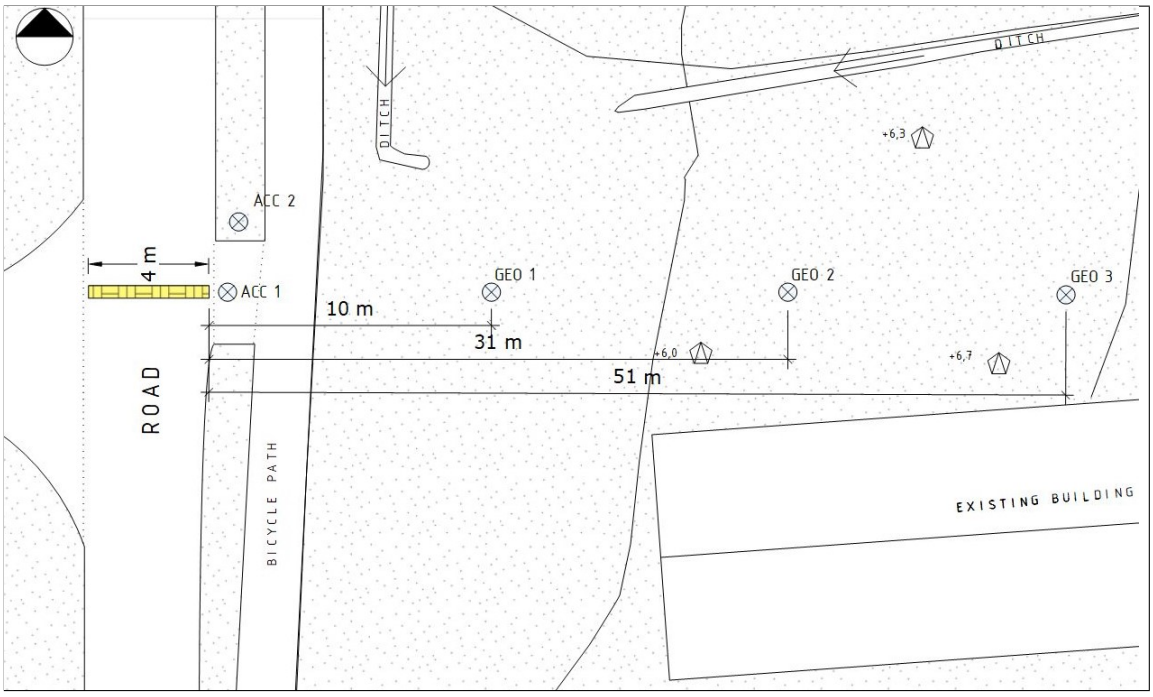

Figure 3.1: The site of measurements.

As shown in the figure, ditches were present on the site, both parallel to the road and parallel to the building on the plot where the measurement was implemented. The

site plan and placement of measurement equipment will be further presented and explained in Subsection 3.1.3. The road on which the measurement was conducted was of pristine condition without any visible unevennesses or cracks. It was also meagerly trafficked with no vehicle passing the site during the measurement. The condition of the road is presented in the figure below:

Figure 3.2: Condition of the road. Camera facing north, away from road-bump position as in Figure 3.1

Furthermore, the site is located within 200 meters from railway tracks trafficked by both cargo and passenger trains. The passages of the trains were monitored in order to be able to distinguish the contribution of the train as a source of ground vibrations.

3.1.2 Material Properties

As the measurement site was part of an on-going project a geotechnical investigation was carried out by Norconsult Fältgeoteknik AB. Some of the drilling points visible in the site plan have been marked in Figure 3.1 as polygons with a triangle. The table below presents the ground condition as found by the geotechnical department.

Table 3.1: The Material Properties of the Ground per in-situ measurements by Norconsult Fältgeoteknik AB

Layer	**Depth**	**Density** ρ	E**-modulus**	**Poisson's** ν	**Damping** h
Surface Clay	0 - 1,5 m	1800 kg/m^3	35 MPa	0,30	0,04
Clay	1,5 - 2,0 m	1620 kg/m^3	15,11 MPa	0,499	0,02
Clay	2,0 - 3,0 m	1620 kg/m^3	22,16 MPa	0,499	0,02
Clay	3,0 - 5,0 m	1670 kg/m^3	21,16 MPa	0,499	0,02
Clay	5,0 - 7,0 m	1750 kg/m^3	28,20 MPa	0,498	0,02
Clay	7,0 - 10,0 m	1720 kg/m^3	33,23 MPa	0,498	0,02
Clay	10,0 - 12,0 m	1770 kg/m^3	38,26 MPa	0,498	0,02
Bedrock	12,0 m -	-	-	-	-

3.1.3 Measurement Implementation

3.1.3.1 Vehicle

The vehicle used for excitation of the vibration was a SCANIA P280L (2016 Model) Truck with two axes (4x2), similar to the one presented in the figure below:

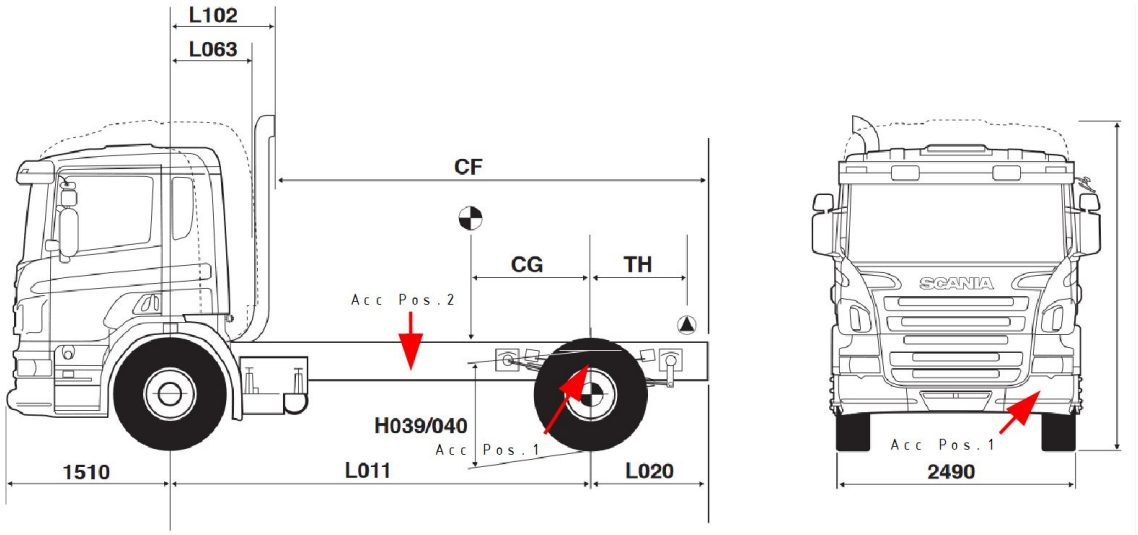

Figure 3.3: The Chassis specification of the truck used in the measurement [27].

The truck was attached with 3 accelerometers during the measurement session as indicated by the red arrows in the figure. These accelerometer positions are presented and explained in detail in Section 3.1.3.3. Moreover the following chassis dimensions are given for the truck used in this measurement :

Table 3.2: Dimensions of the Truck

Dimension	**Length**
L011	4,3 m
L020	1,2 m
CF	4,6 m

A 2-axis vehicle was specifically chosen in order to limit the amount of impulses and allow a easier interpretation of measurement results. The vehicle was fully loaded with macadam and had the following weight and load distribution:

Table 3.3: The load distribution of the truck used in the measurement

Total load:	15000 kg
Front axis load:	6700 kg
Rear axis load:	8300 kg

3.1.3.2 Speed Bump

The speed bumps used for the excitation of vibrations were of the type: *Farthinder "Wake up"* and had the dimensions as in the following figure:

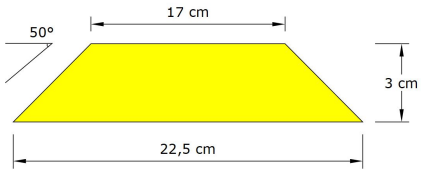

(a) Dimensions of the Speed Bump.

(b) The Speed-bumped used [28]

Figure 3.4: The Speed-bump used in measurement session

A single speed bump has the total length of 2 meter, hence two were used and placed next to each other. These speed bumps were not fixed to the road in any way, but rather laid freely on the pavement. In high velocities the truck caused the speed bumps to slightly shift positions which was corrected after the passage. The positioning of the speed bump in relation to the measurement plot can be seen in Figure 3.1.

3.1.3.3 Accelerometers

A total of 5 accelerometers were used in the measurement session. 3 accelerometers were attached to the vehicle in order to investigate the different resonances of the vehicle components. 2 accelerometers were placed closely to the speed bump as driving point measurements. The two accelerometer positions on the ground are denoted in Figure 3.1 as circles with a cross. A detailed description of the accelerometers follows:

Accelerometer 1

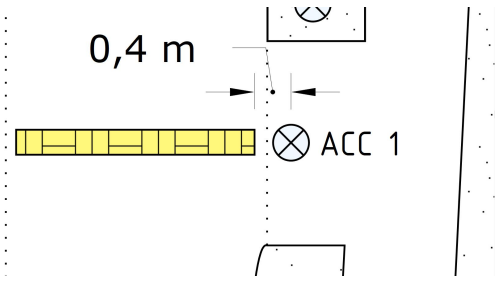

(a) Accelerometer 1 Position

(b) Accelerometer 1 placement

Figure 3.5: Positioning and placement of Accelerometer 1.

Accelerometer 1 is a high sensitivity (500 mV/g) triaxlar piezoelectric accelerometer with a operating range of 0,07 - 6000 Hz and a resonance frequency at 9000 Hz. It was the accelerometer closest to the source, located 0,4 m from the edge of the speed bump on the pavement. It was attached to a thin metal plate which was glued to the road surface.

Accelerometer 2

(a) Accelerometer 2 Position

(b) Accelerometer 2 placement

Figure 3.6: Positioning and placement of Accelerometer 2.

Accelerometer 2 is of the same type as Accelerometer 1, also logging data for two directions only. It was placed a little further from the speed bump in the soft soil in order to be able to place it beneath the surface of the ground. A hole was dug with an approximate depth of 30 cm. The accelerometer was placed on a metal plate which was fixed to the bottom of the pit. The accelerometer was then covered by macadam as shown in Figure (b) of Figure 3.6.

Accelerometer 3 & 4

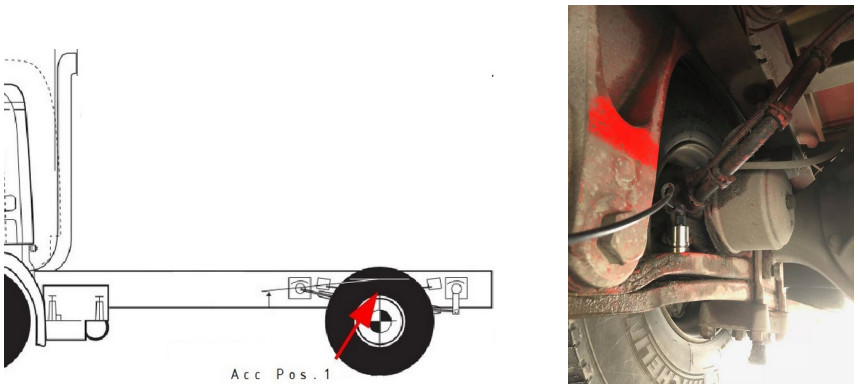

(a) Accelerometer 3 & 4 Position

(b) Accelerometer 3 & 4 placement

Figure 3.7: Positioning and placement of Accelerometer 3 & 4

Accelerometer 3 & 4 were placed on the back axis of the truck as shown in the figures 3.3 and 3.7 (Acc Pos.1). Note that the photograph included in Figure 3.7 only shows one of the used accelerometers as the second was attached after the picture was taken. The accelerometers were attached to the axis by magnets on a previously cleaned surface. The accelerometer shown in the picture (Accelerometer 3) is a high sensitivity accelerometer with a sensitivity of 1000 mV/g and a linear frequency range between 0,1 - 4000 Hz. The resonance frequency of the accelerometer is 7000 Hz. In this measurement only the Z-direction was analyzed.

As Accelerometer 3 was of a very high sensitivity a second accelerometer (Accelerometer 4) was attached as backup, in order to not have to redo the measurements if the data from Accelerometer 3 would be disrupted from the harsh impulses of a truck passing a speed bump. Accelerometer 4 was placed just next to Acceloremeter 3 and attached in the same fashion. It was Industrial Accelerometer with a sensitivity of 100 mV/g and a frequency response between 0,3 - 10,000 Hz. Its resonance frequency was 27 kHz.

No Accelerometer was placed on the front axis since it was practically impossible to place the Accelerometer in a way that generated sufficient results. The different between the suspended mass and unsuspended mass was hard to spot for the front axis in the same time as the truck's frame made it impossible to reach the undercarriage of the truck.

Accelerometer 5

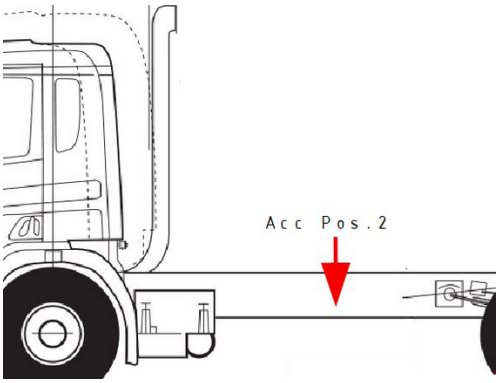

(a) Accelerometer 5 Position

(b) Accelerometer 5 placement

Figure 3.8: Positioning and placement of Accelerometer 5

The 5th accelerometer used was attached to the chassis (Acc Pos. 2 in figures 3.3 and 3.8) in order to see the effect of the damped mass on the vehicle body. Accelerometer 5 was of the exact same type as Accelerometer 3 (Sensivity of 1000 mV/g) and was also registering data in the Z-direction only. It was attached by a magnet as shown in Figure 3.8.

3.1.3.4 Geophones

Another set of equipment that was used to register ground vibrations were Geophones. The Geophones were placed out as shown in Figure 3.1. Geophone 1 was supplied with a trigger set to activate at the velocity level of 0,2 mm/s. As the trigger was activated for the geophone closest to the road it caused all the other geophones to start registering data. The figure below shows the deployment of one of the geophones along with the geophone positions:

(a) Set up of Geophone 1 **(b)** All the Geophone locations

Figure 3.9: The Geophone setup along with its location on the measurement plot, (a) is facing towards west and (b) towards east.

The placement and distances from the road edge for the geophones are presented in Figure 3.1. The geophones record the peak particle velocity within the range of 1 - 1000 Hz and meet the equipment requirements set by Swedish Standard *SS 460 48 61*. The geophones were placed below the ground and recorded vibrations in the Z-direction.

3.1.3.5 Measurement Procedure

The implementation of the measurement was as following; firstly, the equipment was set up and calibrated. The equipment was laid out as in accordance to Figure 3.1, Section 3.1.3.3 and 3.1.3.4. After calibration and check of the acquisition-station the measurement begun with a trial run. The trail run was intended to ensure that the triggers on the geophone worked and that the acquisition stations logged data correctly. Afterwards the actual measurement commenced per the following order:

Table 3.4: Measurement Runs

Velocity	Passages	Start Time
V = 10 km/h	4	10.35
V = 20 km/h	4	10.41
V = 30 km/h	4	10.45

The driver was instructed to keep at the given velocity while passing over the speed bump. The measurement was further logged onto a recording camera which placement can be seen in the Figure below along with placement of the entire setup for the measurement:

Figure 3.10: The setup of the measurement

The recordings from a camera were also used for visual inspection of displacement of the different truck-components when the truck passed over the speed bump. The snapshots from the recording are presented below with yellow tape being the reference point on the different vehicle elements:

Figure 3.11: Snapshots of the truck passing the camera at V = 20 km/h.

The surrounding was monitored during the measurements and abnormalities were noted (e.g. train-passages). The acquisition of data was controlled by the participants and the supervisor simultaneously as the measurement was conducted. Finally, the used equipment for this measurement is presented in the table below:

Table 3.5: The Equipment used for the measurement

Equipment	Serial Number	Comments
SVANTEC Aquisition Station	20870	Tri-channel analyzer
2x Accelerometers type KS48C	16121/16120	Frequency range (0.1 - 4000 Hz)
2x Accelerometers type KS823B	10077/10078	Frequency range (0.7 - 6000 Hz)
1x Accelerometer DYTRAN 3176B	3944	Frequency range (0.3 - 10000 Hz)
Geophone Acquisition Station	x	FRED06 System
3x Geophone type SM 6	x	Frequency range (1 - 1000 Hz)
2x RION SA-78	x	Acquisition for Acc. 1 & 2
2x Speed Bumps	x	Type "Wake up" L=2 m
Camera w/ Tripod	x	x
Cables & Batteries	x	x
Leica Pinmaster	x	Laser meter
SCANIA P280L	x	4x2 Truck

3.2 Modelling of Source Model

In order to be able to investigate the effect of different types of vehicle parameters as varying loads and stiffness parameters a source model was set up.

3.2.1 Description of the Model

The source model is constructed as a mass spring damper system with 4 degrees of freedom, to better resemble the dynamic behavior of a truck. The initial model consisted of a mass spring damper system with two degrees of freedom, per previously presented Figure 2.8 but was later changed into a mass spring damper system with 4 degrees of freedom since the dynamic behavior of a heavy vehicle was better represented by using a more complex model [38]. Below is a visualization of the model:

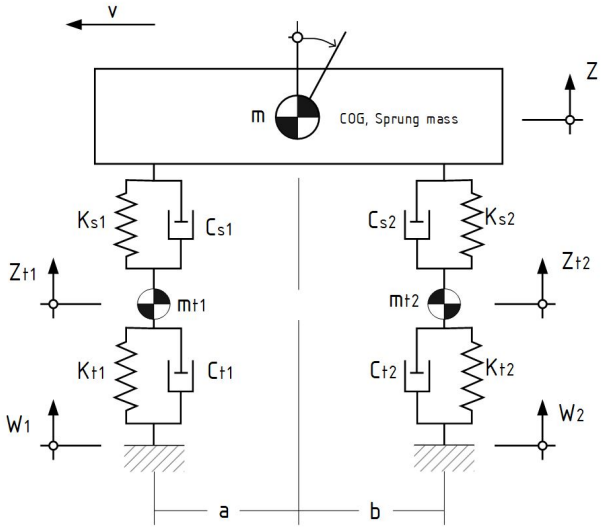

Figure 3.12: Multi degree of freedom system, Adapted from reference [38]

Initially the model did not have any damping at the wheel, but rather only between the unsprung and sprung mass. The damping between the wheel and pavement was added to be able to resemble the half vehicle model as modelled in the guiding Reference [38]. The set-up shown in Figure 3.12 gives the following equations of motion:

$$\ddot{z} = -k_{s1}\left(z - \theta \cdot a - z_{t1}\right) - c_{s1}\left(\dot{z} - \dot{\theta} \cdot a - \dot{z}_{t1}\right) - k_{s2}\left(z + \theta \cdot b - z_{t2}\right) \ldots \\ -c_{s2}\left(\dot{z} + \dot{\theta} \cdot b - \dot{z}_{t2}\right) + F_Z \tag{3.1}$$

$$I_y\ \ddot{\theta} = \left[k_{s1}\left(z - \theta \cdot a - z_{t1}\right) + c_{s1}\left(\dot{z} - \dot{\theta} \cdot a - \dot{z}_{t1}\right)\right] \cdot a - \ldots \\ \left[k_{s2}\left(z + \theta \cdot b - z_{t2}\right) + c_{s2}\left(\dot{z} + \dot{\theta} \cdot b - \dot{z}_{t2}\right)\right] \cdot b \tag{3.2}$$

$${}_{t1}\ddot{z}_{t1} = F_{z_{t1}} + k_{s1}\left(z - \theta \cdot a - z_{t1}\right) + c_{s1}\left(\dot{z} - \dot{\theta} \cdot a - \dot{z}_{t1}\right) - k_{t1}\left(z_{t1} - w_1\right) - \ldots \\ c_{t1}\left(\dot{z}_{t1} - \dot{w}_1\right) \tag{3.3}$$

$$_{t2}\ddot{z}_{t2} = F_{z_{t2}} + k_{s2}\left(z + \theta \cdot b - z_{t2}\right) + c_{s2}\left(\dot{z} + \dot{\theta} \cdot b - \dot{z}_{t2}\right) - k_{t2}\left(z_{t2} - w_2\right) - ... \\ c_{t2}\left(\dot{z}_{t2} - \dot{w}_2\right) \tag{3.4}$$

Where the quantities are presented per the table below:

Table 3.6: Quantities of the Equations of Motion for the Source-model

QTY:	Description:	QTY:	Description:	QTY:	Description:	QTY:	Description:
m	upper mass	c_{s2}	damping const. of rear axis damper	$\dot{z}_{t1}/\dot{z}_{t2}$	velocity of front/rear axis mass	ω_2	1st derivative of the road profile for rear axis
m_{t1}	front axis mass	c_{t1}	damping const. of front axis tire	$\ddot{z}_{t1}/\ddot{z}_{t2}$	acceleration of front/rear axis mass	F_{zt1}	the external force on the front axis.
m_{t2}	rear axis mass	c_{t2}	damping const. of rear axis tire	θ	pitch angle	F_{zt2}	the external force on the rear axis.
k_{t1}	spring const. for front axis wheel	z_{t1}	displacement of front axis	$\dot{\theta}$	1st derivative of the pitch angle	F_Z	the external force on the upper mass.
k_{t2}	spring const. for rear axis wheel	z_{t2}	displacement of rear axis	$\ddot{\theta}$	2nd derivative of the pitch angle	a	length from the centre of gravity and front axis
k_{s1}	spring const. of suspension of front axis	z	displacement of the upper mass	ω_1	road profile for front axis	b	length from the centre of gravity and rear axis
k_{s2}	spring const. of suspension of rear axis	$\dot{z}$	velocity of upper mass	ω_2	road profile for rear axis	I_y	the moment of inertia around the y-axis
c_{s1}	damping const. of front axis damper	$\ddot{z}$	acceleration of upper mass	$\dot{\omega_1}$	1st derivative of the road profile for front axis		

To be able to calculate the dynamic response of the heavy vehicle a road bump must be added as input to the system. In the created model the force is equal to zero if the road profile is flat. Hence, some kind of road irregularity is needed to excite the model.

The input that was used initially was the input measured during the measurements, but this resulted in problems with vehicle speed where some velocity levels created a road profile which coincided with the vehicles second resonance frequency that enhanced the force amplitude. This resulted in some contradicting results, which disproved the fact that the force increases with higher vehicle speed.

To avoid this problem the speed bump was simplified to the "drop off phase", where the vehicle falls from the top of the speed bump. The drop off speed was created so that the incline became steeper with a higher velocity. This resulted in higher force at higher velocities which agrees with the previously presented theory. In the figure below the difference between the initial road profile and the corrected one is presented:

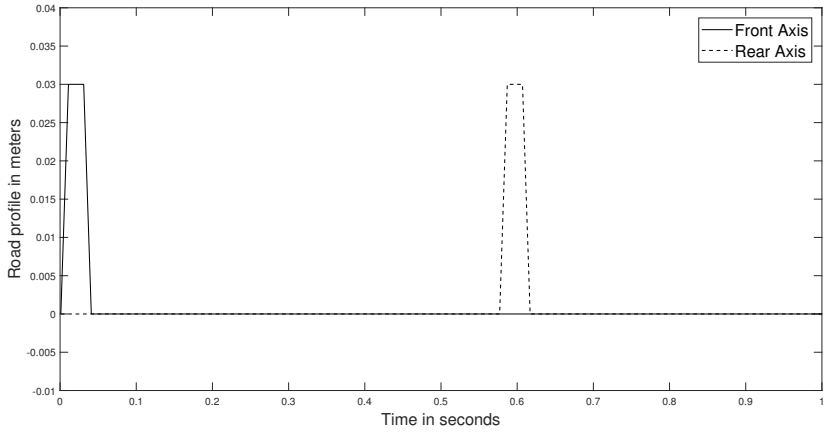

(a) Initial Road Profile

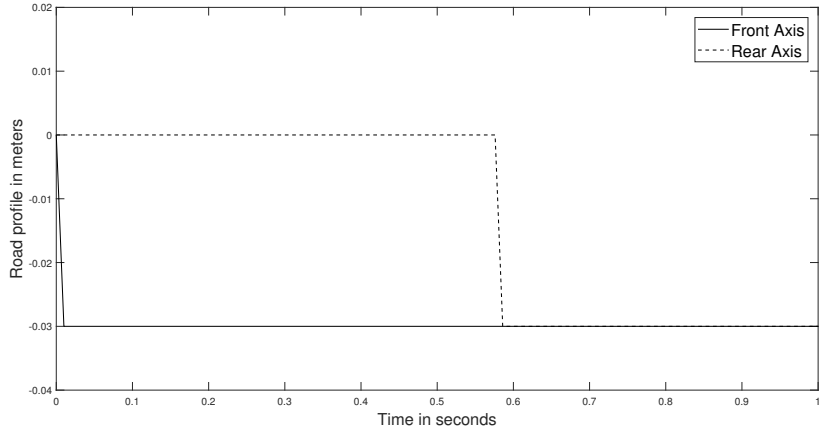

(b) Corrected Road Profile with only the "Drop-off" section

Figure 3.13: Initial and Final Road Profiles for the Source Model

The SIMULINK model that was used to simulate this vehicle passage can be found as a graphical presentation in Appendix A.

All of the used parameters were predefined in MATLAB. In the model, INPUT1 is the road profile for the first axis of the car and INPUT2 is the road profile for the second axis. INPUT1 also contains a delay proportional to the distance between the axis and the velocity.

SIMULINK uses the predefined *ode*-functions that exist in MATLAB which stands for ordinary differential equation. The *ode*-functions calculates a solution for each time step iteratively. The choice of which *ode* function to use in SIMULINK is made by the model automatically. For the given case the SIMULINK chooses *ode3* which is based on the Bogacki–Shampine method. *ode3* computes the next time-step as an explicit function of the state and the state derivative. The state derivative is computed by using the Bogacki-Shampine Formula integration technique [39].

The output produced by the SIMULINK model is the resulting time signal for

the passage. The time-step in the model is set in a way that corresponds to a suiting sampling rate. The sampling rate was 1000 samples per second as it was approximately the same amount as in the measurements.

3.2.2 Implementation and validation

The implementation consisted of a number of steps, firstly, it was of importance to analyze the retrieved measurement data. During the analysis it was realized that the most consistent results were found when the vehicle speed was 20 km/h.

The force at the vehicle speed 10 km/h was to low to be accurate since the impulse of the speed bump passage was damped to fast. At 30 km/h two of the passages contained a peak at 10 Hz and one at 15 Hz. The peak at 15 Hz cannot be explained by the intended model and was therefore questioned. The two measurements that contained this peak were investigated and by the recorded videos of the measurements they could be connected to the speed bump being knocked away by the passing truck. The speed bump moved during the passage of the front wheels passage, which created an unevenness between the two wheels for the rear axis. This unevenness may be the reason to why a second peak was recorded at 15 Hz. More detailed and thorough analysis of the measurement results is presented in Section 4.1.

To be able to ensure that the force the source model generates is correct, the position of the closest accelerometer was used as a driving point and input in the SOLVIA model. The same distances and material parameters were inserted into the SOLVIA model as were measured during the geotechnical survey and the actual measurement. Thus, the measurement results from the nearest accelerometer were matched towards the source model. Therefore the desired force for the passage of the front and rear wheels over the speed bump can be found iteratively by changing the force until the measurement and the model gives the same result at the driving point, in a trial and error approach.

For both the measurement data and the model passages the found time signal for the impulse is cut after 0.5 seconds. The cut off of the time signal is set to 0.5 seconds since the axle hop frequency can be considered to be damped after 0.5 seconds. The reason to why all of the time signals need to be the same length is due to the usage of the Fast Fourier Transform. Combined with different time lengths of the same signal, it will give altering amplitudes of the same time signal in the frequency domain. Therefore, all the signals need to be the same length. This is effect is showcased for an arbitrary signal as the one below:

$$A(t) = e^{-t} sin(\omega t) \tag{3.5}$$

The same signal has been transformed twice, one using the total integration time of 5 seconds and one for 10 seconds.

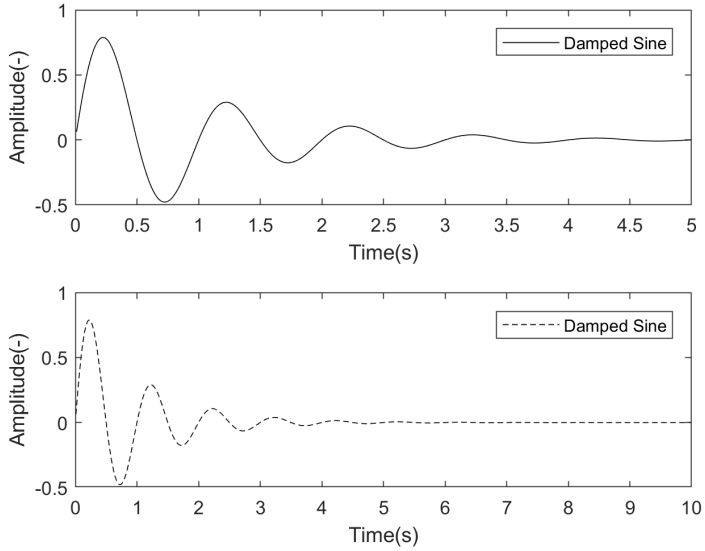

(a) Time signals with different time lengths

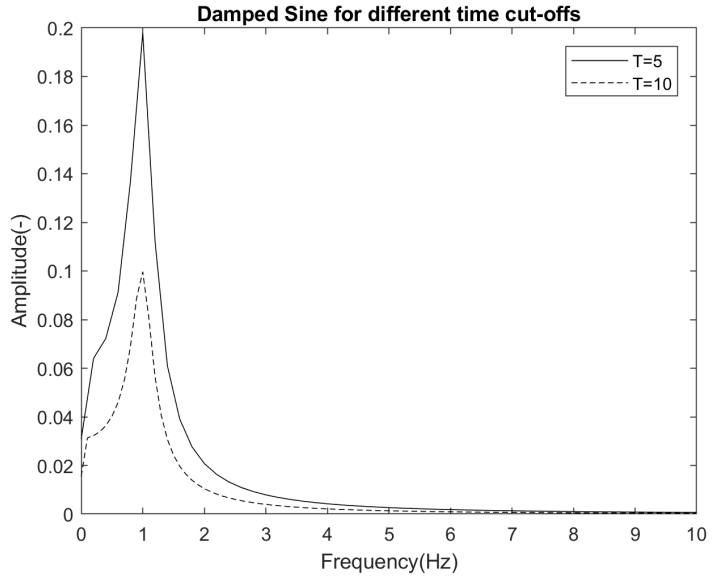

(b) Amplitude comparison between the signals

Figure 3.14: Amplitude given by the fast Fourier transform of different time signal lengths

However, a 0,5 second long signal would give a resolution of 2 Hz which is far from satisfactory. Therefore, another method was used to gain a higher frequency resolution.

The implementation of this method resulted in the division of the front axis passage and the rear axis passage were divided into two five second time signals. After the fast Fourier transform has been performed on these time signals the values are scaled by multiplying with 10 to get the same amplitude as the 0,5 second time

signal provided. The example below shows that this will not create any errors:

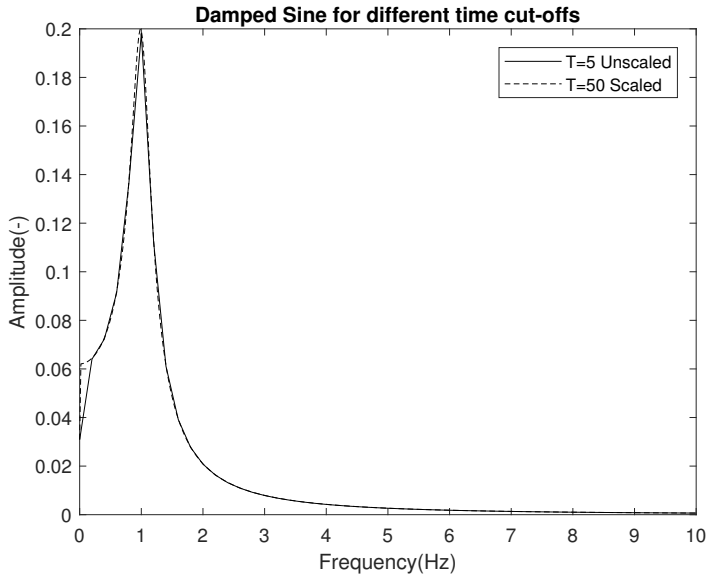

Figure 3.15: Amplitude Scaling Example

Thus, by Figure 3.15 the two signals can be considered to be the same which shows that this is an effective way to improve the frequency resolution without altering the amplitude.

Due to the front and rear axis being separated into two different time segments it is possible that some of the ground vibrations induced by the front axis will be found in the rear axis time segment if the impulses are too close in time. Since it is impossible to avoid this problem in the measurements, this needs to be taken into consideration for the half vehicle model where the axes can be seen individually.

Initially the model parameters were set as seen below, since they were the model parameters used in [38] for a half vehicle model:

Table 3.7: Initial Parameters of the Source Model, as per Reference [38].

Parameters	Value	Parameters	Value
m	8800 kg	k_{s2}	400 kN/m
k_{s1}	300 kN/m	c_{s2}	4000 Ns/m
c_{s1}	2000 Ns/m	m_{t2}	450 kg
m_{t1}	350 kg	k_{t2}	1800 kN/m
k_{t1}	1000 kN/m	c_{t2}	1 kN/m
c_{t1}	500 Ns/m	I_{yy}	50000 kgm^2
a	2.54 m	b	1.16 m

These parameters were later adjusted to better fit the results of the desired front and rear axis forces.

Some parameters can be found or could be calculated. The total load, the distances from the center of gravity to front and back axis and the front and back axis loads. The other parameters are adjusted to fit the input force in the SOLVIA model within a reasonable range. The final parameters for the truck that were used in the measurement can be seen below:

Table 3.8: Final Parameters of the Source Model.

Parameters	Value	Parameters	Value
m	14450kg	k_{s2}	240 kN/m
k_{s1}	150 kN/m	c_{s2}	4000 Ns/m
c_{s1}	2000 Ns/m	m_{t2}	350 kg
m_{t1}	200 kg	k_{t2}	900 kN/m
k_{t1}	480 kN/m	c_{t2}	1500 Ns/m
c_{t1}	600 Ns/m	I_{yy}	45000 kgm^2
a	2.365 m	b	1.935 m

Using the data obtained by Accelerometer 3 the acceleration on the back axis was acquired. This acceleration was used as an indication for the time signal of the acceleration in the SIMULINK model. From the acceleration from the measurement of the back axis, the damping and the resonance frequency is found. The amplitude of the acceleration cannot be found as the correct one, since the amplitude will differ depending on where on the axis the accelerometer is placed. Closer to the wheel the acceleration amplitude may be greater than in the middle of the suspension axis.

The half vehicle model was modelled as a point source in SOLVIA. The point source will represent the passage of both axes and will therefore be the combined force of the front and rear axis contribution. The resulting force generated by the source model and its validation process is broadly presented in Section 4.2.

3.3 Finite Element Method

In order to effectively approach the question of issue of this thesis a FEM model was created with the provided FEM program, SOLVIA Finite Element System.

SOLVIA is a tool for linear and nonlinear analysis of displacements, stresses and temperatures under static or dynamic conditions. As the program is completely text-based and lacks a graphical user interface most of the geometry and boundary condition setting were done through a developed MATLAB code specifically developed to generate a working ANSI-file for the SOLVIA software to answer the questions-of-issue of this thesis.

The FEM Model was used to generate results within a frequency range of 1 - 15 Hz with a frequency step of 0,2 Hz.

3.3.1 Modelling of the Ground Model

Following section describes the geometry, material and model properties of the generated ground model used in this thesis along with methods used to ensure correct boundary conditions and model behaviour.

3.3.1.1 Geometry and Material Properties

The final ground model is a 48 x 48 meters big model with a depth of 12 meters. The depth of the model was governed by the Geotechnical Survey at the Measurement plot described in Section 3.1.3. At a depth of 12 meters rock was struck, hence the ending of the model with fixed boundaries, causing reflections as it would in reality. The geometry of the ground model used is shown in the Figure below:

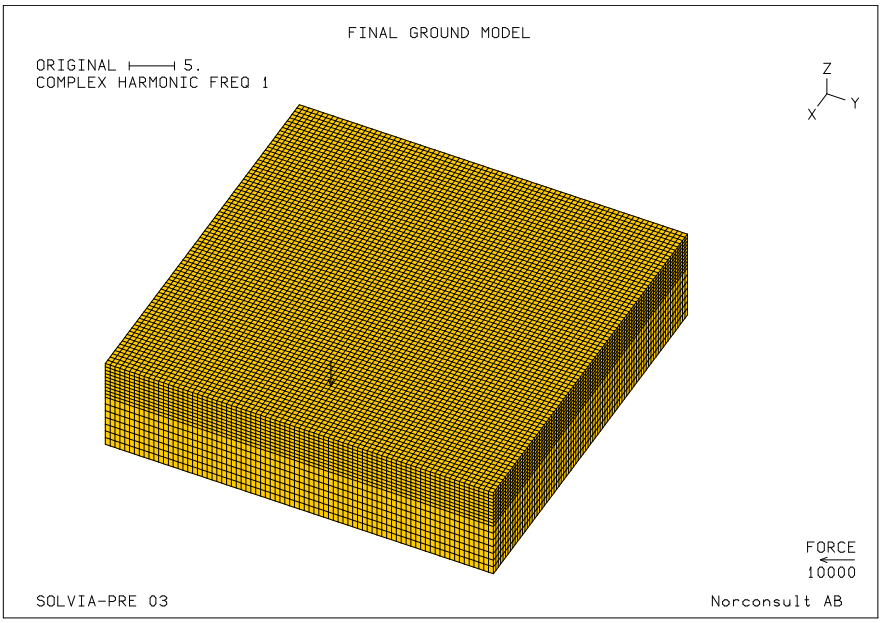

Figure 3.16: The Base Ground Model

The material properties used in the model are presented in Table 3.1. The first layers of Surface crust and clay have been given the finest mesh. One material property is unknown and it is evaluated during the validation progress. This material property is the damping of the soil and is denoted as H, which stands for hysteric damping. This parameter is initially set to 0.02 since it has previously been deemed as successful when evaluating vibrations in clay.

3.3.1.2 Mesh-size

The model consists of free rectangular elements with varying element size where the guiding rule was to have elements small enough to allow for at least 6 nodes per the shortest wave length. The highest frequency of interest is set at 15 Hz which gives the shortest wave length of 3,6 meters (for a shear wave). Hence, the distance between 2 nodes cannot be greater than 0,6 meters in order to satisfy the 6-node per wavelength condition.

Due to calculation-time limitations, the finest mesh was implemented adjacent to the surface. The further away from the surface the rougher the mesh. This decision was motivated by the characteristics of the propagation for the certain waves of interest. The body waves are of most relevance in the near field of the source, hence the lack of need for a finer mesh at the bottom of the model. Due to that the surface waves are of most interest making it necessary to allocate as much as calculation power to the areas where its effect is observed, being directly adjacent to the model surface.

The Mesh-size is also limited by the boundary conditions, disallowing it to be too coarse as the implemented damping method used at the boundaries required a maximum length between nodes of 5 meters. This condition has been greatly satisfied with this mesh where the maximum distance between two nodes is 0,6 respectively 0,5 meters, the boundary conditions are further explained in Section 3.3.1.4.

3.3.1.3 Excitation Force

The force used for excitation is a frequency dependent force input curve calculated using the source model that has been described in detail in Section 3.2. The FEM implementation of this source is as a single vector, normal to the surface of the model acting on one node as a point source. The resulting input force and its validation process can be found in Section 4.2.

It is essential to point out that the FEM model assumes steady-state excitation and is time independent as no time-signal is used as input. Thus, the input excitation is assumed to have acted on the structure well before the measured results and will continue after having reached the steady state. The choice of this method was used as it simplified the calculation process in FEM and is further discussed in Section 5.1.

3.3.1.4 Boundary Conditions

As the ground model was to represent a semi-infinite medium it was of utterly importance to ensure no reflection from the vertical boundaries of the model. This is implemented in different ways when modelling ground in FEM and for this certain model a technique called Perfectly Matching Elements (also referred to as Perfectly Matching Layers) was implemented.

Perfectly Matching Element or Perfectly Matching Layers is a method used to create the correct boundary conditions for a continuous medium. The problem with finite element programs is the reflections caused within the model from boundaries which are not desired. To be able to create perfect matching elements, the boundaries of the model need to be completely absorbing.

To be able to get completely absorbing boundaries the following equation needs to be equal to zero:

$$r = \frac{Z_1 - Z_2}{Z_1 + Z_2} \tag{3.6}$$

Here, Z_1 is the impedance of material 1 (Guiding Medium) and Z_2 is the impedance of material 2 (the void) where the equation can only be 0 if Z_1 and Z_2 are equal to each other. To be able to achieve this, the impedance of material 1 needs to be found. The impedance of material 1 is dependent on the density, the Poisson's ratio, the Young's modulus, the longitudinal wave speed and the transverse wave speed. As the model is finite but should represent a semi-infinite medium it is technically impossible to have the same impedance in a solid medium and the medium past the model boundary (in this case Material 2), hence need of PML/PME.

The PML uses a radiation damping coefficient to avoid wave reflection by rewriting the dynamic equation of motion at the boundaries. Essentially, the PML acts as a spring in the normal or tangential direction of the boundary depending on the wave type. The damping coefficient is:

$$\tau_R = \rho c_i \tag{3.7}$$

where ρ is the material density and c_i is the wave speed in the medium, calculated per the previously presented Equations 2.18, 2.22 and 2.45.

In order to be effective, the PML must match the mesh and is bound by the surface area of the boundary with the correct damping coefficient. This means that when applying the PML to a real model, the PML is dependent on both the mesh and the surface area it acts on. It also differs at the model's corner, at the model's edge or if it is in the middle of the models surface. When the node is at the corner of the surface the area it represents is only 1/4 of the area that a non-connected node has, and if it is at an edge it is only 1/2 of the area a non-connected node has. The formula also changes dependent in which direction in the model the PML is desired. Since ground vibrations consist of different types of waves that excite the structure in different directions the boundaries need to be absorbing in all the directions.

The PML is then validated by evaluating the impedance and compliance functions as well as considering the phase at the excitation point where it should be flat. More detailed description of the PML can be found in Reference [37].

3.3.2 Modelling of Buildings and Foundations

As the base for the paramateric study, three different foundation types were chosen and studied as briefly presented in Section 2.2.2. These foundation solutions were then applied to two buildings, one referred to as *"the big"* and the second being *"the small"* building due to the size of the constructions. The different base structures were created in SOLVIA and are briefly presented in the sections below:

3.3.2.1 Big vs. Small

The two constructed buildings are to represent regular buildings that are constructed in Sweden. The *"big"* building is to represent a multi-apartment block. It has the dimensions of 15 x 39,6 meter with the long side of the building facing the source of vibrations. The house is constructed with 5 floors where the distance between slabs is set to 2,6 meters. All building elements (slabs and walls) have been given the thickness of 300 mm.

The *"small"* building is to represent a regular single-family house and has been constructed as a single floor house with dimensions of 9 x 14,4 meter. All load-carrying elements in the *"small"* building have been given a thickness of 150 mm, both of the constructions are shown in the figure below:

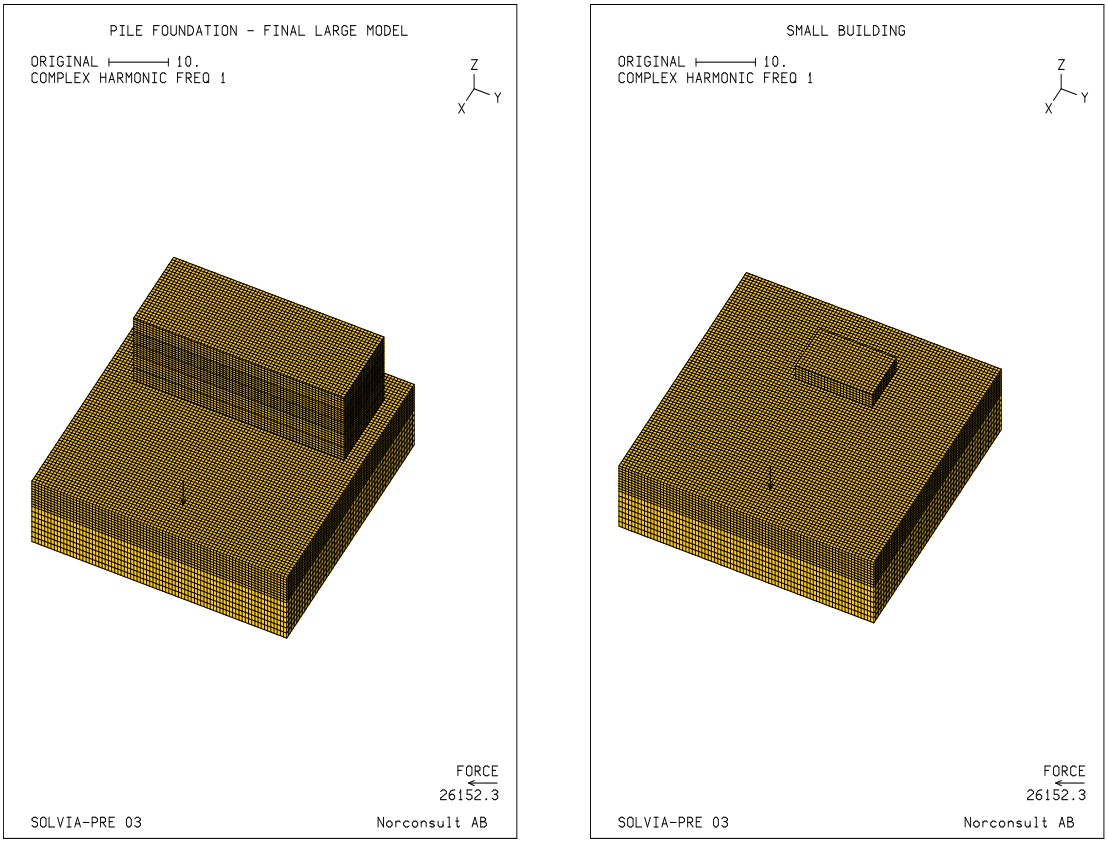

(a) The *big* building **(b)** The *small* building

Figure 3.17: The building constructions for the FEM analysis of Big vs. Small

This thesis focusses on the transfer between the foundation and ground depending on different foundation types, thus the effect of vibrations on the higher floors is of secondary importance as reliability cannot be ensured that the transfer functions between floors are correct. Rather the purpose of the floors is to supply a mass that can be considered representative in these kind of buildings.

Both the *"big"* and *"small"* building have been constructed using concrete, per this thesis limitations and have the following material parameters:

Density, ρ	**Young's Modulus,** E	**Poisson's Ratio,** ν
2400 kg/m^3	30 GPa	0,3

It is of importance to point out that the structures have no other loads applied than the mass of the construction elements. The models consist of the plates and outer walls, no other elements are inserted on the floors.

Important to notice is that no damping coefficient was used in SOLVIA when modelling the concrete elements. The reason to why no damping coefficient was used was that it would arguably not affect the focus of the thesis and there were some uncertainties regarding how the damping should be applied. To avoid potential errors the damping was not applied.
The following sections will in detail describe the modelling of the different foundation types that were applied for both building types:

3.3.2.2 Slab-on-grade Foundation

The first chosen parameter was a Slab-on-grade foundation which is one of the most used foundations due to its economic advantages alongside other attributes that have been briefly presented in Section 2.2.2.1.

For the *big* building the slab has a thickness of 0,3 meter with 0,15 meter above and 0,15 meter below ground level respectively. For the *small* building the slabs thickness was changed to 0,15 meter (75 mm above and 75 mm below ground) in order to see the effect of the vibrations on a slab with a much lower mass.

3.3.2.3 Basement Foundation

The basement foundation was chosen as the second parameter of interest. The basement is made up of the same material parameters as the slab edge and has a total depth of 2,70 meters. For the *big* building the basement model has a slab resting at the depth of 3 meters with a thickness of 300mm. The foundation walls are 0,3-meter-thick and support a top plate with a thickness of 300 mm. The plates have been modelled as solids while the walls as shells.

Similarly to the Slab Foundation, the thickness of the building elements was altered to investigate the effect of the vibrations. The second setup (*small* building)

was made up of walls and slabs with a total thickness of 150 mm, making the basement 2,85 meters deep. The figure below shows a section of the basement foundation with the *big* construction setup:

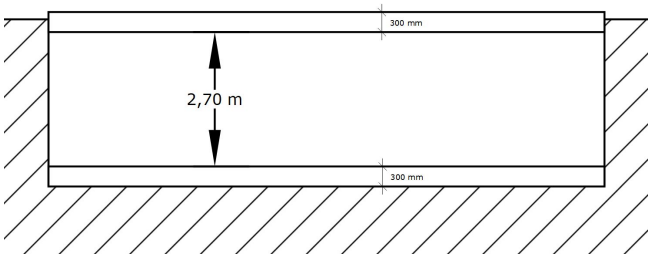

Figure 3.18: Section of the model - Setup for the *big* building with element thickness set at 0,3 meters

3.3.2.4 Piling Foundation

Lastly, a piling foundation was implemented. The piles were attached to the previously used basement foundation in accordance to the following piling plan for the *big* building:

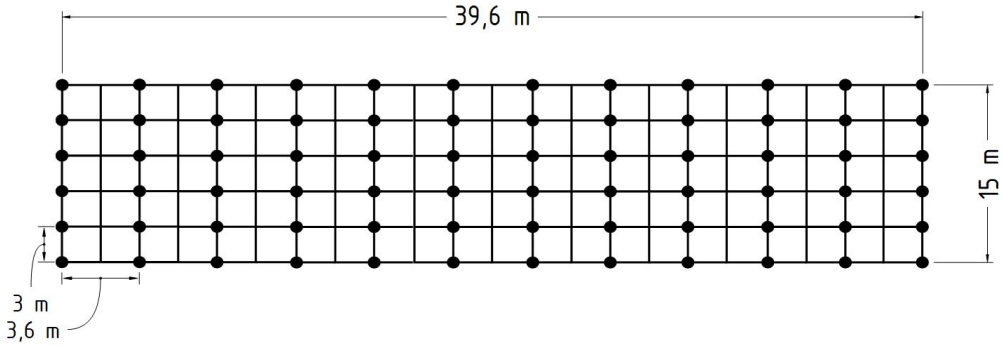

Figure 3.19: The Piling plan of the *big* building

The piling plan for the *small* building had a similar distance relation between piles, per the following plan:

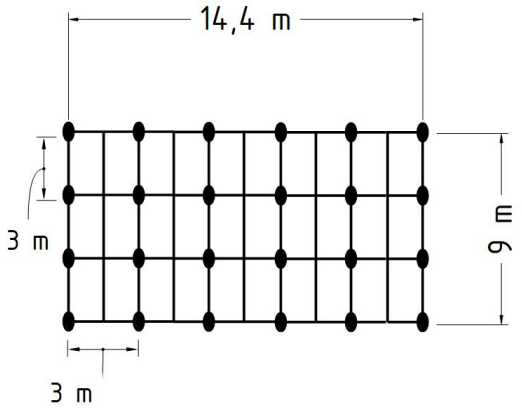

Figure 3.20: The Piling plan of the *small* building

The piles were constructed using truss elements while the rest of the model remained an elastic solid. The piles were given the dimensions of 270 mm x 270 mm with material data corresponding to concrete. The piles go as deep as the ground model and attach to the base of the model which is fixed in order to represent the rock-bed. All other elements are uniform with the previous parameter, Basement foundation.

The piling foundation model was also implemented in two thickness setups where the altering parameter was the thickness of the walls and slabs. The parameters of the piles stayed the same disregarding of the thickness parameter used for the remaining elements. The material parameters used for both the material parameters and piles were:

Density, ρ	**Young's Modulus,** E	**Poisson's Ratio,** ν
2400 kg/m^3	30 GPa	0,3

with the model section looking as following for the *big* building thickness setup:

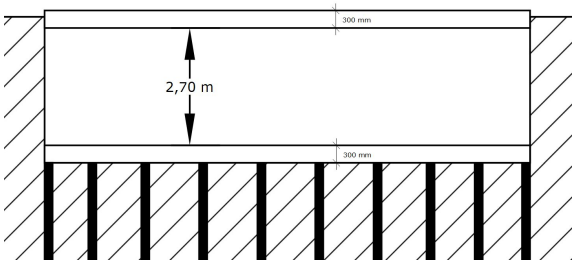

Figure 3.21: Section of the Ground Model with Basement Pile foundation

3.3.3 Parametric study

Following section presents the method which is used to obtained results in the parametric study which has been the main objective of this thesis.

The comparison is mainly focused on the transfer function between ground and

foundation. Thus, the most relevant points to consider is a point at the added structure (e.g. the slab) compared to the empty base model at the exact same measurement point (with varying height depending on the construction element). Secondly, the nodes in focus are the nodes at the slab edge, first floor edge and basement floor edge versus the same exact point at ground level in the plain base model (See point 1, 4 and 6 in Figure 3.22).

The parametric study also considers other points on the building such as in the middle of the ground floor, on the basement and so on. The nodes from where data is extracted is presented in the figure below to allow easy identification of results:

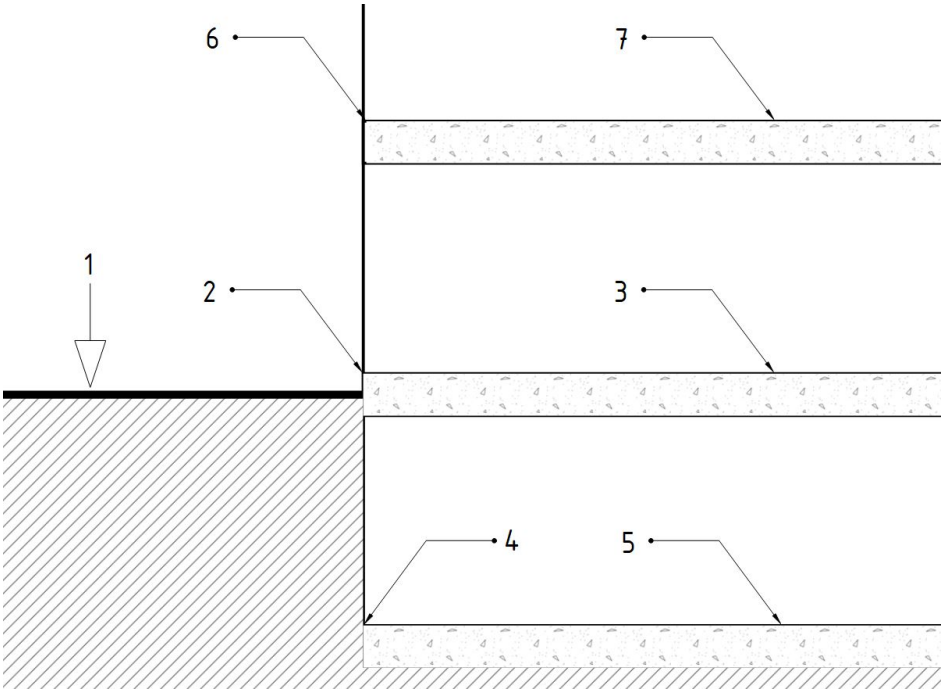

Figure 3.22: Measurement nodes for the FEM model

Here, the arrow denotes the force input along with all the measurement points. Point 1, 4 and 6 are located on the edge of the long side towards the source while 3, 5 and 7 are located in the middle of the plates.

For the Base model only point 1,2 and 3 were extracted as it lacks a structure. For the Slab on grade models, only point 1,2,3,6 and 7 were extracted as they lack a basement. The remaining models had all the measurement points. The base model measurement points are always on the ground level (Z = 0) while for the constructions the points always rest on the edge of the element. Note that not all results will be presented as the thesis does not aim to obtain transfer functions between different floors of building but rather between ground and building.

The result presentation is done in a parameter-by-parameter fashion finishing the chapter with a summary. The broader discussion of the results is found in Section 5.3.

4

Results

4.1 Measurement Results

Following section presents the measurements results from the measurement session that are considered to be of relevance.

4.1.1 Accelerometer 1 and 2

4.1.1.1 Vehicle Speed = 10km/h

The first set of figures present the acceleration measured by the driving point accelerometers, per Section 3.1.3.3. Accelerometer 2 is the accelerometer in the soft soil while Accelerometer 1 is the accelerometer attached to the road surface.

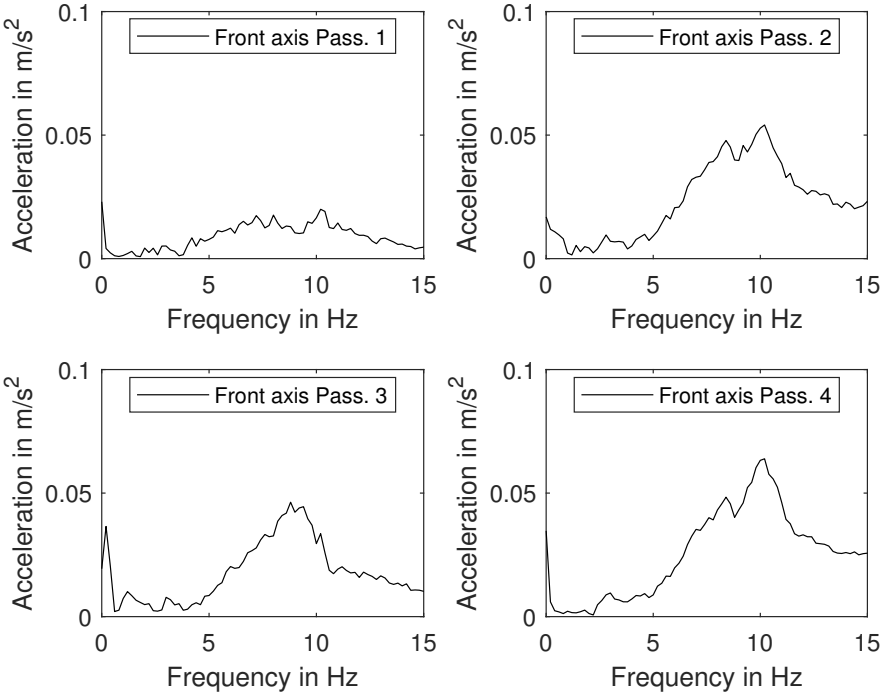

Figure 4.1: Acceleration for front axis passages for Accelerometer 2

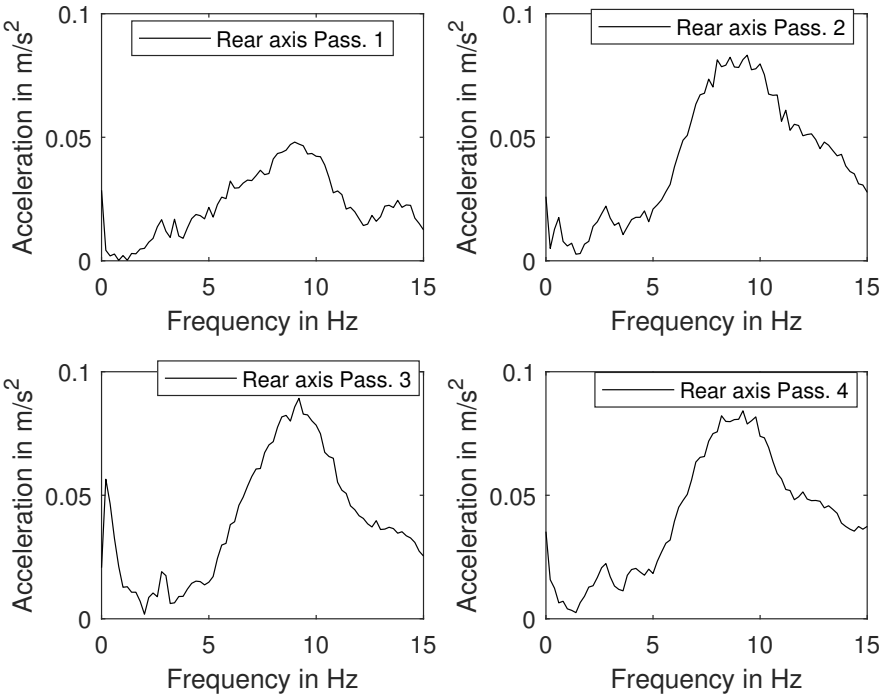

(a) Acceleration for rear axis passages for Accelerometer 2

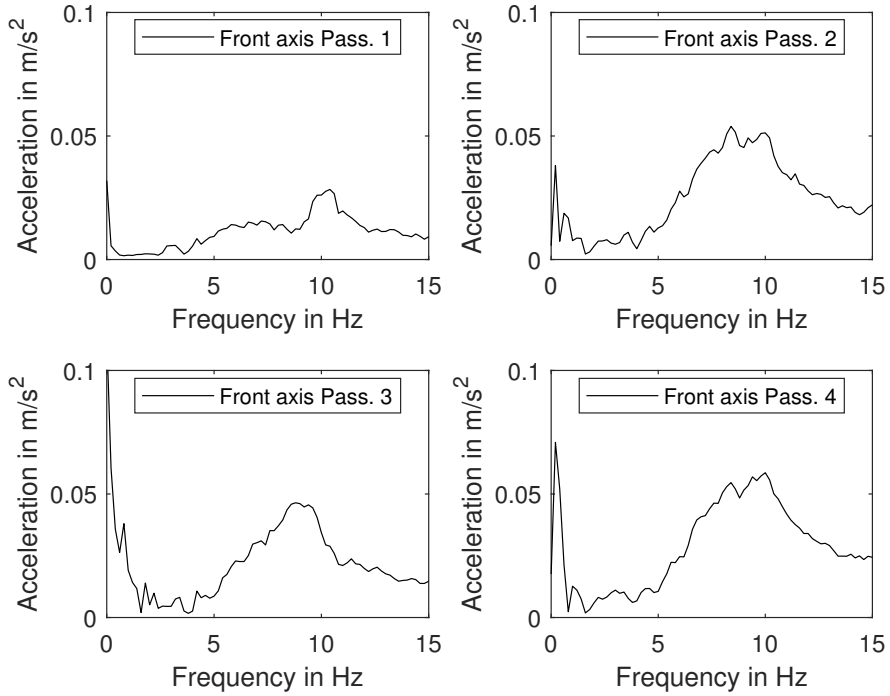

(b) Acceleration for front axis passages for Accelerometer 1

Figure 4.2: Acceleration of the rear and front axis passages for Accelerometer 1

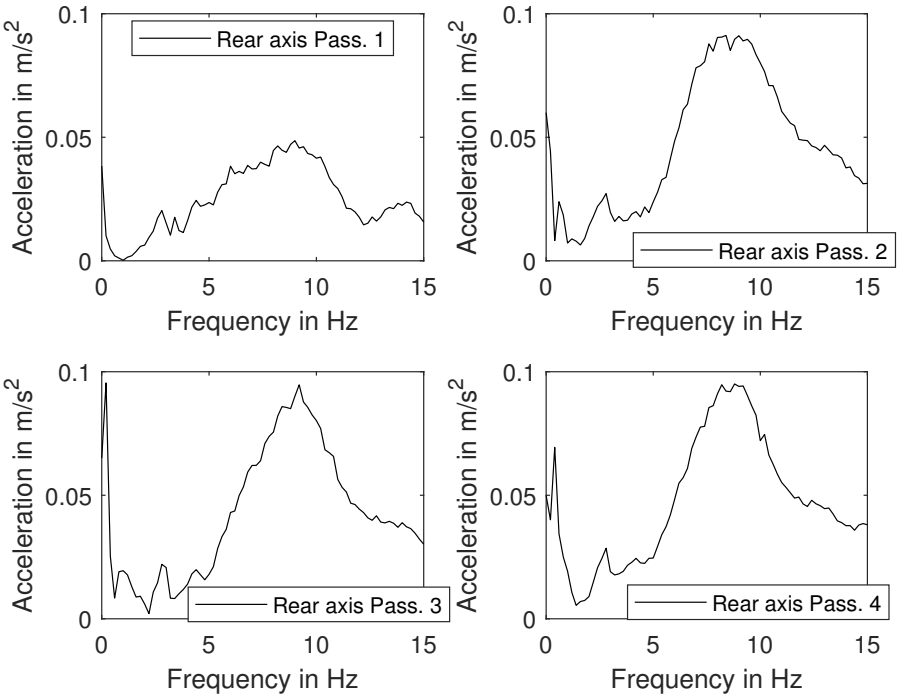

Figure 4.3: Acceleration for rear axis passages for Accelerometer 1

Considering Figures 4.1, 4.2 and 4.3 it is distinguishable that the first passage of the four was unsuccessful as its frequency characteristics is noticeably different from the 3 other passages. This could be explained by the fact that this was the first live run after the test run and the truck operator might have failed to keep the requested velocity or hit the speed bump at an angle. Thus, the decision is made to exclude the first pass from the average acceleration calculation for the passages at V = 10 km/h, shown in the figure below:

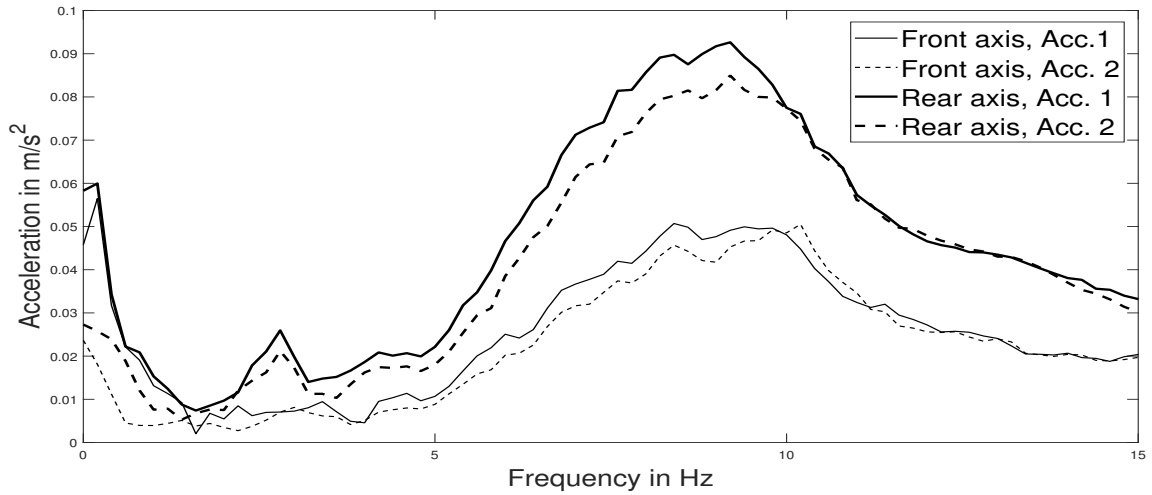

Figure 4.4: Average Acceleration for Accelerometer 1 and 2 for each axis at 10 km/h without first passage

The total contribution from both axes is calculated through simply adding the contribution of the front and rear axis in the frequency domain, the result in presented below:

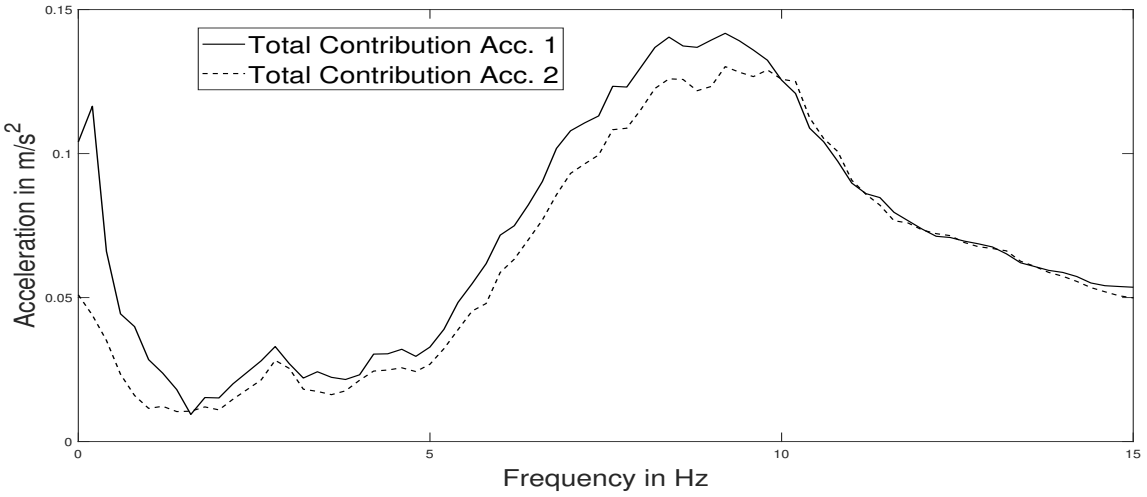

Figure 4.5: Average Acceleration for Accelerometer 1 and 2 at 10 km/h for both axes without first passage

4.1.1.2 Vehicle Speed = 20km/h

Same set of results is presented for Accelerometer 1 and 2 for V = 20 km/h:

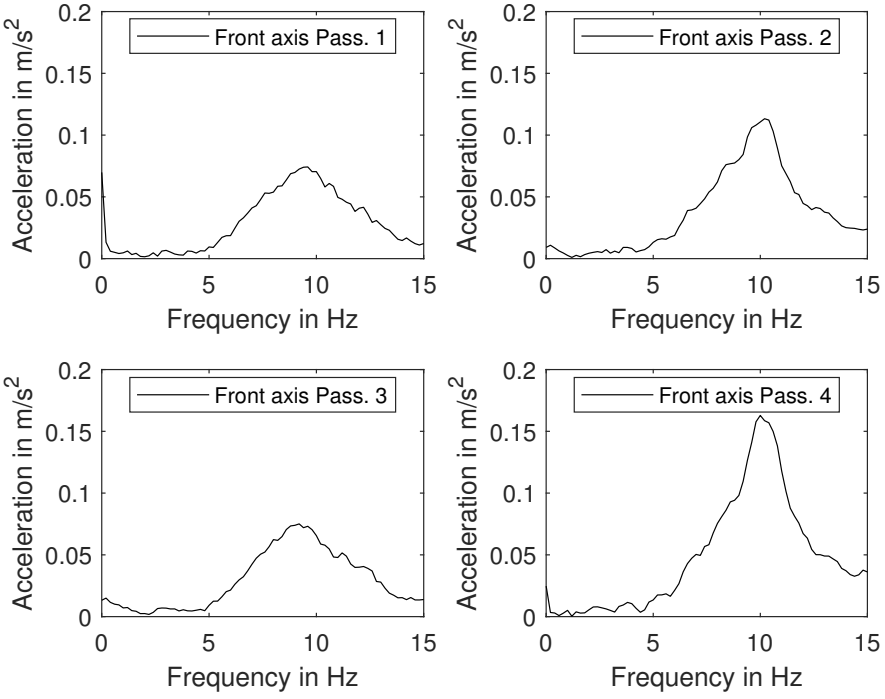

Figure 4.6: Acceleration for front axis passages for Accelerometer 2

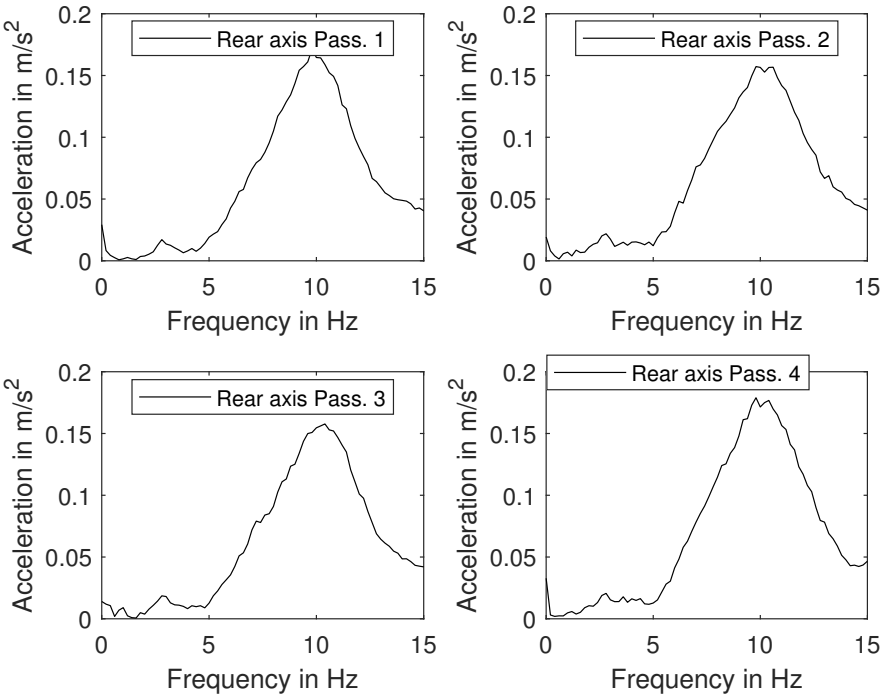

(a) Acceleration for rear axis passages for Accelerometer 2

Figure 4.7: Acceleration for rear axis passages for Accelerometer 2, at v = 20km/h

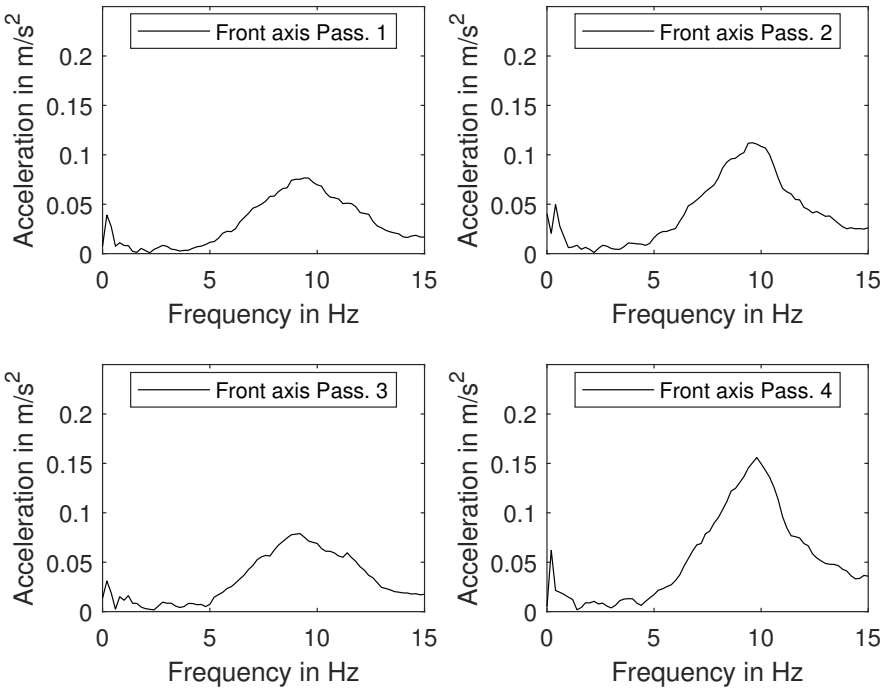

(a) Acceleration for front axis passages for Accelerometer 1

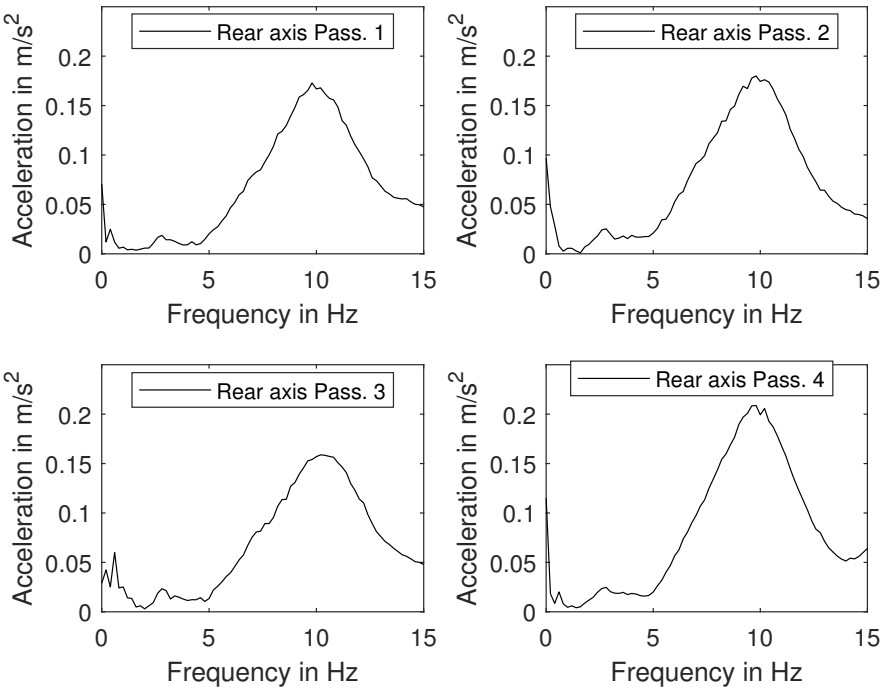

Figure 4.8: Acceleration for rear axis passages for Accelerometer 1, at v = 20km/h

The results found in Figures 4.6, 4.7 and 4.8 are found to be uniform for all the passages, thus, all the passages result made up the arithmetic mean of the front and rear axis contribution and are presented in the table below:

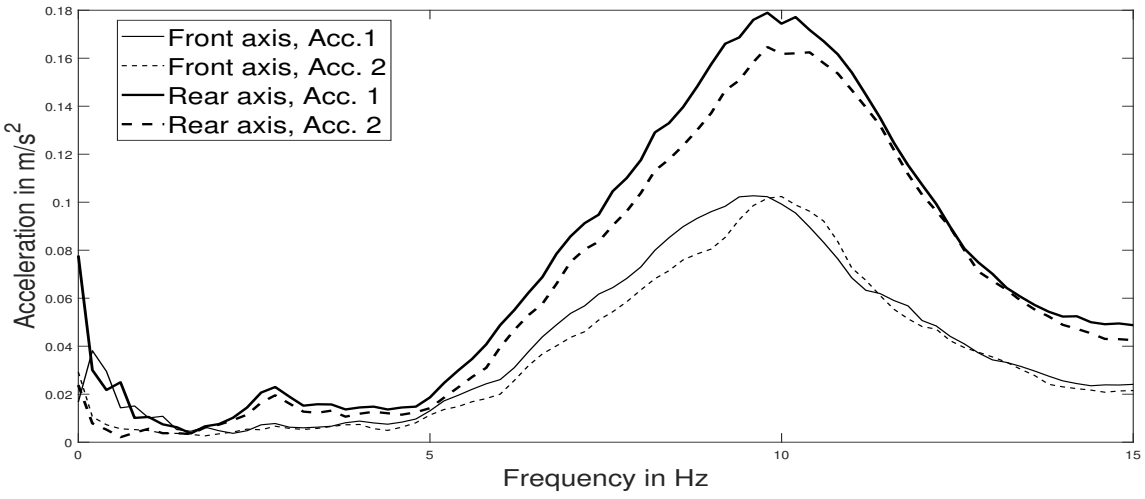

Figure 4.9: Average Acceleration for Accelerometer 1 and 2 for each axis at 20 km/h

with the summed up contribution as following:

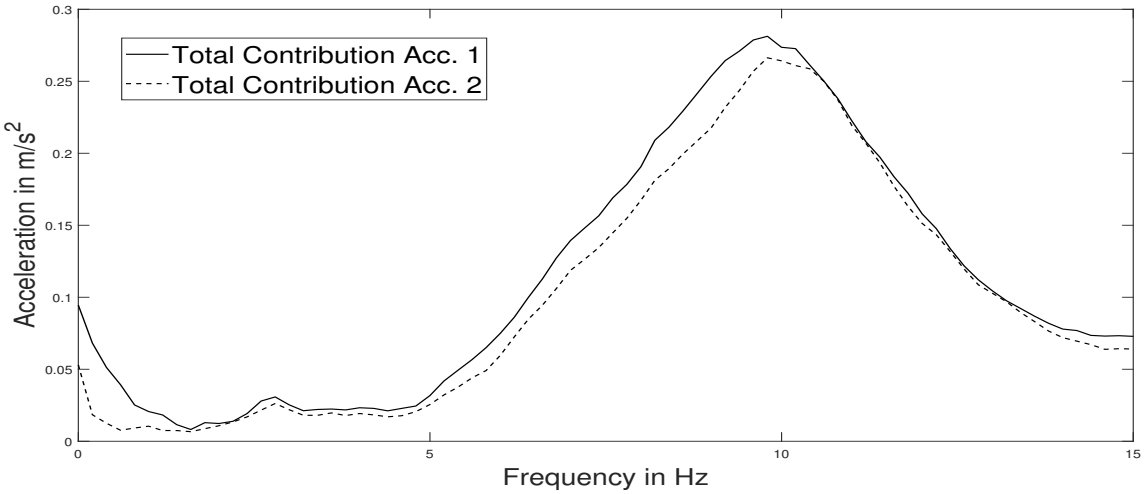

Figure 4.10: Average Acceleration for Accelerometer 1 and 2 at 20 km/h for both axes.

4.1.1.3 Vehicle Speed = 30 km/h

The third set of results for Accelerometer 1 and 2 is for the highest velocity-run at 30 km/h and is presented below:

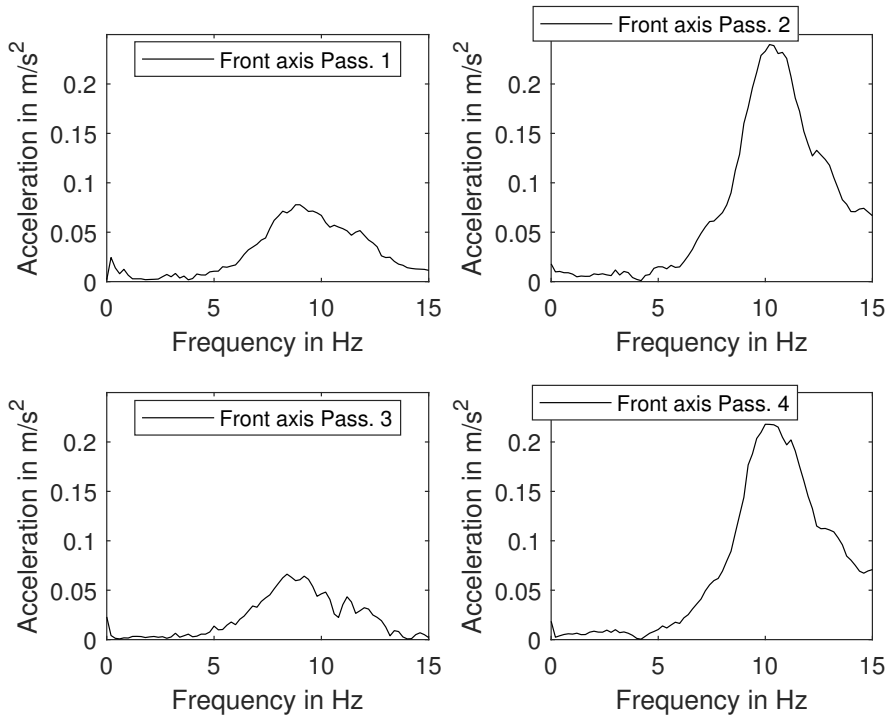

Figure 4.11: Acceleration for front axis passages for Accelerometer 2

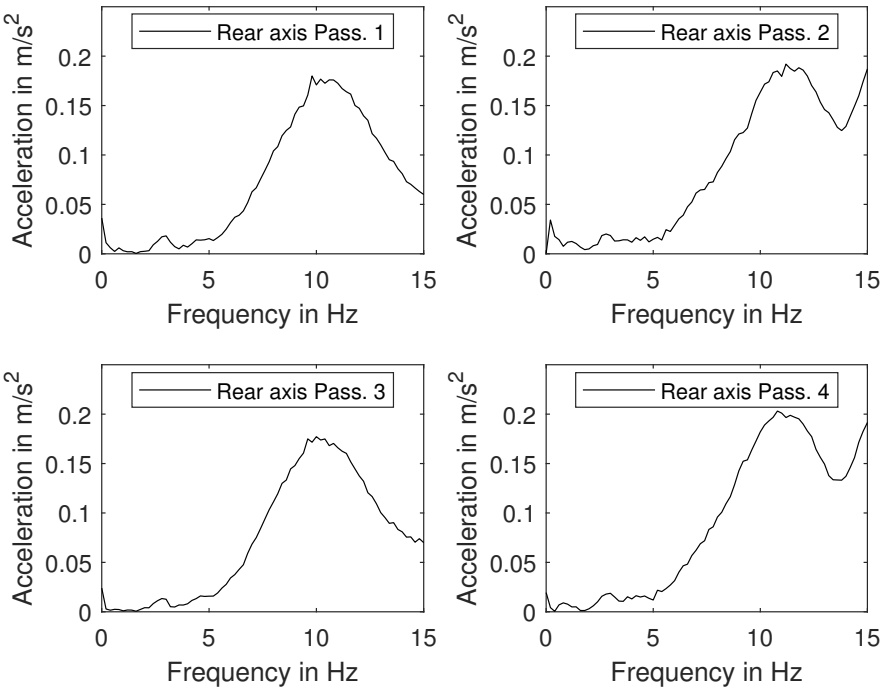

(a) Acceleration for rear axis passages for Accelerometer 2

Figure 4.12: Acceleration for rear axis passages for Accelerometer 2, at v = 30km/h

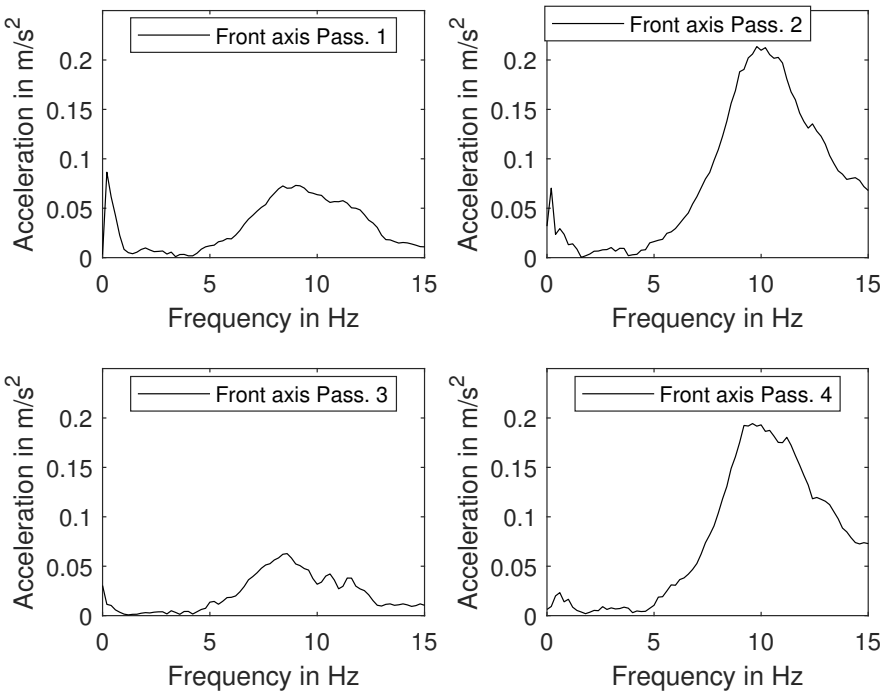

(a) Acceleration for front axis passages for Accelerometer 1

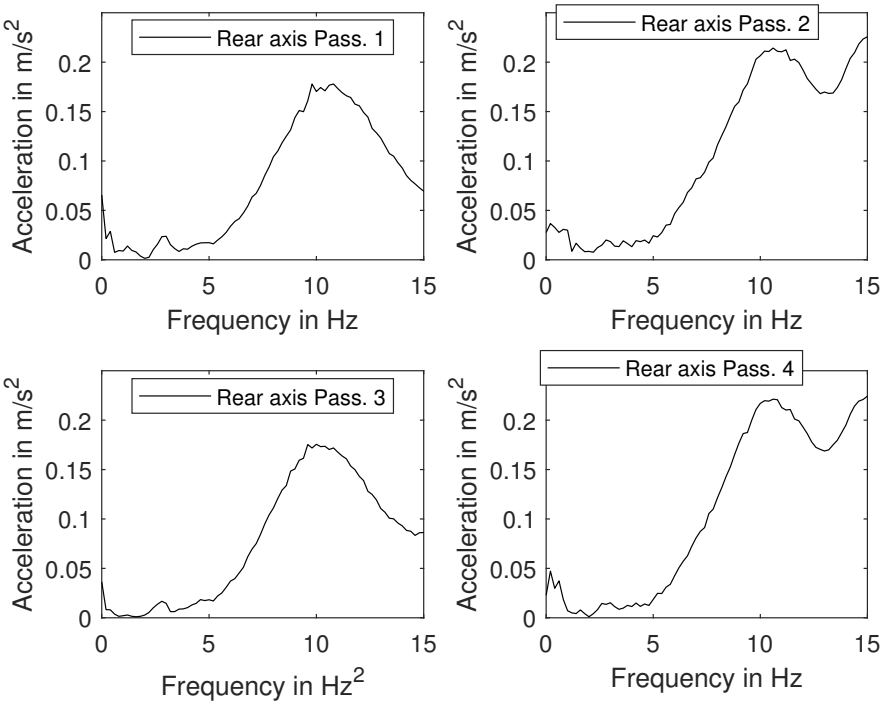

Figure 4.13: Acceleration for rear axis passages for Accelerometer 1

The main difficulties encountered when measuring at V = 30km/h included the fact that the speed bumps were not attached to the surface of the road making them prone to moving at contact with the front axis. Due to that both the second and fourth passage is excluded from the averaging process as video recordings and data showed that the speed bumps altered position between the two axes, making the results unusable. The averaging of Passage 1 and 3 is presented in the figure below: With the total contribution summed up as following:

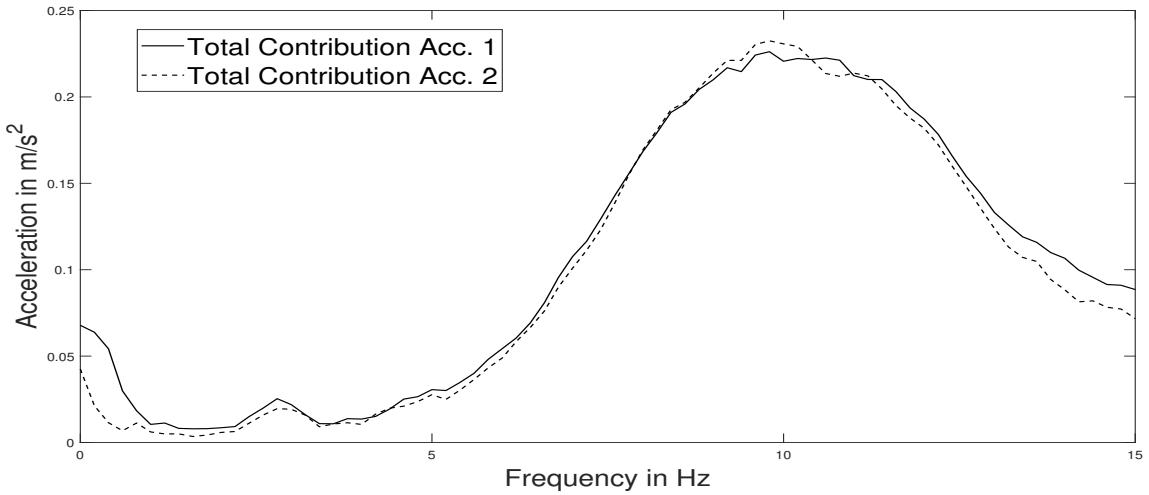

Figure 4.14: Average Acceleration for Accelerometer 1 and 2 at 30 km/h for both axes without second and fourth passage

4.1.2 Geophones

Following section presents the relevant geophone velocity levels that have been obtained during the measurement. The setup and indexing of the Geophones have been explained in detail in Section 3.1.3.4.

The measured data from the geophones is further presented in Section 4.3 where it is used to validate the FEM model. The model does not contain all of the geophones since Geophone 3 is positioned 51 meters away from the speed bump passage which is too far for a reliable result. Therefore, only results from Geophone 1 & 2 will be presented.

4.1.2.1 Vehicle Speed = 10 km/h

For 10km/h the average results for each axis separately and together are shown since it has previously been decided that 20km/h is the reference speed.

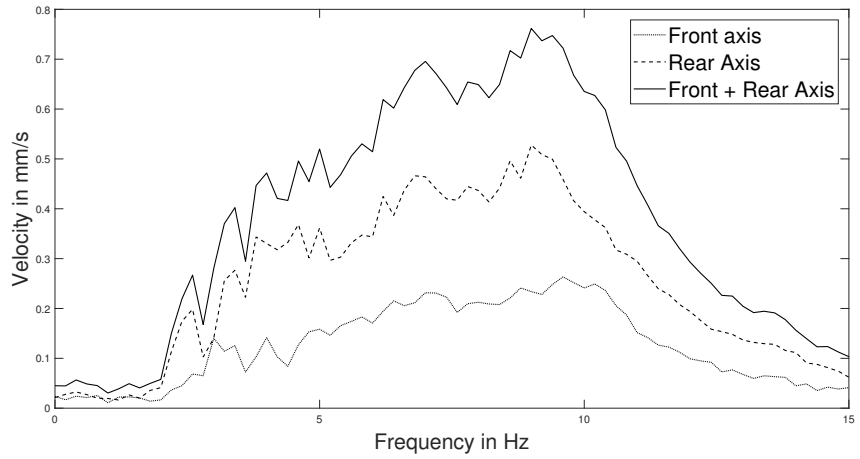

(a) Average velocity for Geophone 1 at 10 km/h for both axes

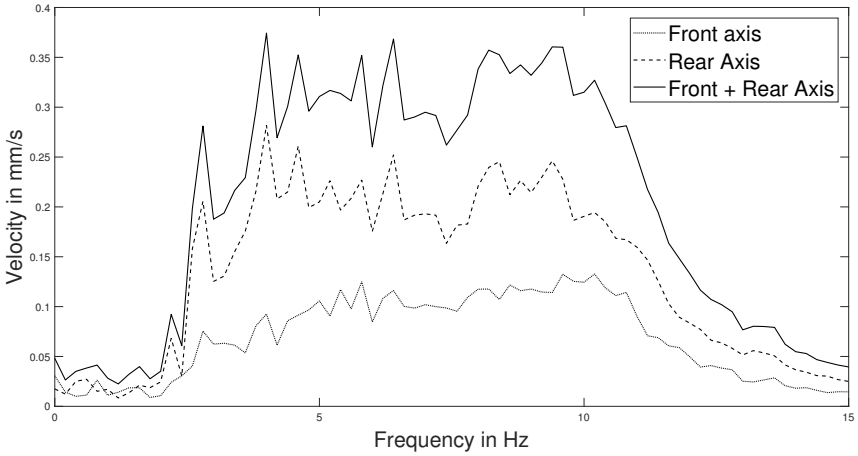

(b) Average velocity for Geophone 2 at 10 km/h for both axes

Figure 4.15: Geophone Measurement Data at V = 10km/h

4.1.2.2 Vehicle Speed = 20 km/h

As the 20km/h measurement data was the average results for each axis separately and together. Each of the passages for each axis will also be shown to prove that all of the passages for 20km/h are consistent.

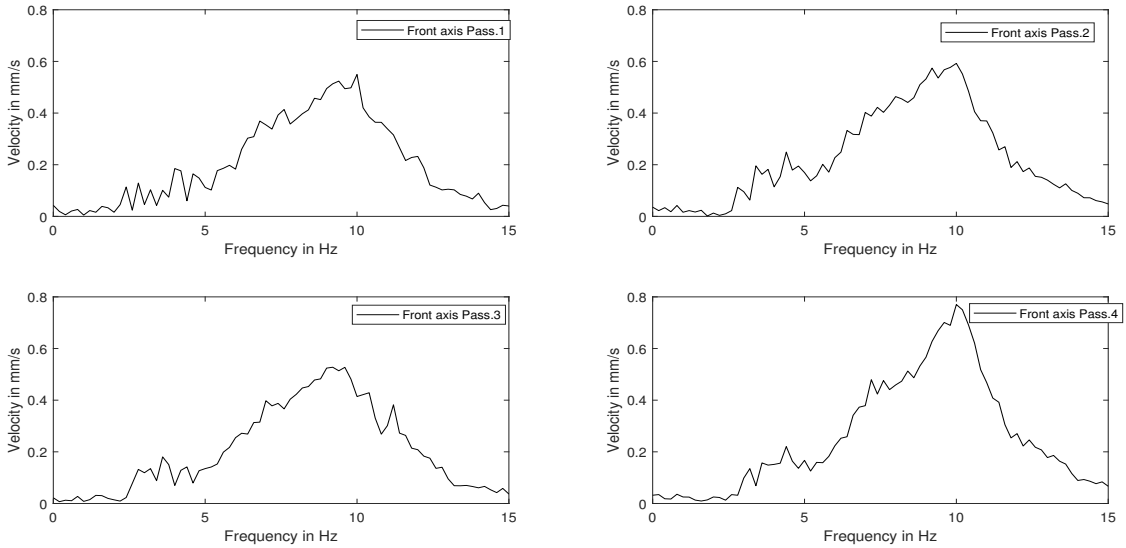

Figure 4.16: Velocity for Geophone 1 at 20 km/h for front axis at different passages

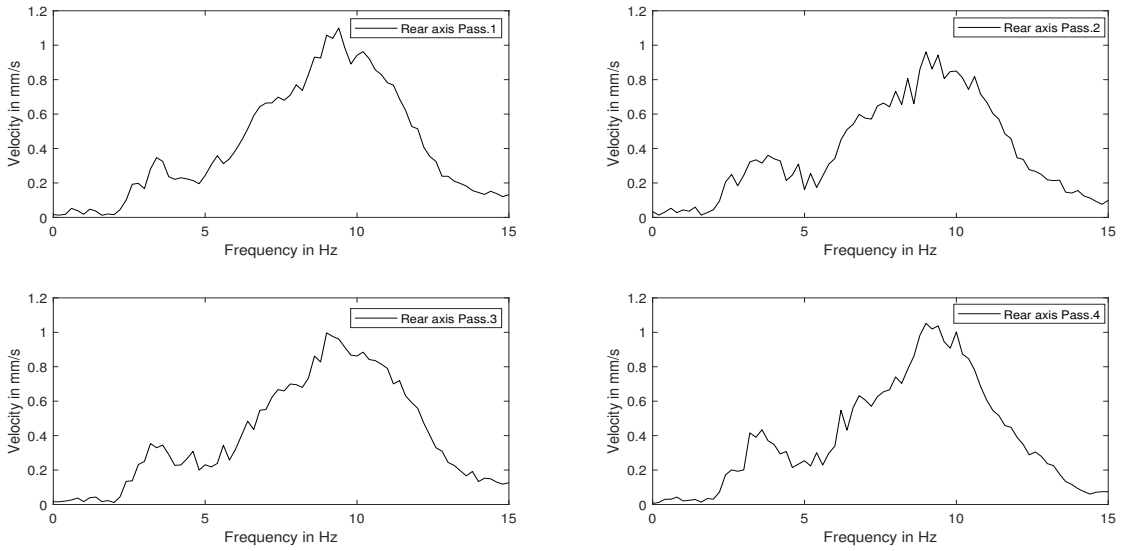

Figure 4.17: Velocity for Geophone 1 at 20 km/h for rear axis at different passages

The Geophone results from the passages at 20 km/h were considered to be of the highest reliability as the speed bump was kept in place and a constant velocity was obtained. Therefore, these results were used as validation of the model at higher distances, see Section 4.2.

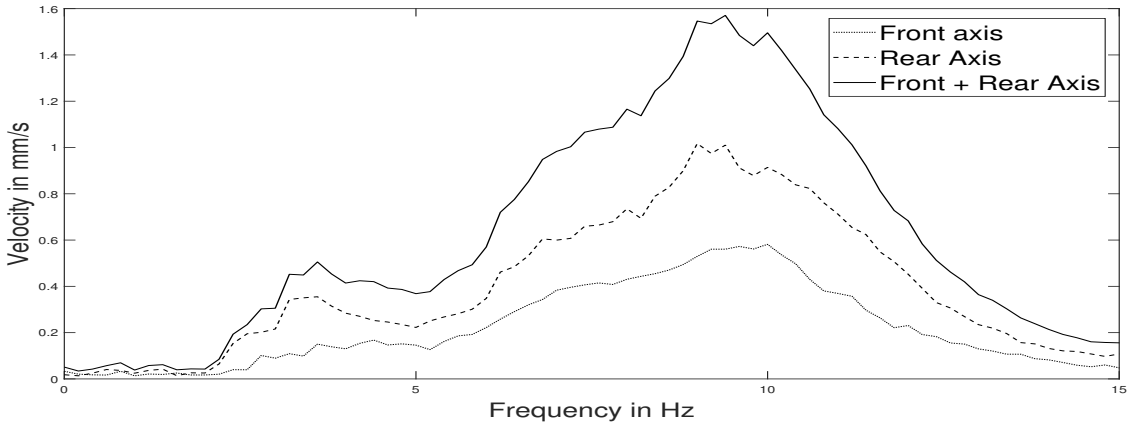

Figure 4.18: Average velocity for Geophone 1 at 20 km/h for both axes

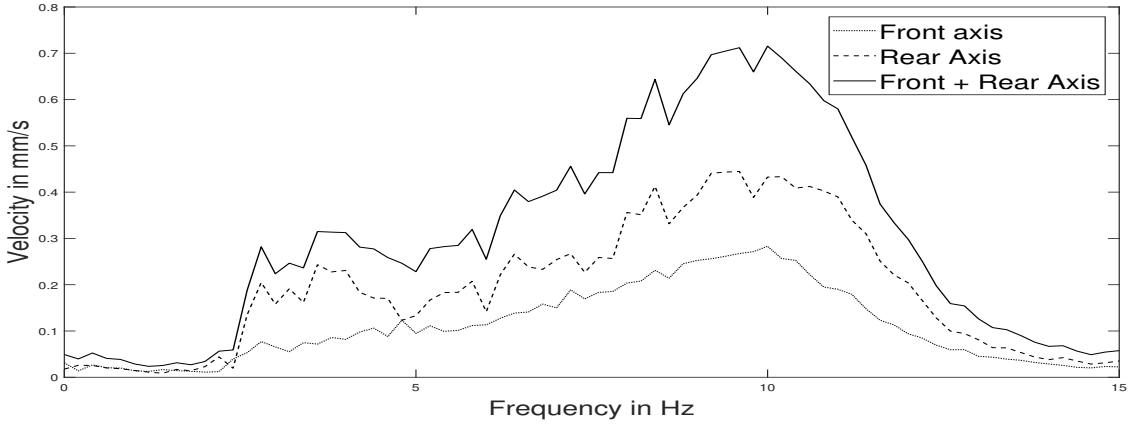

Figure 4.19: Average velocity for Geophone 2 at 20 km/h for both axes

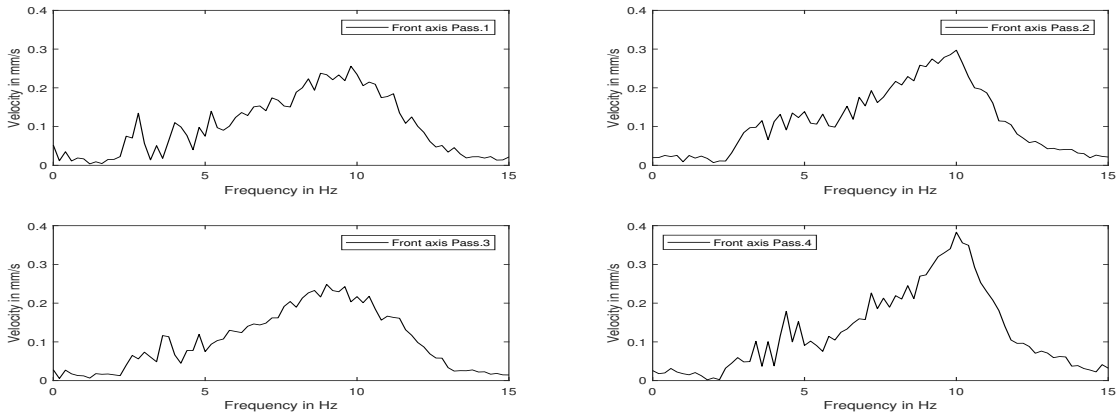

Figure 4.20: Velocity for Geophone 2 at 20 km/h for front axis at different passages

The results obtained from the passages at 30 km/h have been excluded due to high non-reliability and non-linear behaviour.

4.2 Validation of Source Model

The validation of the model is based on the procedure described in Section 3.2. The goal of the validation is to ensure that the generated Source Model corresponds well with the measured accelerometer results and is confirmed using SOLVIA FEM.

The measured acceleration at Accelerometer 1 (representing the Driving Point) is compared to the FEM-model with the generated induction of vibrations by the Source Model. As Accelerometer 1 was considered to be the most reliable due to its proximity to the source, the Source Model was fine-tuned to generate a force which corresponded to the found measurement results. The results are presented in the frequency domain within a range of 1 - 15 Hz, as some uncertainties appeared below 1 Hz, which is further explained in Section 5.1.

Firstly, the comparison of the acceleration caused by the rear axis is presented and compared alongside the input force that was then used to achieve good correlation between the measurement and the FEM model:

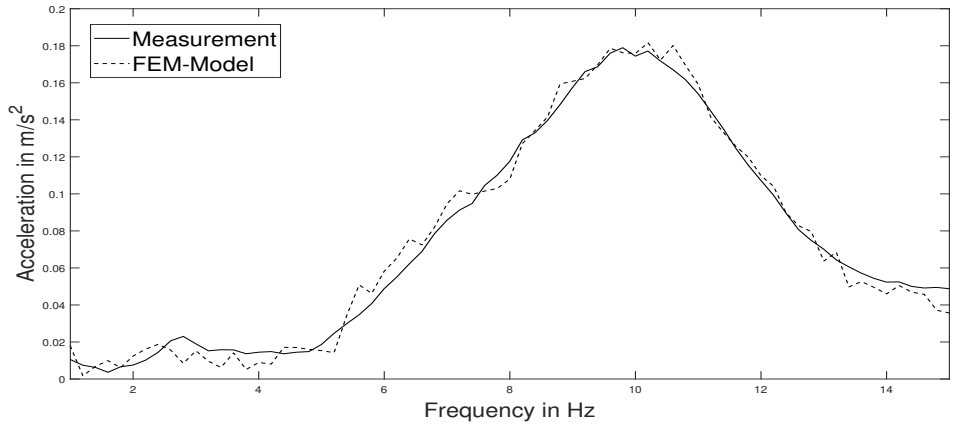

(a) Acceleration at Acc.1, rear axis

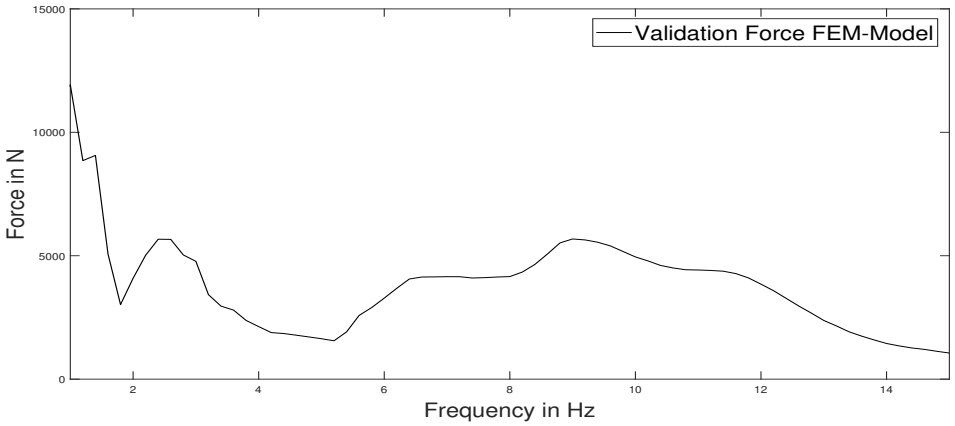

(b) Validating Force in FEM-Model for rear axis

Figure 4.21: Rear Axis Acceleration and Input Force comparison

The validation force as seen above is not exactly following the desired mass-spring behaviour. Therefore, when fine-tuning the models the focus was put on finding the correct levels in the frequency region of interest, between 8 - 15 Hz. The adapted SIMULINK model is shown together with the validation force in Figure 4.22 for the rear axis where the validation force FEM-model is the back-traced force required in accordance to the measurement results:

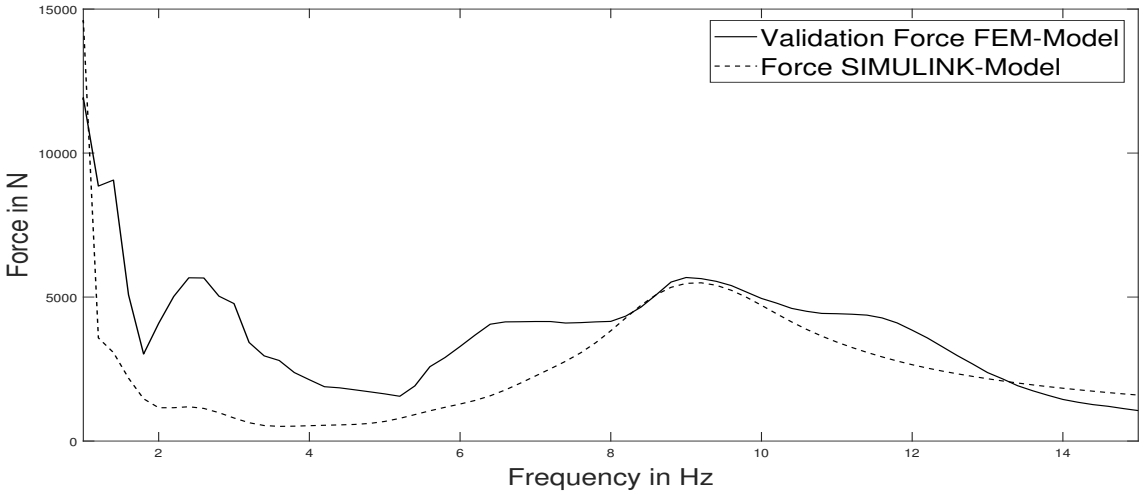

Figure 4.22: Validating Force and SIMULINK model force for rear axis

To be able to tune the force that the passage causes the SIMULINK models acceleration in time is compared to the measured acceleration. As the amplitude cannot be confirmed to be correct the resonance frequency and the damping of the time signal is in focus. This is presented in Figure 4.23. Here, the upper signal is the band-pass filtered (in the range of 0.1-20 Hz) Accelerometer 3, which is the accelerometer attached to the rear truck axis (see Section 3.1.3.3 for detailed description) and the lower one is the SIMULINK final result for the rear axis:

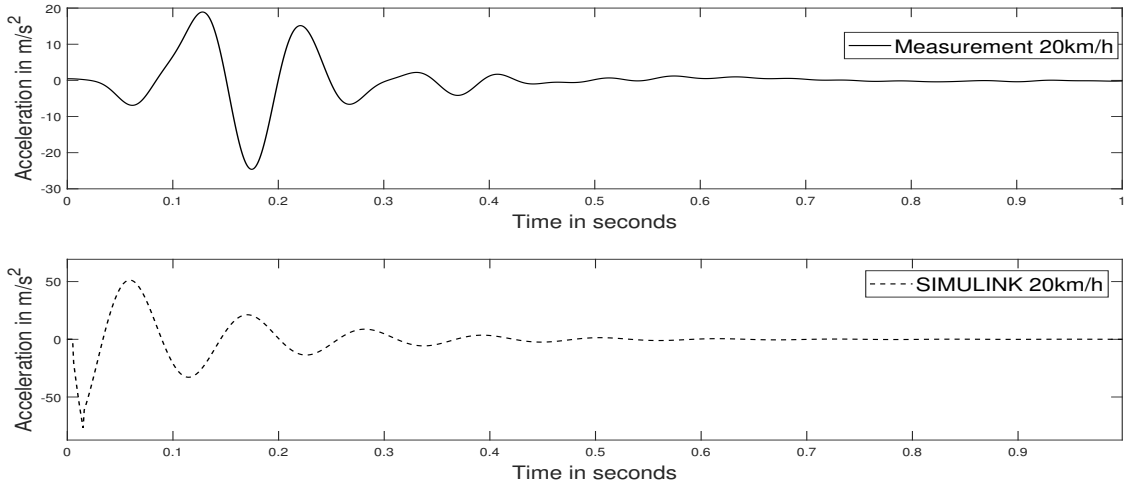

Figure 4.23: Accelerometer 3 compared with SIMULINK model time domain

As showcased above - these signals are not exactly same in amplitude and as the speed bump passage was modified in SIMULINK they are put out of phase in the time domain. The damping of the signals are approximately the same and in Figure 4.24 it is distinguishable that they have a similar frequency peak.

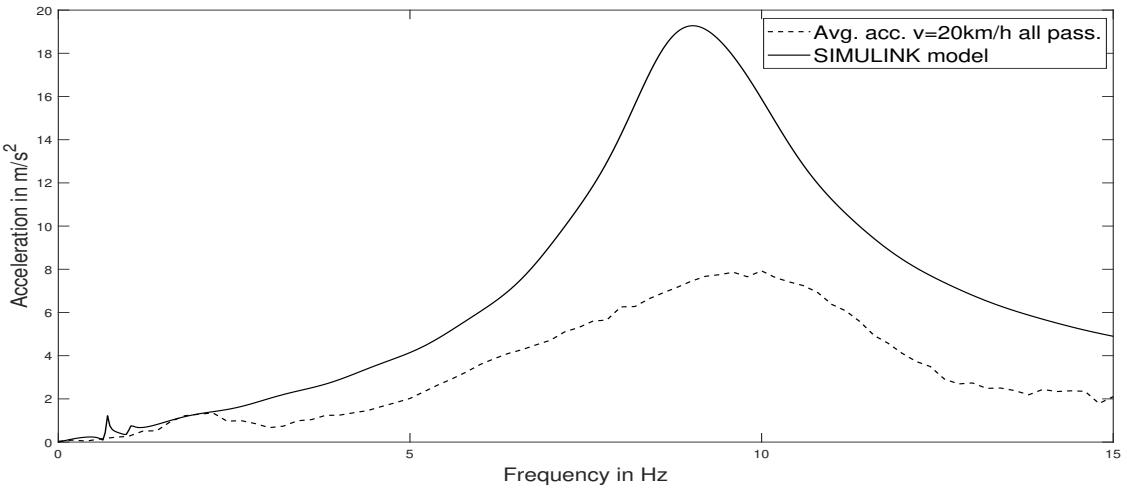

Figure 4.24: Accelerometer 3 compared with SIMULINK model in frequency domain

The same procedure is repeated for the front axis. The only major difference is that no comparison between the SIMULINK and measurement can be done for the front truck axis, as the all of the accelerometers used during the measurement were placed on the rear axis (technically impossible to place on the front axis). The comparison between the average acceleration for the passages at 20 km/h compared to the FEM-model can be seen in Figure 4.26:

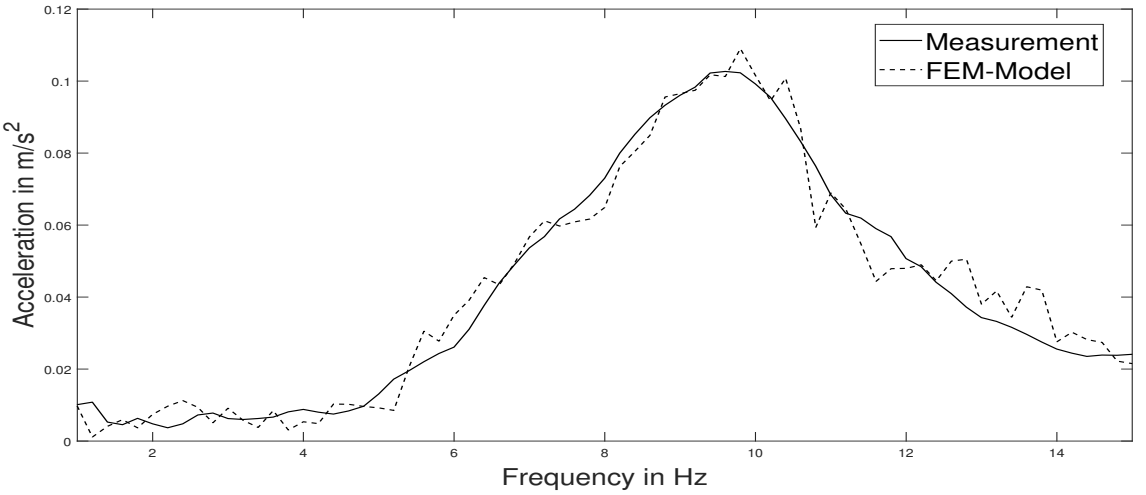

Figure 4.25: Acceleration at Accelerometer 1, front axis comparison

This results in the following force that was used as input from the truck:

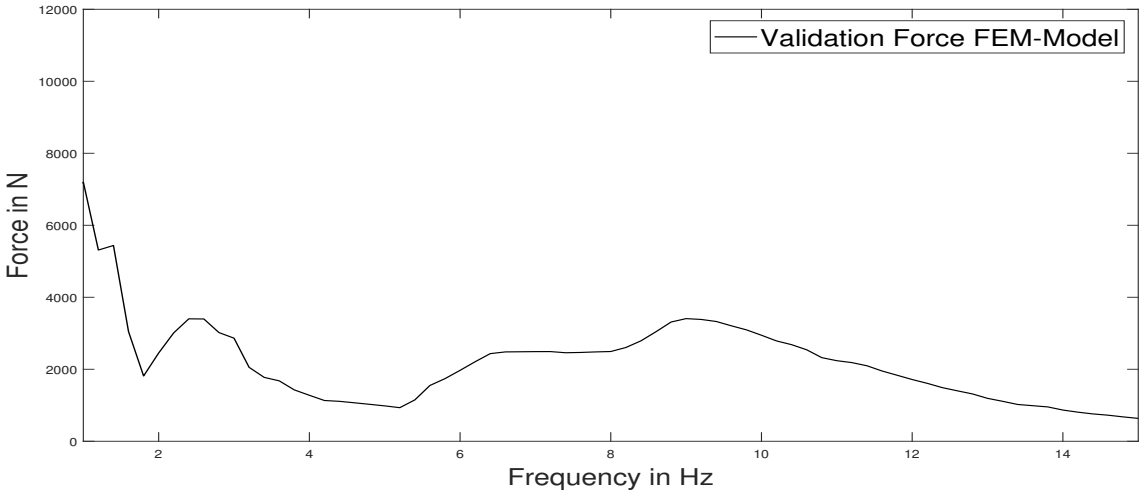

Figure 4.26: Input Force Validation, front axis comparison

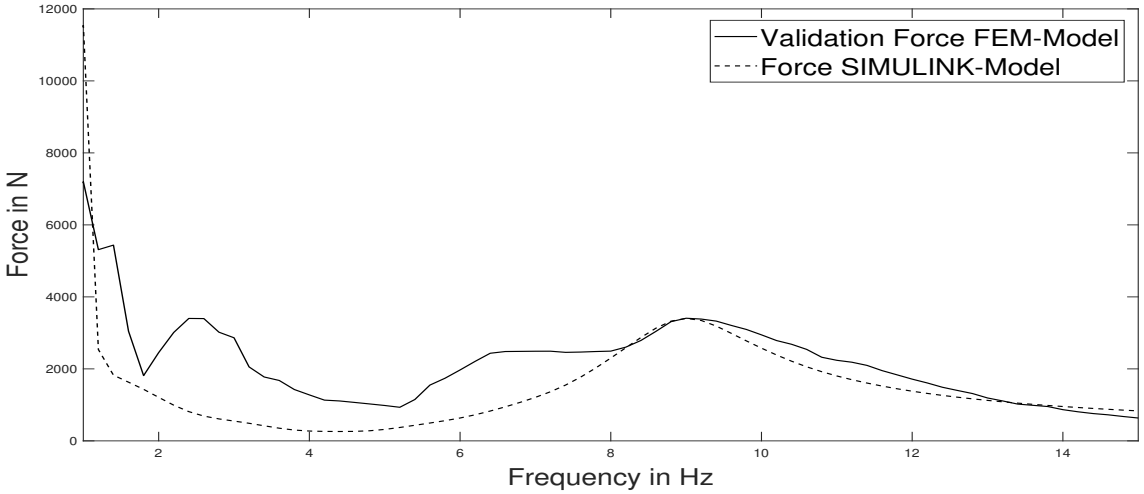

Figure 4.27: Validating Force and SIMULINK model force for front axis comparison

The validation force did not follow the exact mass spring behavior for the front axis either which resulted in the same limitation and focus when adapting the SIMULINK model for the front axis as for the rear axis.

The final SIMULINK model that is used to represent a heavy vehicle passing over a speed bump in the final FEM model is the total contribution combined from both the front and rear axis. This force is also used as a tool for the validation of the Ground Model and the ground accelerometers and geophones are validated against it. This final SIMULINK model force input is shown in the figure below with both axis presented individually and combined:

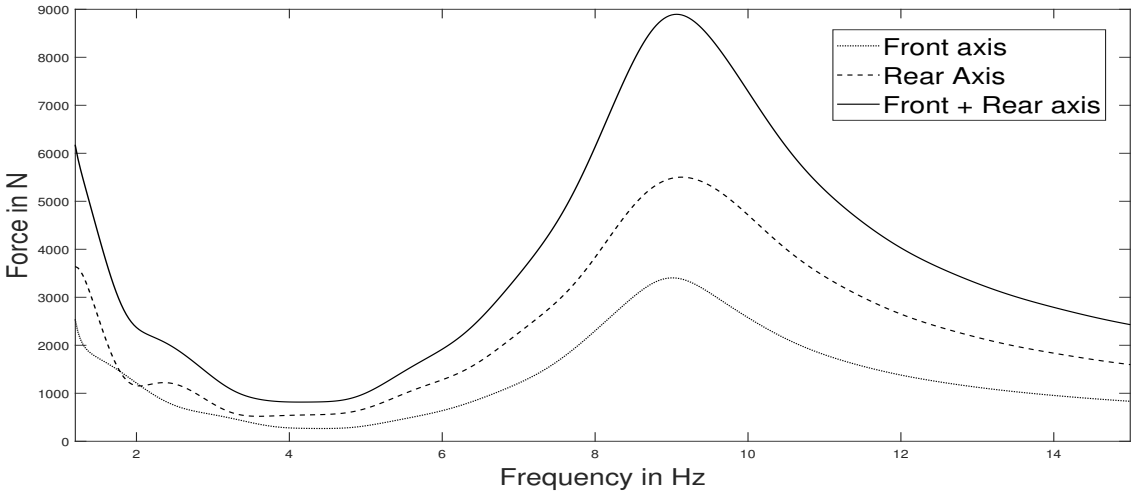

Figure 4.28: Vertical force for rear and front axis, SIMULINK model

4.3 Validation of FEM Model

Similar to the previous section, the FEM Model was validated using the results from Accelerometer 2, Geophone 1 and Geophone 2 and compared with the FEM-model results. Here, the input force is the validation force which was used to be able to retrieve the correct levels for Accelerometer 1, as per the validation process in Section 4.2. The comparison between measurement and the geophones are done to confirm that the amplitude levels and frequency characteristics of the results are reasonable.

The results are presented below, starting with the comparison between Accelerometer 2 and the rear axis force:

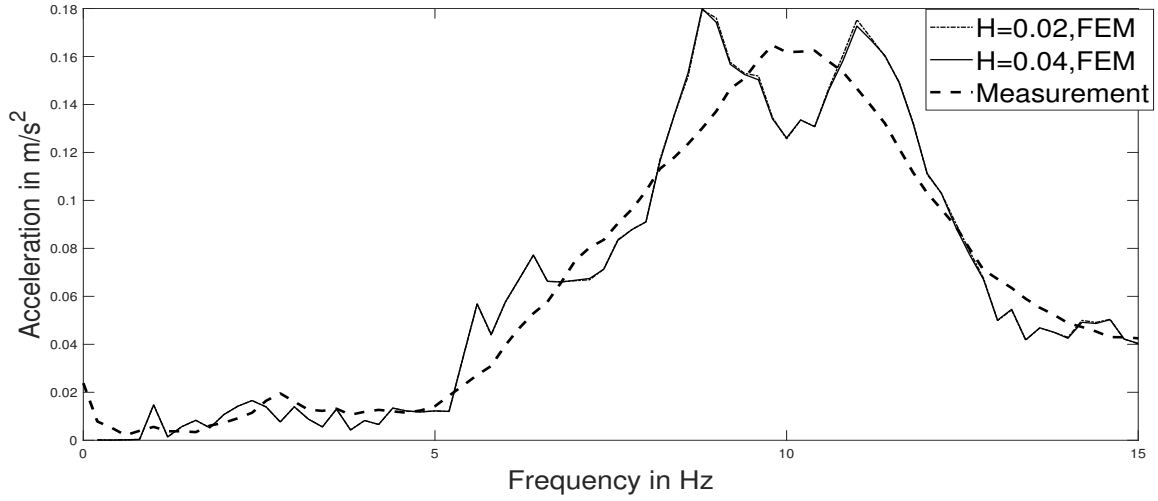

Figure 4.29: Accelerometer 2 comparison with rear axis force as reference force

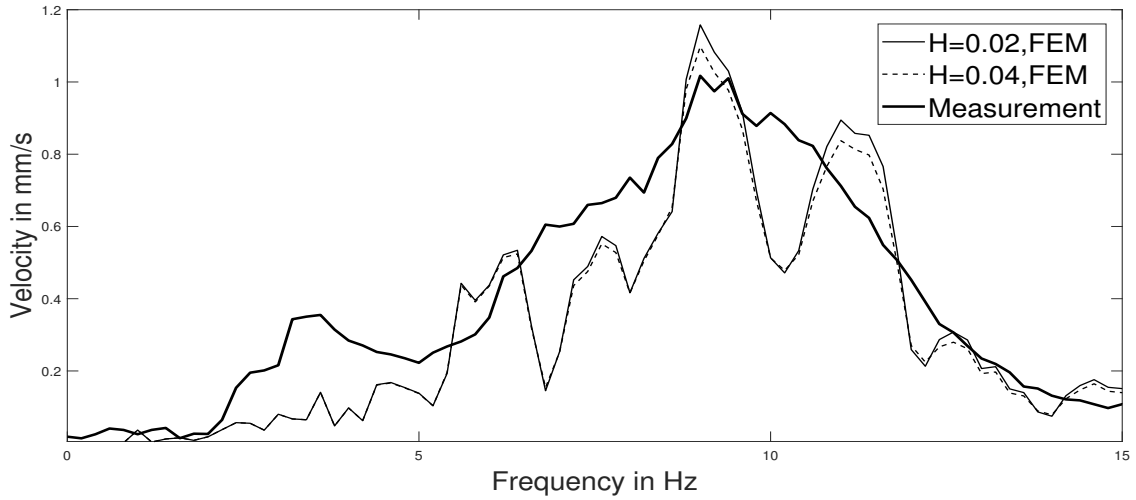

Figure 4.30: Geophone 1 comparison with rear axis force as reference force

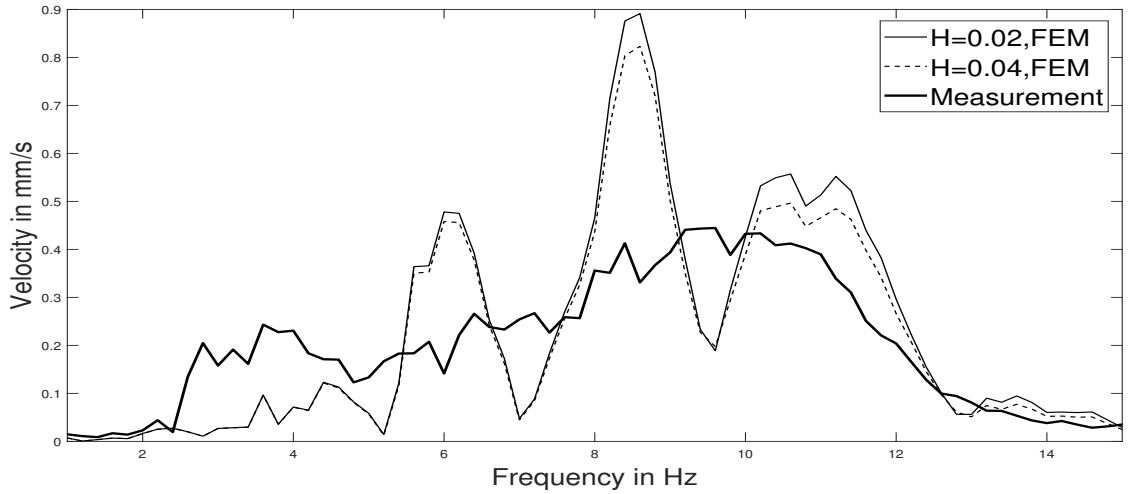

Figure 4.31: Geophone 2 comparison with rear axis force as reference force

One of the FEM parameters that was undergoing change as part of fine-tuning the model was the damping coefficient, here denoted as H. Initial set to 0.02 for the top layer was later changed to 0.04 to obtain more correct results. The damping coefficient in the model is contributing to the materials stress and strain relations. As seen in Figure 4.30 and 4.31, the change of damping to 0.04 gave better results while in Figure 4.29 the changes was barely visible.

As seen above, not all the figures have a good correlation with measurement vs. model, which could be expected since the reality is much more complex than the model. In the model it is easier to spot modes/reflections, as the geophones positions sometimes can be found in maximum/minimum of the ground model for different frequencies. To visualize this problem the vibrations levels are shown for the ground model for different frequencies in Figure 4.32. This problem does not indicate that

the ground model does not work as intended since the reflections between layers and the bedrock are to be expected.

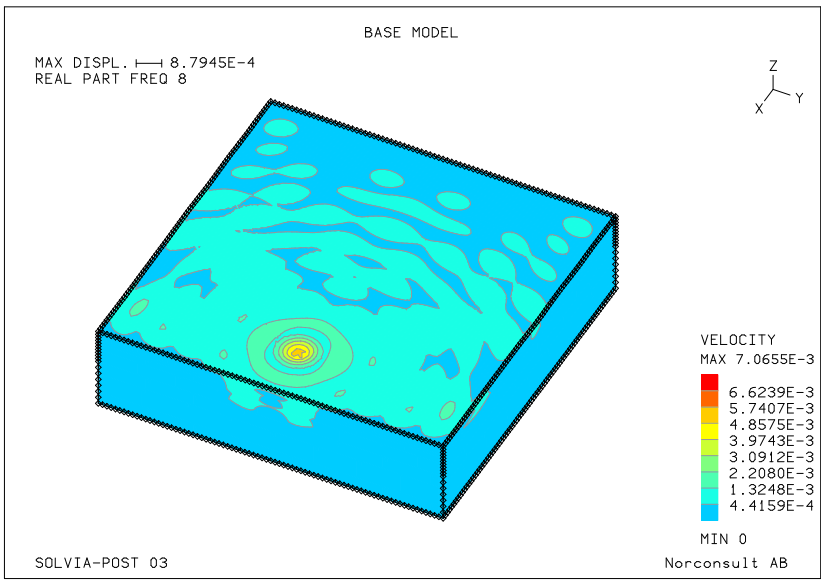

(a) Velocity of for the Base model shown for 8 Hz.

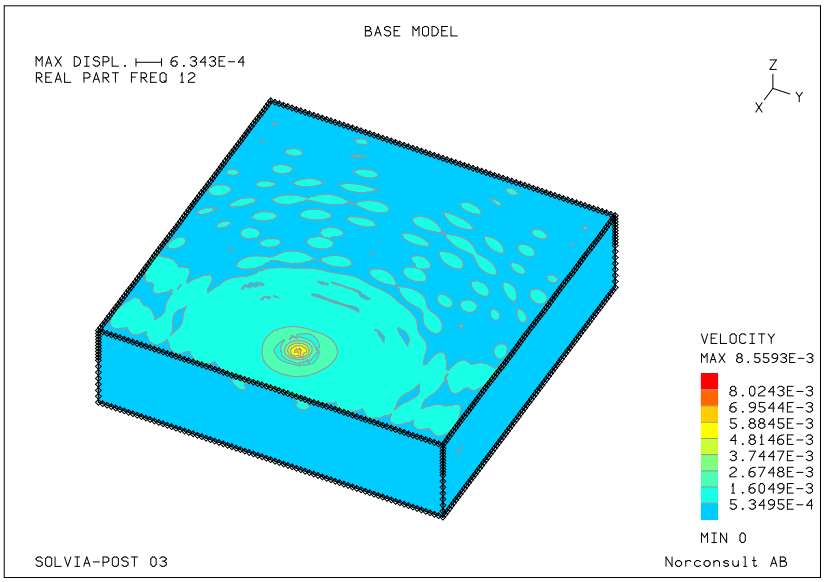

(b) Velocity of for the Base model shown for 12 Hz.

Figure 4.32: Velocity levels spreading of the Base Model depending on Frequency

4.4 Validation Process Summary

The final results of the validation process are presented in this section. Here, both the fine-tuned FEM Model and Source Model are combined and compared to the measurement results. The force input is the combined force of both axes of the vehicle as generated by the Source Model and the results are the transfer function given by the FEM Model:

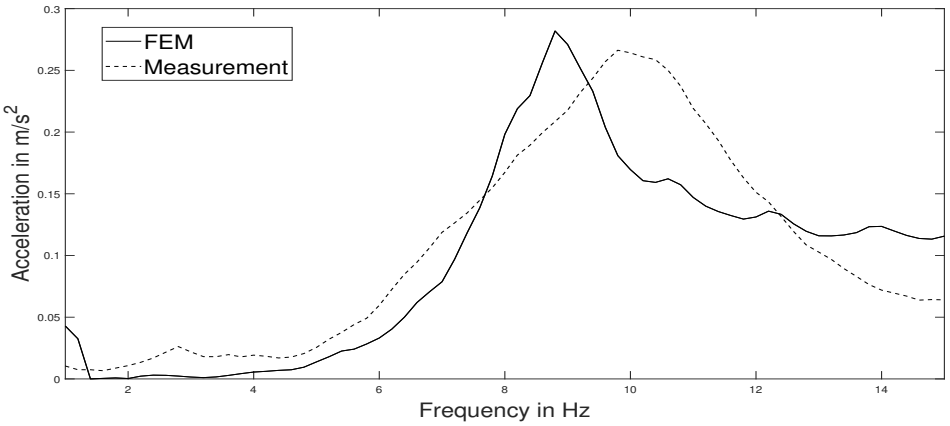

(a) Accelerometer 2 comparison between the measurement and FEM model with the total force from the source model as input force.

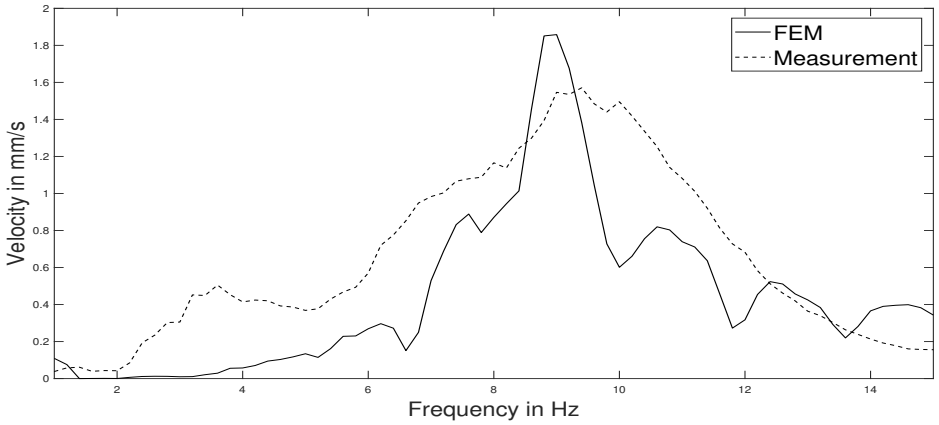

(b) Geophone 1 comparison between the measurement and FEM model with the total force from the source model as input force.

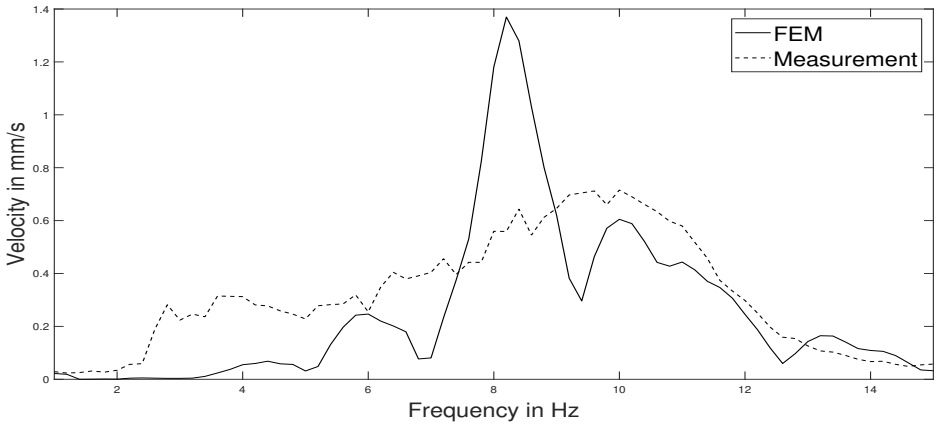

(c) Geophone 2 comparison between the measurement and FEM model with the total force from the source model as input force.

Figure 4.33: Summary of the Validation Process for the Different measurement data

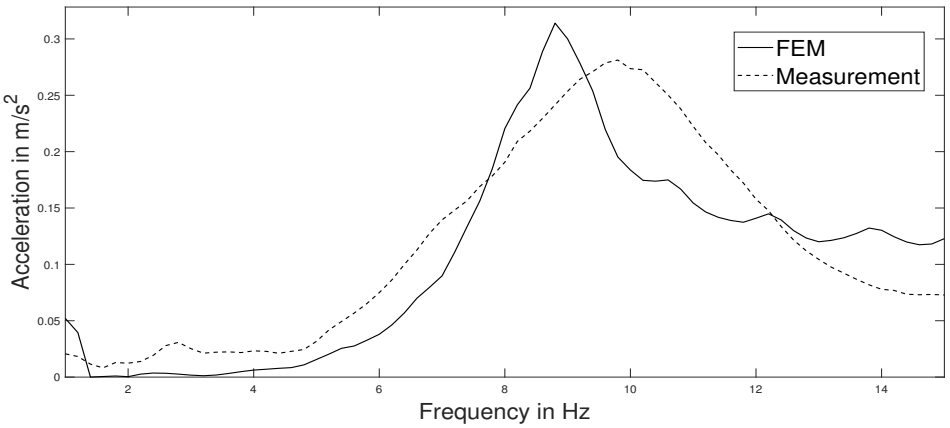

Figure 4.34: Accelerometer 1 comparison between the measurement and FEM model with the total force from the source model as input force.

As seen in the figure above, the levels and peak frequencies are not always correlating well. The difference between measurement and the model is increasing as the distance between the excitation point and the measurement point increases. Since the model force assumes that the excitation is a steady state excitation, resonances and reflections within the model are more pronounced, which is further discussed in Section 5.1. Therefore, the overall levels should be the most important data to compare. The overall levels are roughly the same even though some frequencies are different in amplitude.

4.5 Parametric Study Results

Following section presents the results obtained in the parametric study which has been the main objective of this thesis. With the validated Ground and Source models the constructions are implemented as previously presented in Section 3.3.2.

4.5.1 The *big* building

Following section presents the results obtained for the *big* building. The main focus is on Measurement Point 2 as in Figure 3.22 due to the character of this thesis. The result section is summarized in Section 4.5.1.4 where the other measurement points are briefly presented. For the *big* building the excitation point is exactly 21 meters away from the buildings edge.

Before presenting the results of vibration in the building induced by the source model the complex harmonic response is computed for all the measurement points presenting the modes of the structure in Figure 3.22:

4.5.1.1 Slab on grade

Following results were obtained when comparing the plain base model with the impact of adding a Slab on Grade Foundation with a total thickness of 300 mm and

a static load comparing to the material load of 5 floors made of concrete:

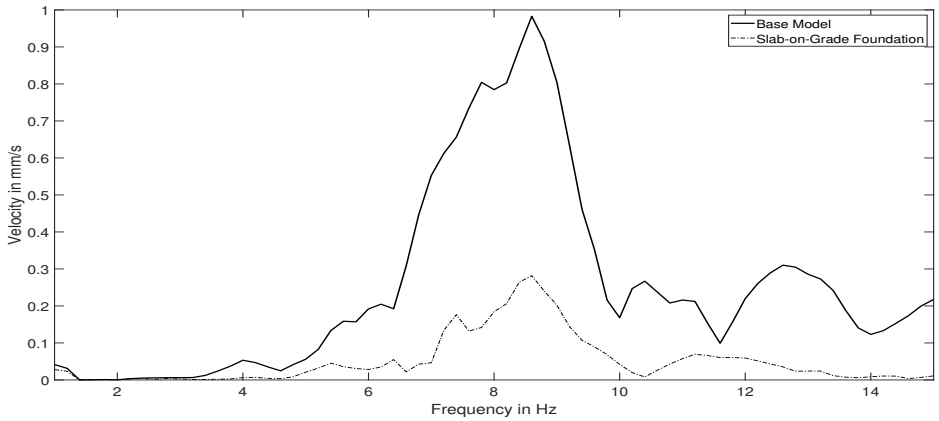

Figure 4.35: Measurement Point 2 in Accordance to Figure 3.22, Base model vs. Slab-on-Grade in the *Big* building

As a parameter, the thickness of the ground-level slab was exchanged from 300 mm to 150 mm. All elements above ground level remained the same in order to provide equal mass acting on structure. The result is presented without the base model result:

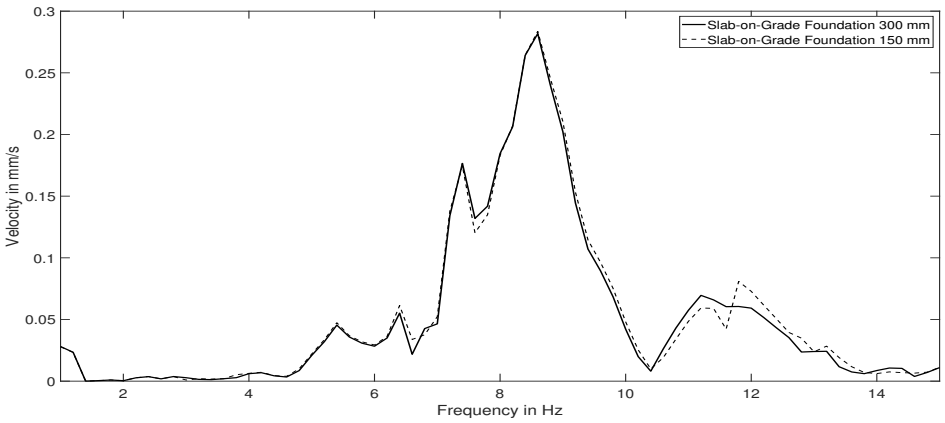

Figure 4.36: Measurement Point 2 in Accordance to Figure 3.22, 300 mm Slab-on-Grade vs. 150 mm Slab-on-Grade in the *Big* building

4.5.1.2 Basement Foundation

Following results were obtained when comparing the plain base model with the impact of adding a basement foundation:

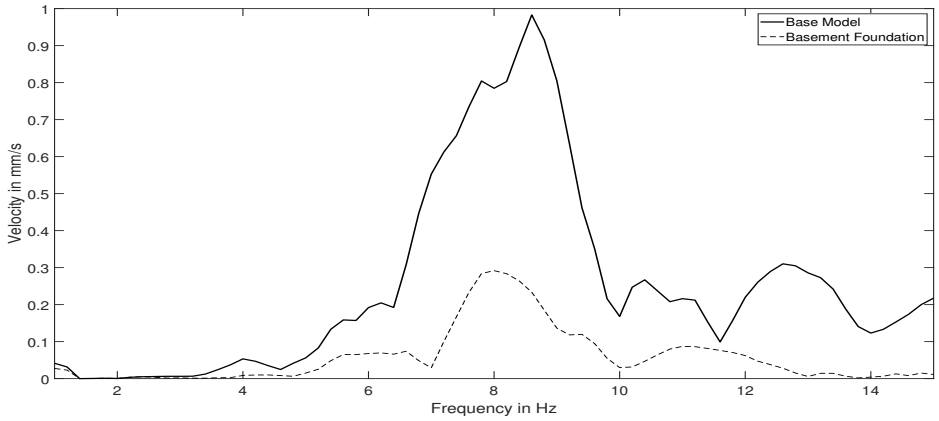

Figure 4.37: Measurement Point 2 in Accordance to Figure 3.22, Base model vs. Basement Foundation in the *Big* building

4.5.1.3 Piled Basement Foundation

The piled basement foundation had the following impact on the transfer between ground and slab:

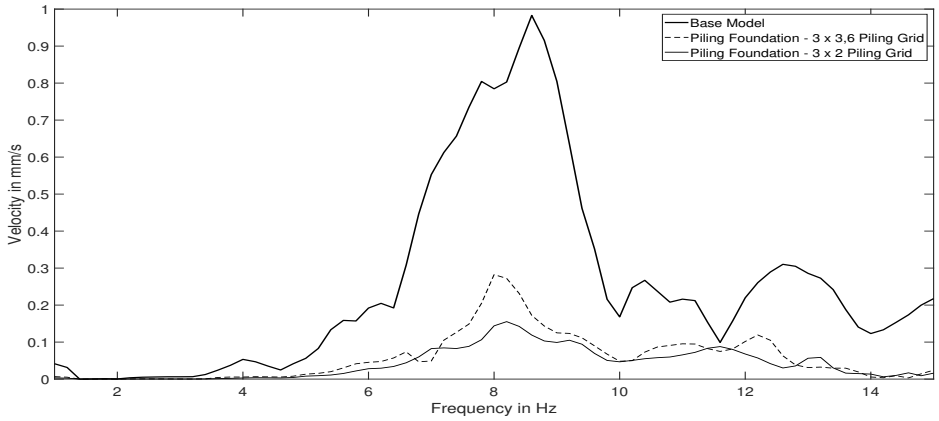

Figure 4.38: Measurement Point 2 in Accordance to Figure 3.22, Base model vs. Piled Basement Foundation in the *Big* building

The Piled Basement Foundation corresponds to the Piling Plan shown in Figure 3.19 in Section 3.3.2. In order to give the previous figure some context, another figure is shown below, with a denser piling plan:

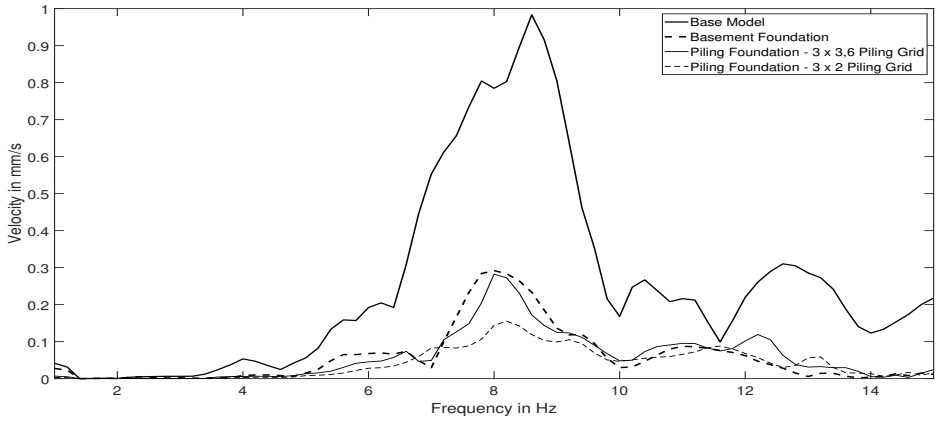

Figure 4.39: Measurement Point 2 in Accordance to Figure 3.22, Base model vs. Piled Basement Foundation in 2 setups along with the Basement Foundation in the *Big* building

The figure shows that the initial piling foundation had a minor impact in comparison to the basement foundation. However, a denser piling foundation shows a much more distinguishable reduction of vibration at the slab edge.

A further parameter that was investigated is the thickness of the Basement Foundation and the Ground-level slab. Their thicknesses were exchanged from 300 mm to 150 mm in order to investigate the effect of element thickness on vibration transfer. The rest of the building elements had the same dimensions. The parameters of the building elements above the ground-level slab remained the same in order to ensure the same mass, the results are presented below:

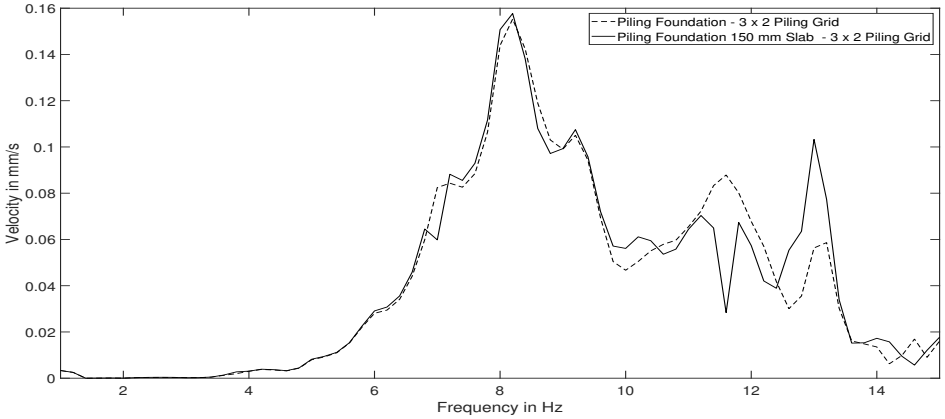

Figure 4.40: Measurement Point 2 in Accordance to Figure 3.22, Piled Basement with 300 mm vs. Piled Basement Foundation with a 150 mm in the *Big* building

4.5.1.4 Summary of *big* building results

The remaining points from Figure 3.22 are presented in the following left-to-right order; Point 2, Point 3, Point 4, Point 5, Point 6 and lastly Point 7 without the base model results:

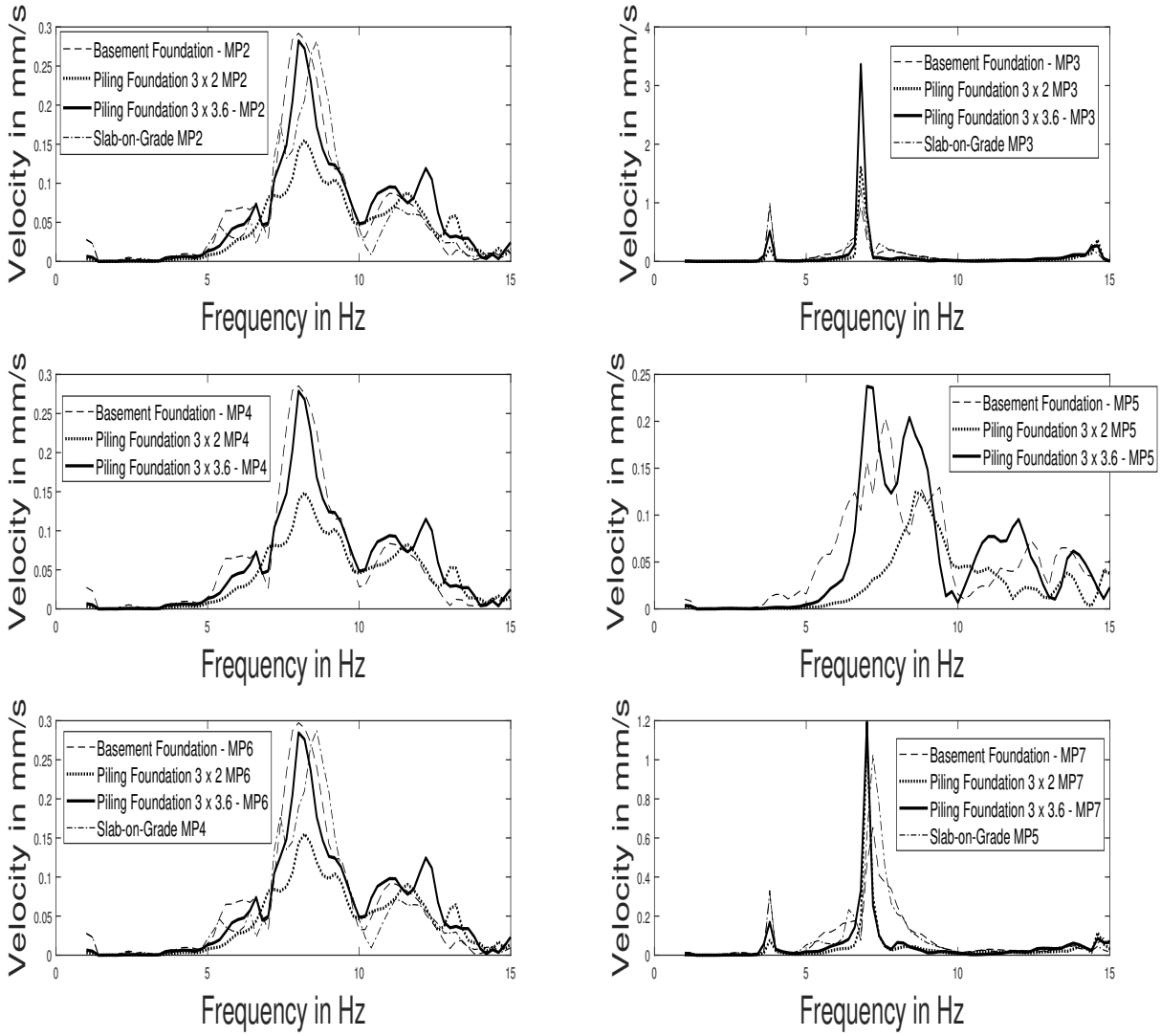

Figure 4.41: Summary of results obtained at Measurement Points 2, 3, 4, 5, 6 and 7 in Accordance to Figure 3.22, for the different parameters in the *Big* building

Along with the summary of the results from the vibration damping between ground and construction measured at Point 2 is presented for all of the constructions that were used for the *big* building:

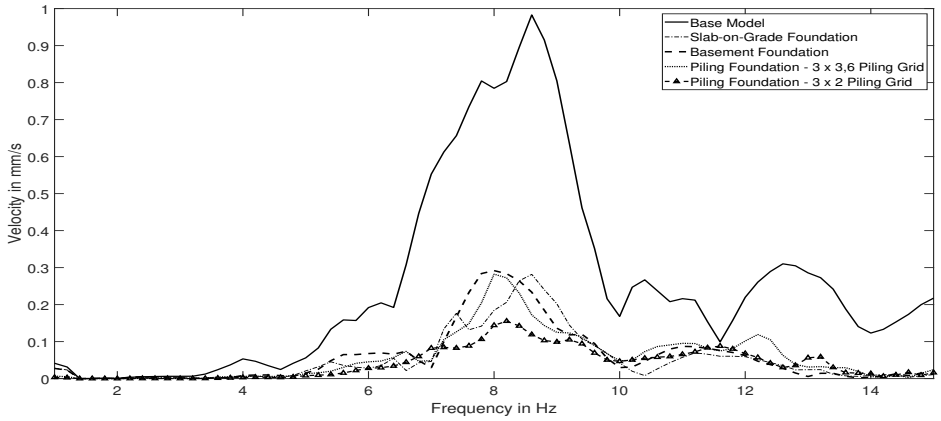

Figure 4.42: Summary of results obtained at Measurement Point 2 in Accordance to Figure 3.22, for the different parameters in the *Big* building

In order to gain better insight into why the different foundation types give some frequency shifts found in Figure 4.41 (e.g. point 7 where piling foundation gives higher values than the slab on grade foundation), the complex harmonic response of the building is shown in Figures 4.43, 4.45 and 4.44 for measurement point 3, 5 and 7. The figure below presents the complex harmonic response of the plate at ground level:

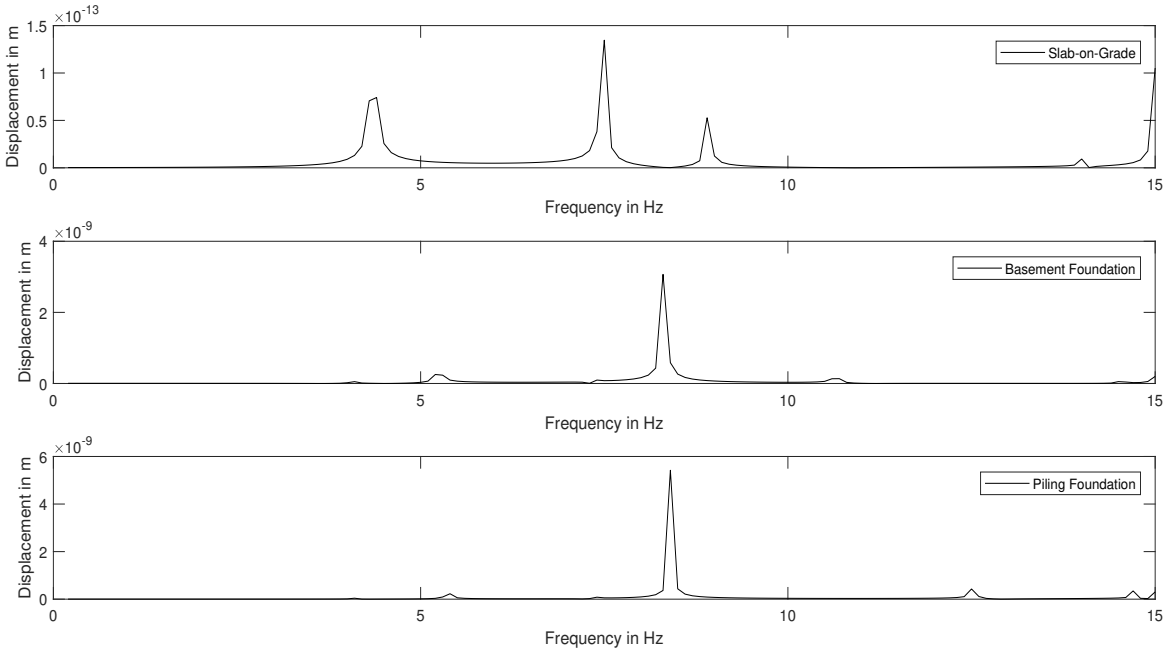

Figure 4.43: The Resonances at the Measurement Point 3 (See Figure 3.22) of the different structures for the *big* building

Followed by the response at the second floor of the building, denoted as Measurement Point 7 in Figure 3.22:

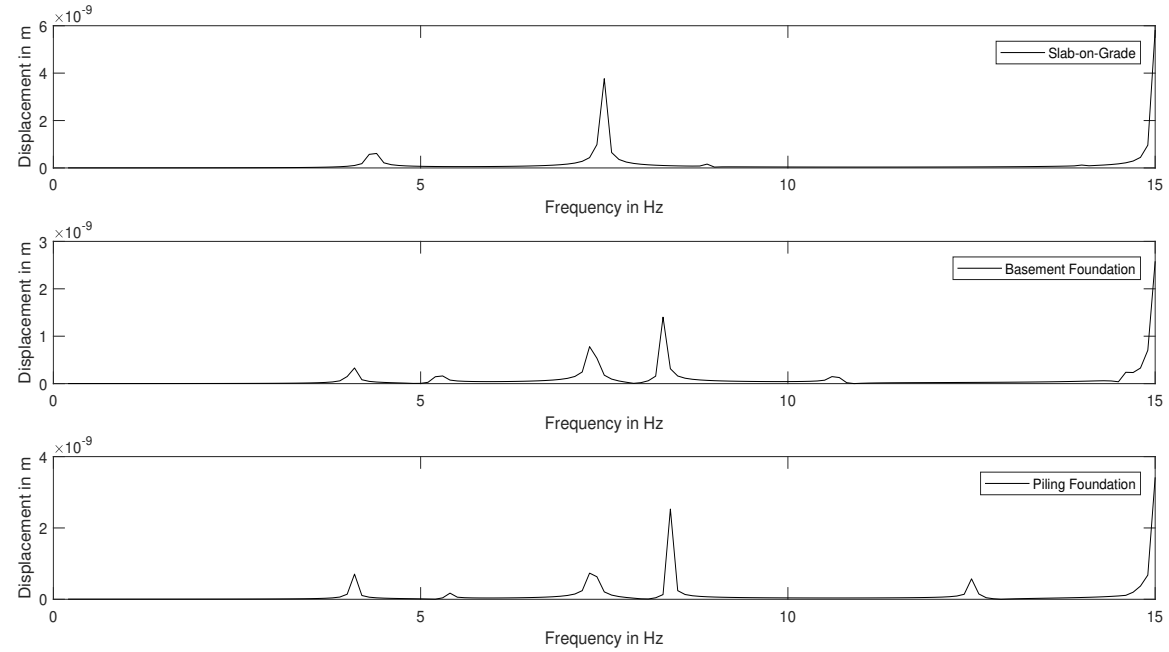

Figure 4.44: The Resonances at the Measurement Point 7 (See Figure 3.22) of the different structures for the *big* building

Lastly, the response is also presented for the basement level slab, at the foundation types when its applicable:

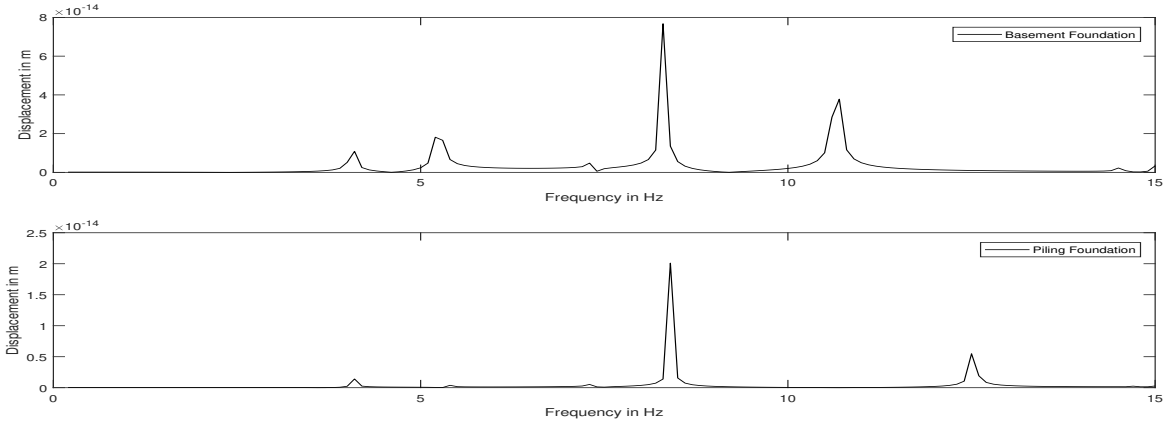

Figure 4.45: The Resonances at the Measurement Point 5 (See Figure 3.22) of the different structures for the *big* building

The floors used in the *big* building have a long span, which means eigenfrequencies of these elements will be in the frequency range of interest (1 - 15 Hz). As the geometry of the plates is not affected by the change of foundation types the mode shapes will be fairly similar with an offset in frequency due to the increased stiffness and mass of the building as the structural measures are added. Hence, only mode shapes for the basement foundation will be showcased in the figure below:

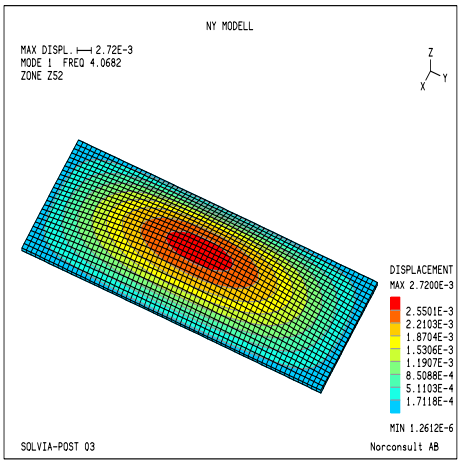

(a)

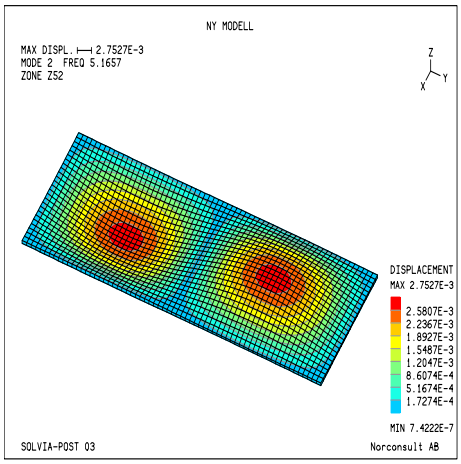

(b)

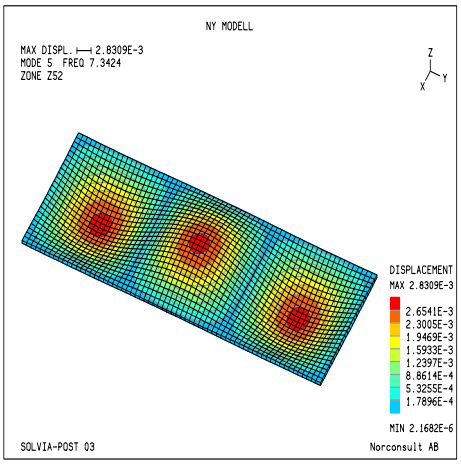

(c)

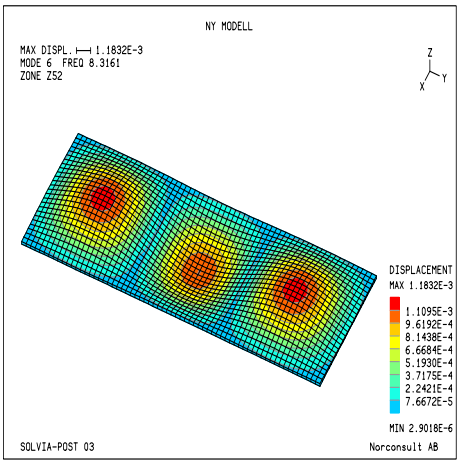

(d)

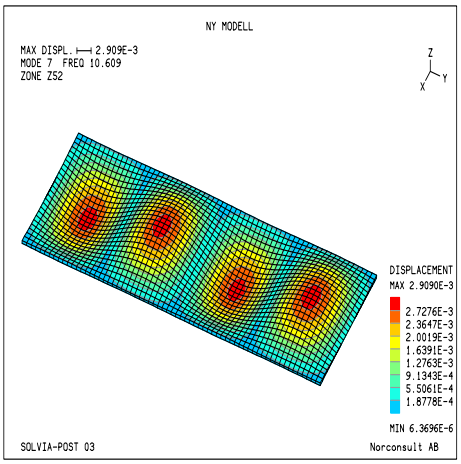

(e)

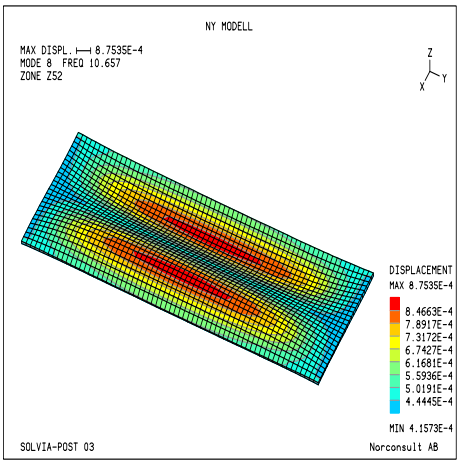

(f)

Figure 4.46: The Mode Shapes of the Second Floor Slab of the *big* building with Basement Foundation, Measurement Point 7 in Accordance to Figure 3.22 with corresponding Harmonic Response showcased in Figure 4.45

4.5.2 The *small* building

Similarly to Section 4.5.1, this section will be focused around Measurement Point 2 with a brief presentation of the measurement results for the remaining measurement points in the summary found in Section 4.5.2.4.

4.5.2.1 Slab on grade

The slab on grade foundation was a 150 mm thick concrete slab with 75 mm below and above ground respectively. The static load that this slab is subjected to corresponds to a one-story concrete building with wall and floor thickness of 150 mm.

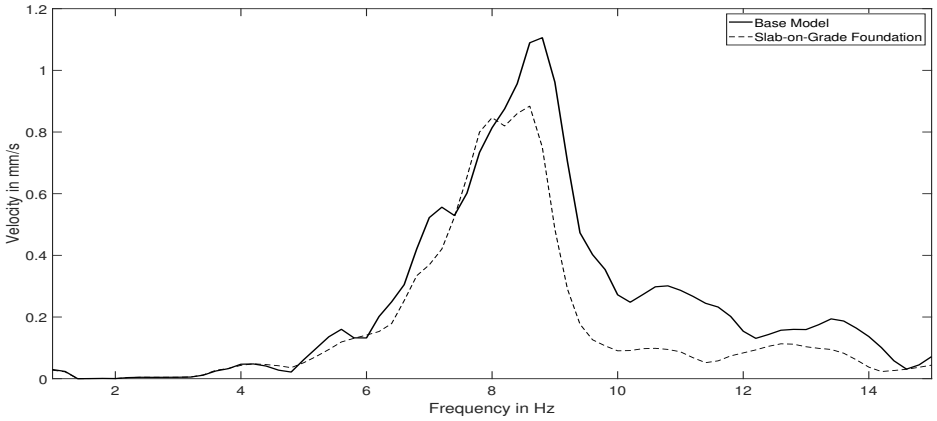

Figure 4.47: Measurement Point 2 in Accordance to Figure 3.22, Base model vs. Slab-on-Grade in the *Small* building

A comparison was made to see how the slab thickness can affect the obtained levels where thickness of the slab-on-grade was exchanged to 300 mm, the results are shown below:

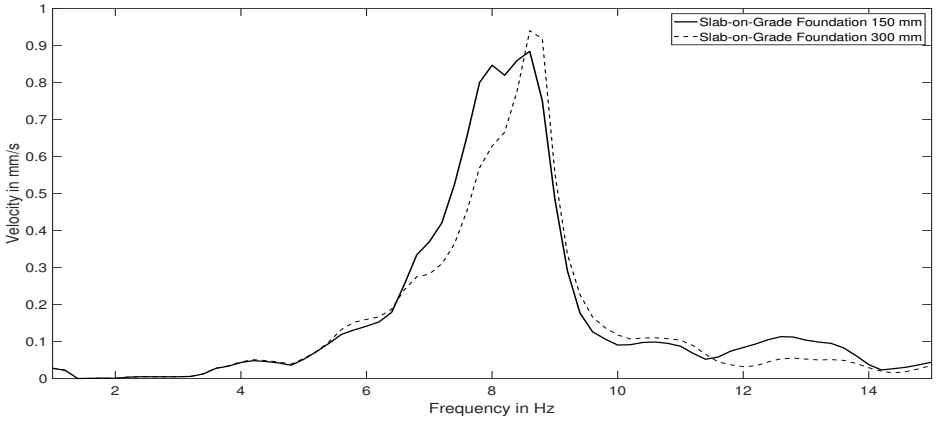

Figure 4.48: Measurement Point 2 in Accordance to Figure 3.22, Slab-on-Grade 300 mm vs. Slab-on-Grade 150 mm in the *Small* building

4.5.2.2 Basement Foundation

Following results were obtained when comparing the plain base model with the impact of adding a basement foundation:

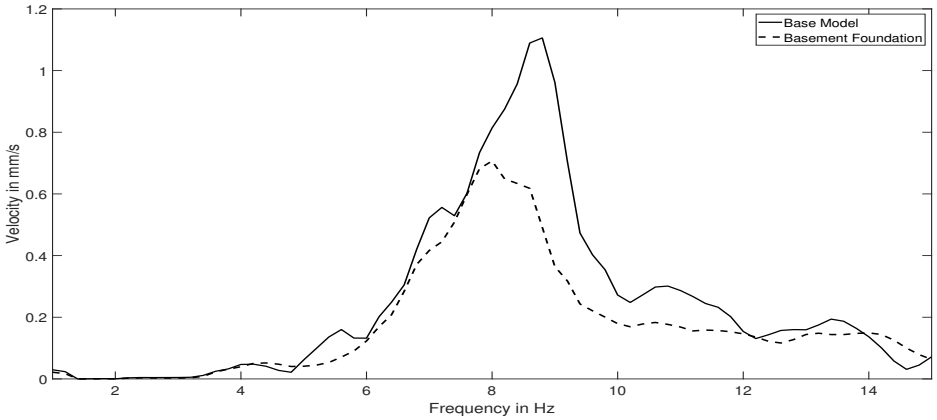

Figure 4.49: Measurement Point 2 in Accordance to Figure 3.22, Base model vs. Basement Foundation in the *small* building

Here, interestingly enough the slab with higher thickness has a higher max level but lower overall level of vibrations.

4.5.2.3 Piled Basement Foundation

The piled basement foundation had the following impact on the transfer between ground and slab for the *small* building:

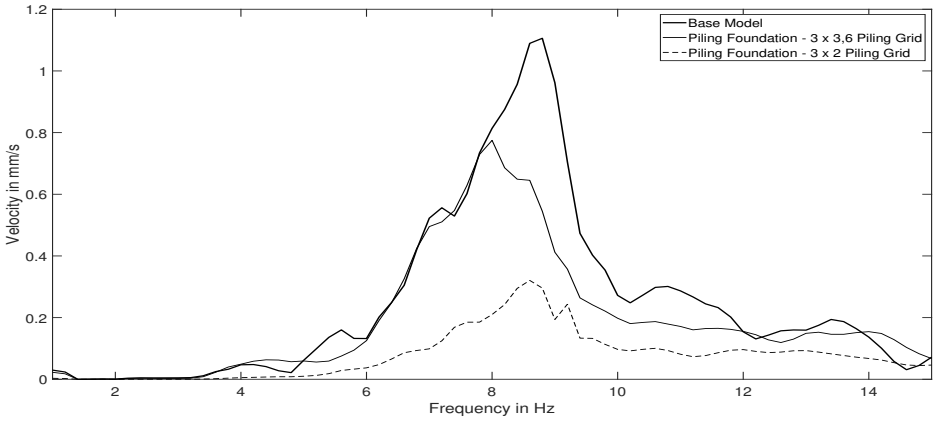

Figure 4.50: Measurement Point 2 in Accordance to Figure 3.22, Base model vs. Piled Basement Foundation in the *Small* building

The Piled Basement Foundation corresponds to the Piling Plan shown in Figure 3.20 in Section 3.3.2. As in the previous section, in order to give the previous figure some context, another figure is shown below, with a denser piling plan:

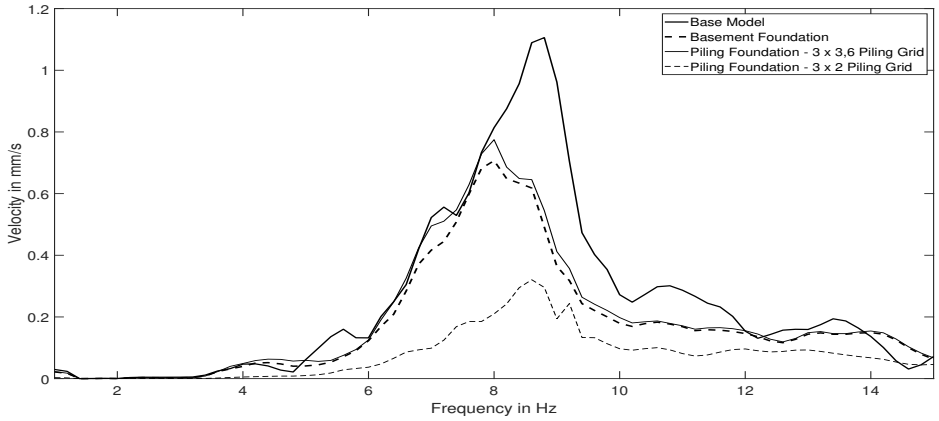

Figure 4.51: Measurement Point 2 in Accordance to Figure 3.22, Base model vs. Piled Basement Foundation in 2 setups along with the Basement Foundation in the *small* building

Very similar to the *big* building, the *small* building shows that the 3 x 3,6 meters piling density will give results that are very similar to the results found by only applying a basement foundation. When applying the denser piling plan the transferred energy is visibly decreased and much more effective at damping than both basement foundation and the piling plan.

In order to gain insight on how the slab and element thickness affects a smaller building a comparison was made where the construction elements below ground-level were doubled in thickness. The static load remained the same as only the base-slab and basement slab and walls had their thickness exchanged to 300 mm. The result is presented below:

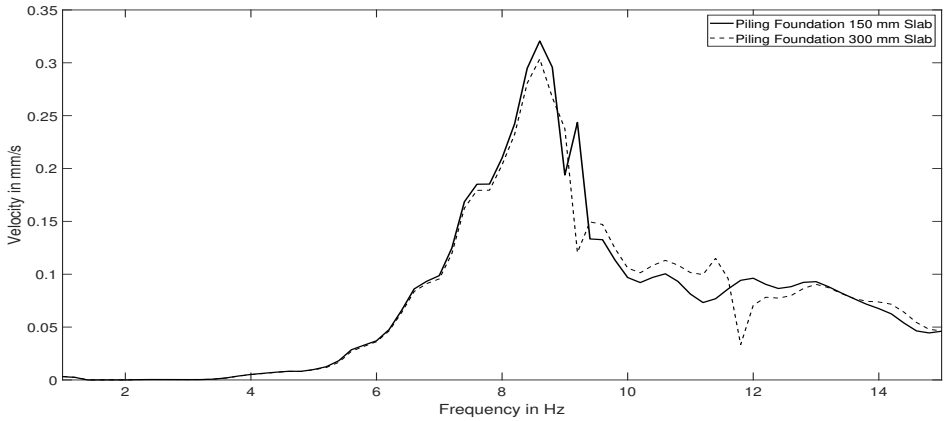

Figure 4.52: Measurement Point 2 in Accordance to Figure 3.22, Thick Piled Basement Foundation (300 mm) vs. Thin Piled Basement Foundation (150 mm) in the *small* building

4.5.2.4 Summary of *Small* building results

Firstly, the remaining points from Figure 3.22 are presented in the following left-to-right order; Point 2, Point 3, Point 4, Point 5, Point 6 and lastly Point 7 without the base model results:

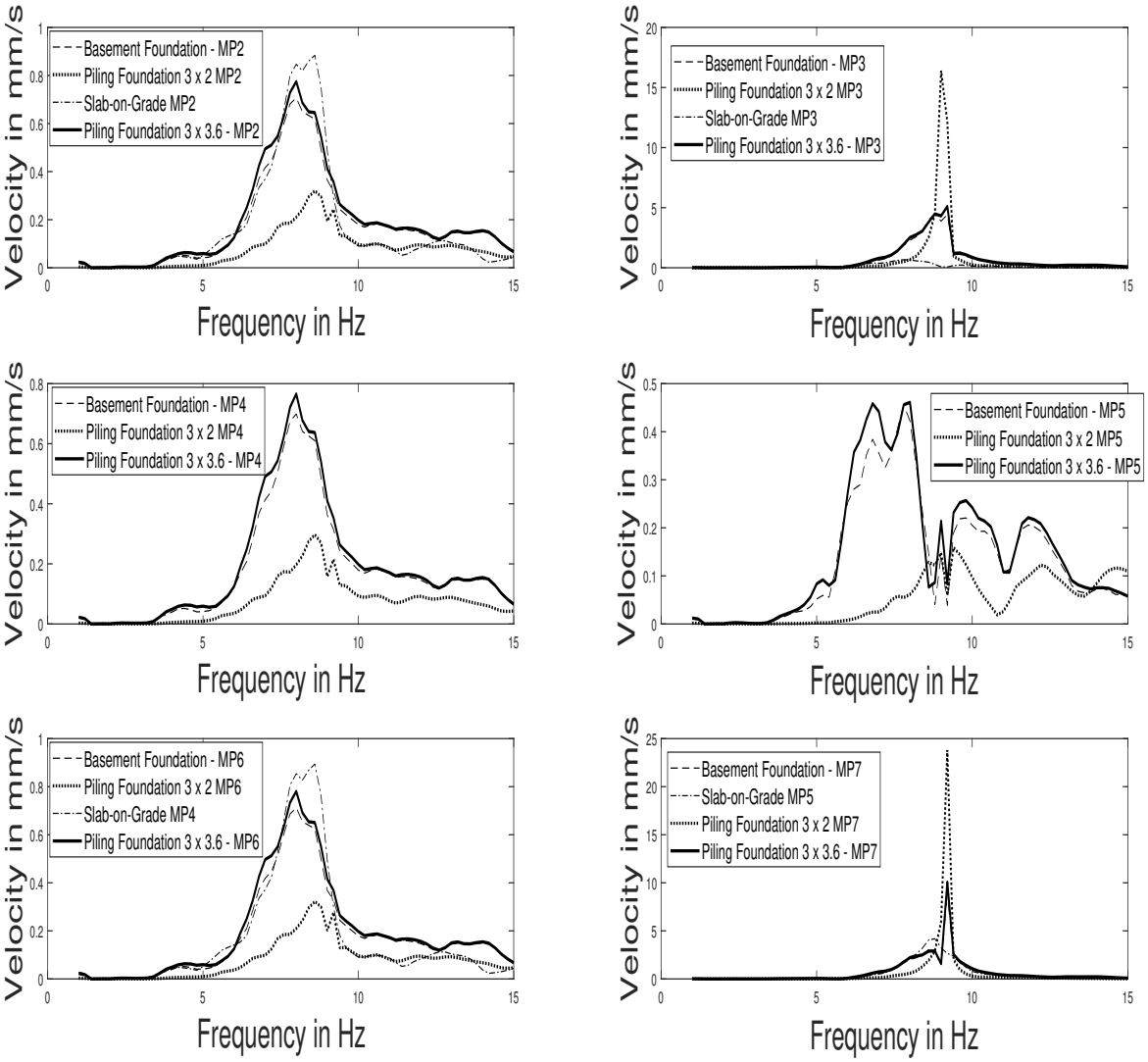

Figure 4.53: Summary of results obtained at Measurement Points 2, 3, 4, 5, 6 and 7 in Accordance to Figure 3.22, for the different parameters in the *Small* building

These are presented although Point 3 and 6 seem to show erroneous results whose absolute value cannot be considered reliable, however it showcases the effect that could be observed as the excitation frequency matches with the resonance frequency of the building element. Secondly, the summary of the results from the vibration damping between ground and construction measured at Point 2 is presented for all of the constructions that were used for the *small* building:

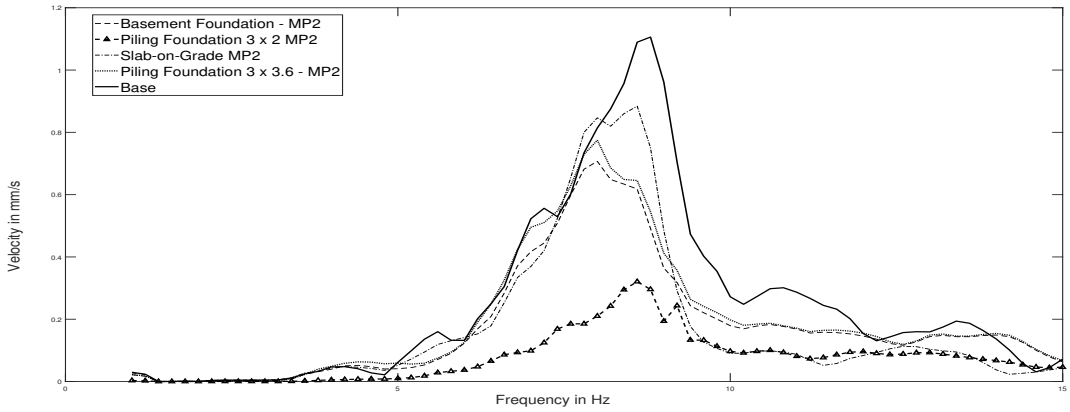

Figure 4.54: Summary of results obtained at Measurement Point 2 in Accordance to Figure 3.22, for the different parameters in the *small* building

Similarly to the *big* building the harmonic response of the small house will be presented in Figure 4.55, 4.57, 4.56 for Measurement Point 3, 5 and 7 as established in Figure 3.22.

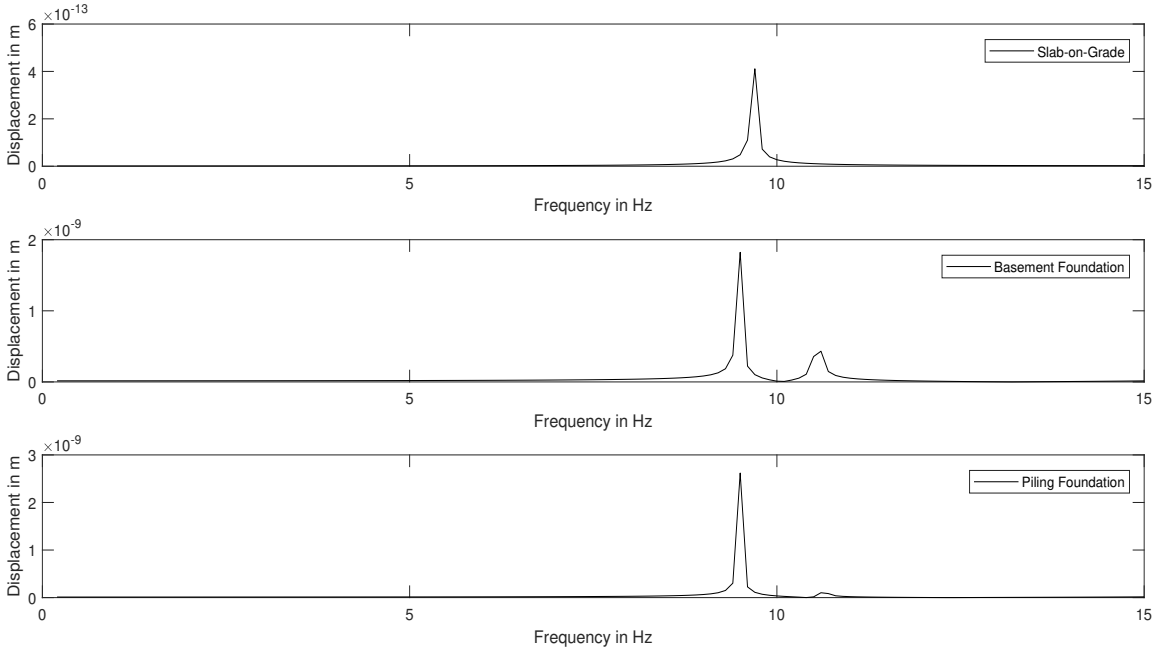

Figure 4.55: The Resonances at the Measurement Point 3 (See Figure 3.22) of the different structures for the *small* building

Followed by the response at the second floor of the building, denoted as Measurement Point 7 in Figure 3.22:

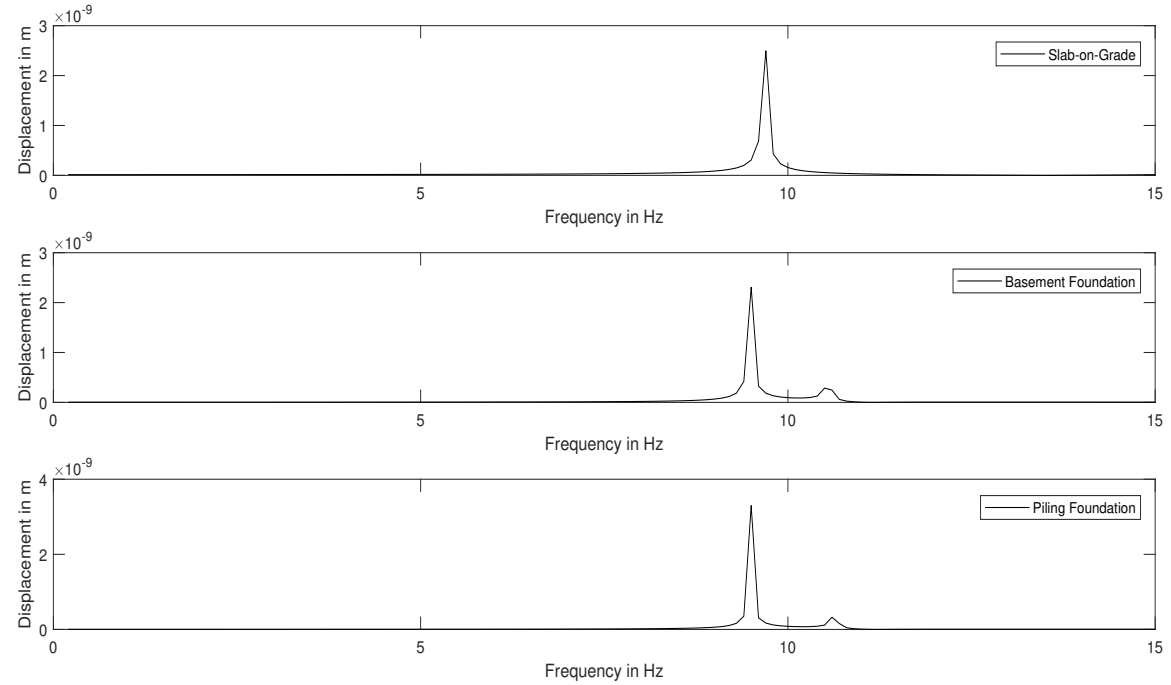

Figure 4.56: The Resonances at the Measurement Point 7 (See Figure 3.22) of the different structures for the *small* building

Lastly, the response is also presented for the basement level slab, at the foundation structures where it is applicable:

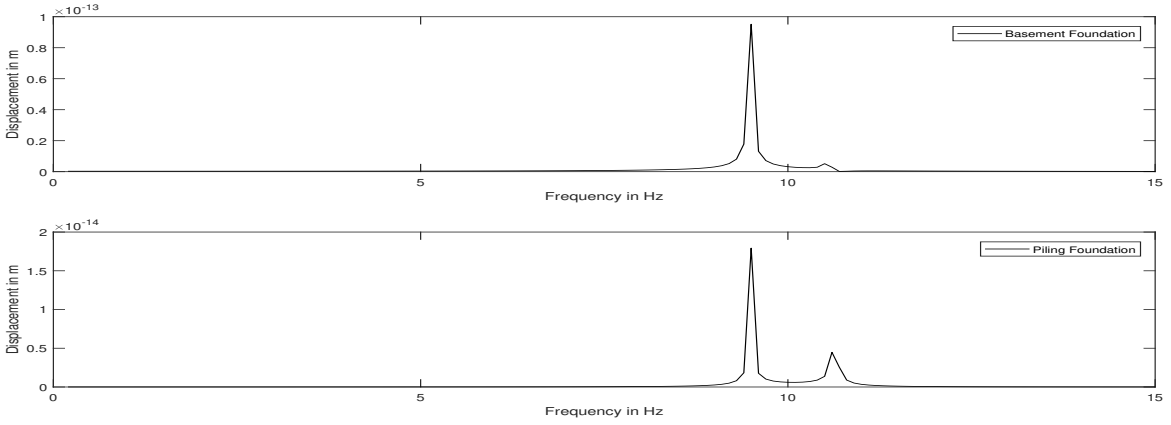

Figure 4.57: The Resonances at the Measurement Point 5 (See Figure 3.22) of the different structures for the *small* building

The span of the plate of the small house is much shorter than of the *big* building and contains only one eigenfrequency in the frequency range of interest, representing the first mode shape. In the small building the upper floor has no mass acting on it which will result in different boundary conditions which will lead to lowering of the first eigenfrequency. As the change of foundation structure did not constitute a

change of geometry or boundary conditions the mode shapes for the different setups will be very similar, once again, with the change only visible when it comes to the frequency at which the mode shape is most pronounced. Thus, only mode shapes of the top floor of the building with a basement foundation will be presented:

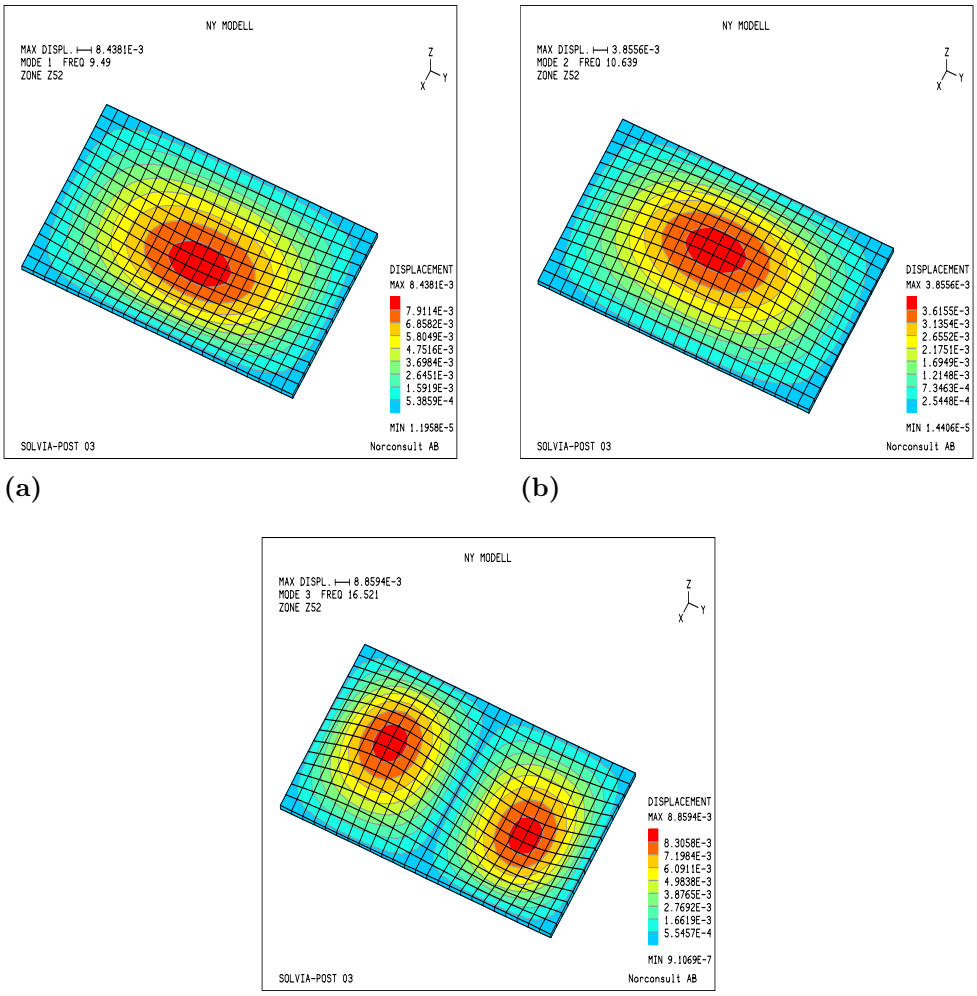

Figure 4.58: The Mode Shapes of the Second Floor Slab of the *small* building with Basement Foundation, Measurement Point 7 in Accordance to Figure 3.22 with corresponding Harmonic Response showcased in Figure 4.57

Note that the second modeshape is outside the span of interest (1 - 15 Hz) and thus not visible in Figure 4.57.

4.5.3 Obtained Transfer Functions

In the previously presented standard *NT ACOU 082* a weighting curve is presented for vibrations, which is similar to the commonly used A-weighting curve in order to resemble human perception. The weighting curve in *NT ACOU 082* is described in dB, but converted into scaling values to be able to apply them on the velocity

levels. As described in *SS 460 48 61* a single value can be evaluated individually if the frequency can be seen as dominant which is applicable for most of the results. Therefore, the weighted peak value for each of the foundation types is used as a single value compared to the peak of the empty model.

As a second parameter, the mean transfer value is also presented to get a better perception on how the foundations types relate to each other and the plain base model. In Figure 4.59 the comfort weighted velocities for the different foundation types are shown for the *big* building. Since the human perception is higher in lower frequencies the weighting curve is decaying over frequency which result in lower vibration levels for higher frequencies. This will also affect which peak frequency which will be used when evaluating the transfer function for the different foundation types.

In Table 4.1 the transfer values for the different foundation types are shown. The peak transfer factor is shown together with the peak frequency of each foundation type.

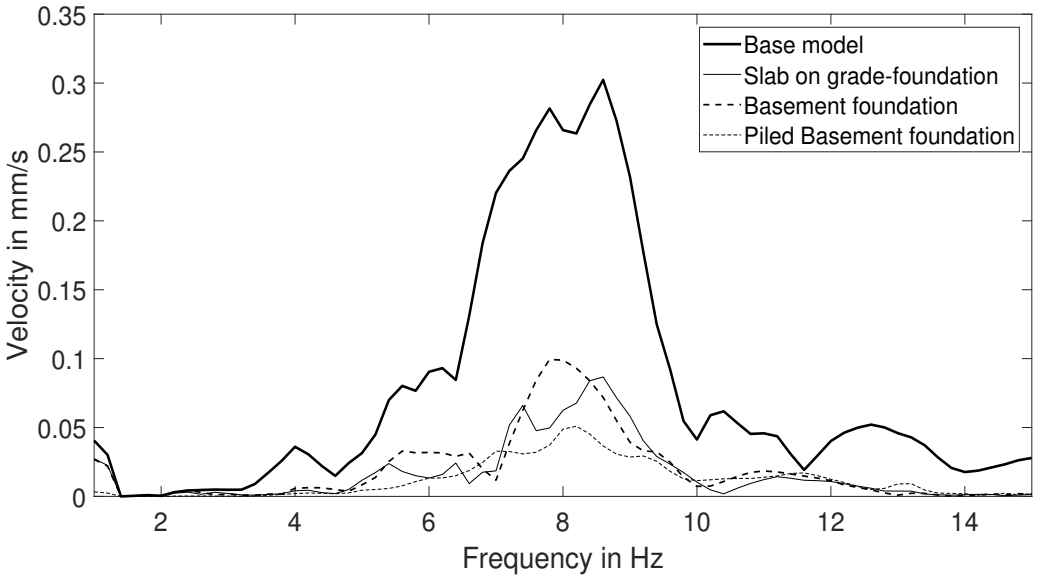

Figure 4.59: Comfort weighted vibration level for the *big* house in accordance to *NT ACOU 082* included as [16]

Table 4.1: Transfer Values for *big* building

Foundation type	Overall transfer value	Peak transfer value
Slab on grade	0.27	0.29 (8.6 Hz)
Basement	0.31	0.33 (7.8 Hz)
Piled Basement	0.15	0.17 (8.2 Hz)

The same procedure as previously described is used for the *small* house. In Figure 4.60 the comfort weighted velocities for the different foundation types is shown for

the *small* building. In Table 4.2 the transfer values for the different foundation types is shown.

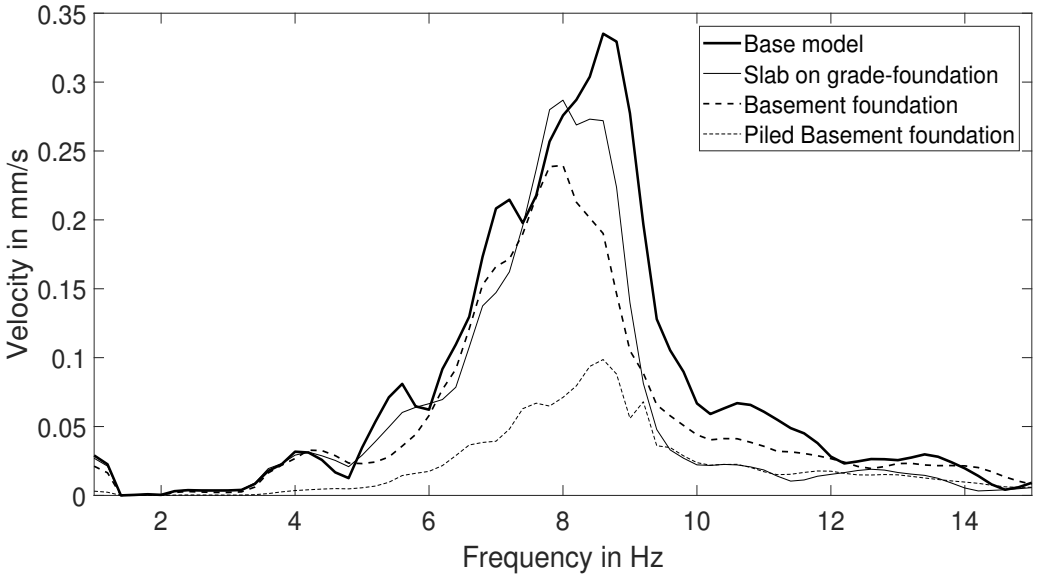

Figure 4.60: Comfort weighted vibration level for the *small* house in accordance to *NT ACOU 082*

Table 4.2: Transfer Values for *small* building

Foundation type	Overall transfer value	Peak transfer value
Slab on grade	0.74	0.86 (8 Hz)
Basement	0.85	0.71 (8 Hz)
Piled Basement	0.32	0.29 (8.6 Hz)

The most notable results which can be seen in the transfer functions values is for the *small* house in Table 4.2 and Figure 4.60 where the slab on grade foundation is better in terms of overall transfer function than basement foundation, but is worse for the peak transfer value than the basement foundation. Another interesting result which can be seen is that the basement foundation is worse than the slab on edge foundation for the *big* building when the weighting values is applied. The peak velocity levels which can be seen in Figure 4.42 are on similar levels but the slab on grade comes higher in frequency than the basement which scaled with the weighting curve gives a lower value.

5
Discussion

The following chapter presents a brief discussion regarding the validity of the Ground and Source model, as well as the suitability of the methods used to generate them.

Further, the chapter presents a reflection upon the given results from the Parametric study and discusses possible error sources and non-linearities that they may present.

5.1 Validation of Source Model

The source model was intended to create a model where different parameters could be exchanged to obtain different forces depending on the vehicle properties such as suspension stiffness, total mass but also vehicle speed and speed bump profile. The parameter altering of the SIMULINK model showed results in line with what was expected from the theory survey for different force levels induced due to different parameters. The local deformation of the rubber compound in the tread layer and the curvature of the tyre affects the relation between the speed bump profile and the profile relevant for the model. The local deformation and curvature works as a low pass filter and results in a smoother profile. However, the SIMULINK model was not able to generate the expected amplitude differences satisfactory for altering vehicle velocities as the measurements suggested it should. This does not mean that used model is unreliable or faulty for the used vehicle velocity of 20 km/h, but indicates that the model cannot provide the correct values for different vehicle speeds by only changing it as a single parameter in it. To be able to create a model that can in an adequate way treat different vehicle speeds the equation of motion needs to involve the horizontal force that the speed bump is exposed to. As the focus of the thesis was not to optimize a vehicle model the used source model was not further developed but can be seen as adequate for the intended purpose.

During the validation progress the model was validated against the total contribution of the passage. This approach was chosen since the time signal of the vibrations overlapped between the two axis and to avoid that truncation error, this approach was used. It would be possible to argue for that it is only the back axis that should be of importance, but with that approach it excludes the front axis affect which would be wrong, especially if the input force would be time dependent.

The final parameters for the source model are similar to the first parameters found

in [38]. As the only confirmed parameters of the truck were the mass and the length between the axes, the parameters had to be found in an iterative way. This does not mean that the parameters are the correct one for the used truck, but they did serve their purpose for this thesis after being validated as described in Section 4.2.

When combining the FEM model with the source model, some limitations had to be applied. The used FEM program SOLVIA assumes steady state conditions when calculating the results in the frequency domain. Therefore it was considered to try to generate a time signal in SOLVIA which could later be converted into the frequency domain. This approach was discussed but rejected since it would be much more time consuming without certainty that it would result in more reliable results. Therefore, the approach that assumed steady state conditions was used which needs to be considered when analyzing the FEM-generated results as the steady state condition assume that the input force is fully built up for all frequencies and the resonances are at their maximal saturation. Therefore, possible resonances in the system will be more pronounced then they are in a real case scenario for this type of outline. In a real case scenario one impulse from a vehicle would not saturate the resonances as much as the FEM-model indicates.

Due to the choosing of steady state conditions and the nature of the impulse the lower frequency limit will be set to 1 Hz for the final results since it is highly unlikely that the low frequency will be excited with the amount of force that the SIMULINK model suggest. As the displacement of the upper mass is not damped within the simulation time the impact of the lower frequency is arguably negligible since the force it creates will be distributed in over a longer distance. This will not affect the frequency range that is of the highest interest which are 7 - 15 Hz.

The initial approach where the road profile had the same size and characteristics as in the measurement did not give satisfying results as described in Section 4.2. The reason to this was that the passing time on the road profile coincided with the axle hop resonance. For the created source model this becomes a problem since the vertical force is described by a simplified 4 degree of freedom system. In reality it is highly unlikely that this problem will occur since the vehicle is much more complex than the 4DOF-system used. As mentioned earlier the impact of the local deformation of the rubber compound in the tread layer and the curvature of the tyre is not taken into account in the model which may also cause problems in the initial approach.

The final results of the validation of the source model can be seen as adequate. The final results can be improved if the entire progress would be done again but due to the focus and purpose of this thesis it is deemed unnecessary. If any additional work would be put on the source model and its validation, it would be to be able to get around the steady state condition which is used in the current one by using a time signal instead of frequency. The problem this would face in model is that each time-step would be calculated individually, and the length of the signal would be at least 5 seconds long to be able to get a sufficient frequency resolution. Since the

sampling frequency in the measurements is between 1000 and 1500 Hz this would result in long calculation times. It is possible that the steady state condition would be possible to solve in other FEM-modelling software, but due to the size of the ground model the programs may cause longer calculation times.

5.2 Validation of Ground Model

The validation of the ground model mainly focused on the correct modeling of two important features of a continuous medium. The first feature was that the model needed to act as a semi-infinite model, i.e. no reflections at the vertical edges of the model. This feature was solved by matching the impedance of the model and putting springs acting as radiation dampers around the model in the different required directions, referred to as the Perfectly Matching Element Method in this thesis. This was later confirmed by ensuring that the phase was flat at the excitation point when the same material parameters were used for all of the layers along with PME applied at the bottom of the model. Nevertheless, when using the actual model with the different material parameters for different layers and with a bedrock surface at the models bottom there will be some reflections and therefore it is hard to validate that this approach works for all of the layers as intended for the final model.

The Perfectly Matching Element Method is a good attempt to ensure no reflection at boundaries and even though it is harder to confirm when using the final model, there are indications that confirm that it is working as intended. The spreading of the force in the model is spherical and the flat phase is almost always achieved for the excitation point excepts for two frequencies around 2 Hz where the model bottom supplies reflections. Furthermore, measurement points were set at arbitrary positions to control for reflections from boundaries and gave satisfactory results. Thus, it is assumed that a semi-infinite ground model has been achieved in the thesis as intended.

The second feature which was important to achieve is that the bedrock is reflective and rigid. To be able to achieve this the nodal points of the bottom of the model were not able to move in any direction. To ensure that this approach worked as intended, the force in all directions for one of the nodes of the bottom was investigated. The results showed that there was no motion in the nodal point which confirmed that the approach worked as intended.

A final parameter that was not obtained during the geotechnical survey was the damping coefficient of the ground. Instead the final model was tested and compared to a lower damping value. The final value was the same value that have been used in previous calculations made by our experienced supervisor Gunnar Widen in SOLVIA for one of his projects in Gothenburg and had better correlation with the measurement than the lower tested one.

5.3 Parametric Study

All of the models that have been used during the parametric study have been complied in the same fashion as previously constructed models using SOLVIA FEM at the acoustic department in Norconsult. No known errors occurred when running the models and during inspection the models appeared to be visually correct. The construction elements could have been connected and built together using different techniques in Solvia, which is why the transfer functions between the different floors in the buildings are not to be considered reliable as that was not a part that was within the scope of this thesis.

The aim of the thesis was to investigate how different foundation types will affect the transfer factors from ground to building for vibrations induced by a heavy vehicle. The usage of in-situ measurements to generate a reliable ground and source model showed to be an effective way of correctly approximating the transfer functions within the ground itself. However, the same level of reliability cannot be reached for the parametric study as no in-situ measurements have been done for houses similar to the ones generated in the FEM modelling.

Although no confirmation of the obtained transfer values could be done as part of this thesis, the result showed good correlation to the theoretically expected values, with some alterations.

Firstly, a parameter that is not considered within the industry-standard transfer factors is the size and mass of the building. Same transfer factors are used whether a multi-story building or a single-family house is the subject of consideration. In accordance to the preformed parametric study the mass on the foundation will have a major impact on the transfer of vibrations. The shown tendency is that a foundation with a higher mass will have significantly lower transfer factor than a smaller construction with a lower mass. As shown in Figure 4.59 and 4.60, the magnitude of the transfer factors will be highly dependent on the mass with the foundation types having a secondary, although important, impact.

A factor to consider is that the source is acting in its steady-state condition which makes its excitation force resemble a train rather than a heavy vehicle. Considering this limitation, one must be reminded that the difference between heavy and light structures might not be as big as the resonances are not as saturated in a real-life scenario as shown in the FEM models. Nevertheless, this approach has been previously used as a successful engineering method at Norconsult and the result generated can be considered moderately reliable.

To further put emphasis on why it is important to investigate the contribution from heavy vehicles Figure 4.53 should be considered, showcasing measurement point 7 (denoted as MP7). In this figure the resonance frequency of the second floor is approximately the same as the peak of the excitation signal. Therefore, the vibration amplitude on this frequency is significantly higher than the rest of the frequencies.

As previously described it is unlikely that the resonance frequency will be as saturated as shown in Figure 4.53 but as the level is unreasonably high, it is likely that this will still be an issue of a different magnitude. To put it in further perspective the distance between the source and the building is 23 meters and the source model is modelled to resemble a medium-sized truck passing over a small speed bump at 20 km/h which is far from an unlikely real life scenario.

It is clear that the resonances of the building affect the transfer function of the different foundations. The eigenfrequencies will be different depending on applied foundation type, most notably between basement and slab-on-grade foundation. Since the vibrations level of the foundation is retrieved on the edge on top of the foundation, these resonances do not have significant impact on the levels, but they do contribute.

As seen for Measurement Point 2 the *big* house in Figure 4.45 the slab on grade foundation has an eigenfrequency around 7.6 and 8.8 Hz while the basement foundation has its at 8.2 Hz. This is distinguishable when comparing the values in Figure 4.42. The same contribution can be found in position 2 for the small house as well, where the basement foundation has its eigenfrequency around 9.5 Hz and the slab on grade foundation has its at 9.7 Hz which can be seen in Figure 4.54.

Since the frequency resolution were 0.2 Hz the final results it is possible that there will be amplifications if the eigenfrequency is fully amplified. It is possible that this is what occurs at Measurement Point 7 (denoted as MP7) of the small building at 9.4 Hz as seen in Figure 4.54.

Another factor to be weighted in is that a structural counter-measurement to reach lower vibration transfer levels will have different effect depending on the receiving structure. The parametric study showed that the difference between a slab-on-grade foundation and a basement foundation will not give as big of a difference as [16] and [23] suggest. These reports suggest a transfer factor amplification difference of 0,2 - 0,4 between a frame-type foundation and a basement foundation while the computed results show an amplification factor difference between 0,05 - 0,15.

The most effective structural counter-measurement showed to be a piling ground however, requiring a dense setup as a to sparse setup has shown to be ineffective and even counter-effective for light structures as presented in Figure 4.51. The piles for both structures were of the same type and another parameter to consider could be the thickness and mass of the piles compared to their ability to reduce vibration transfers. This parameter was not investigated, instead the parametric study proved that the thickness of the foundation components (thickness of slab and/or thickness of basement structural elements) has little to no effect for heavy structures and a minor effect for light constructions as shown in Figure 4.48.

In general, this has been a reoccurring characteristic noticeable throughout the parametric study. The structural measures for lower transfer factors have a higher

and more distinguishable effect in lighter and smaller constructions while for heavy and large buildings their impact will be limited to lowering the resonances of the construction if correctly dimensioned, as observable in Figure 4.42 and 4.54.

6
Conclusion

The parametric study showed no significant difference between basement foundation and slab on grade foundation. The piled basement foundation was found to be the most efficient alternative to lower vibrations, but only if the piling was dense enough. The parametric study also showed that a lighter and smaller house was easier to excite which provided higher transfer values for all the different foundation when comparing the light and heavy structure. The thickness of the different foundations did not provide any notable difference, rather the static load was the governing factor.

The source model approach assumes steady state condition of the excitation which resulted in some uncertainties where reflections/resonances were more pronounced than in a real case scenario, but was deemed as the sufficient approach due to calculation time and choice of FEM-modelling software.

Lastly some of the results obtained in the parametric study did not fully correlate with the currently used reference values and standards, especially the impact of basement foundation compared to slab on edge foundation and that different sizes of buildings are treated the same way.

The difference between basement and slab on grade foundation in this thesis cannot be deemed as confident enough to prove the standard wrong but possible question its results. This thesis proves that the size of building is of significant importance when estimating the transfer values, which is a parameter that the standards does not consider.

7
Future Work

This Parametric study is an introduction to what could have been an infinite project, comparing parameter after parameter. This chapter presents the subjects that are considered the most interesting for further investigation.

For once, the computation of a source model could be investigated individually to be able to successfully generate the correct vertical force for varying vehicles velocities, along with other adjustable parameters such as stiffness and mass. An analytical approach with measurements as validation could result in a model that could be further used in similar thesis project. It would also be of interest to investigate different types of vehicles to see how well the current source model compares to them and if this simplified model could be used to generate the input force of other vehicles such as buses.

A good future thesis project would be a continuation of this thesis with a higher level of measurements. The most interesting validation would be to measure the transfer factors on site and then compare it with the FEM modelling by using the same procedure as used in *NT ACOU 082*.

As seen in the results of the thesis the different piling foundations gave different results. It would be interesting to investigate how different amount of piles would change the transfer values for the building. It would also be of interest to investigate more parameters such as different soil properties and different materials on building as this is not investigated in this thesis. As a continuation of what this thesis conclusion it would also be of interest to investigate the weight of the building by trying to find some kind of numerical relation between weight, size and the transfer values.

Bibliography

[1] F.E. Richart, Jr., J.R. Hall, Jr. & R.D. Woods (1970) *Vibrations of Soils and Foundations.* Englewood Cliffs, N.J.

[2] Augusta Neto, Mari, Amaro Ana, Roserio Luis & Cirne Rogerio Leal Jose (2015) *Engineering Computation of Structures: The Finite Element Method* Springer International Publishing.

[3] Uppsala University Lecture Notes (2015) *Elasticity and Elastic Waves* Uppsala University - Department of Earth Sciences

[4] P. Kelly (2011) *Solid Mechanics - Part II.* University of Auckland - Department of Engineering Science

[5] Allshookup.org (n.d.) *Types of Earthquake Waves*
URL: http://allshookup.org/quakes/wavetype.htm (Visited on 2019-03-15)

[6] UPSeis - An educational site for budding seismologists (2006) *Types of Seismic Waves* URL: http://www.geo.mtu.edu/UPSeis/waves.html (Visited on 2019-03-15)

[7] Nazarchuk Zinoviy, Skalskyi Valentyn & Serhiyenko Oleh (2017) *Acoustic Emission: Methodology and Application (Foundations of Engineering Mechanics).* Springer International Publishing.

[8] Landau, L.D. & Lifshitz E.M. (1970) *Theory of Elasticity.* Pergamon Press.

[9] Incorporated Research Institutions for Seismology (n.d.) *Rayleigh-wave motion* URL: https://www.iris.edu/hq/inclass/animation/284 (Visited on 2019-03-15).

[10] H. Lamb (1904) *On the propagation of tremors over the surface of an elastic solid.*. The Royal Society Publishing.

[11] Al-Hunaidi M.O & Rainer J.H (1991) *Remedial Measures for Traffic-Induced Vibrations at a Residential Site. Part 1: Field Tests.* Canadian Acoustics.

[12] M. Mhanna, M. Sadek & I. Shahrour (2011) *Prediction And Mitigation Of Traffic Induced Ground Vibrations In An Urban Zone.* WIT Transactions on

the Built Environment.

[13] Divett. T & Cenek. P (2008) *Quantification of Noise and Vibration Effects Arising from Higher Mass Limits for Heavy Vehicles*. Opus International Consultants Limited.

[14] Swedish Standards Institute (2004) *SS 460 48 61 Vibration and shock - Measurement and guidelines for the evaluation of comfort in buildings*. Svensk Standard.

[15] Swedish Standards Institute (2017) *SS-EN ISO 8014-1:2017 Human response to vibration - Measuring instrumentation - Part 1: General purpose vibration meters*. Svensk Standard.

[16] Nordtest method (1991) *NT ACOU 082 - Vibration and Shock, Evaluation of Annoyance*. NORDTEST

[17] European Environment Agency (2015) *Noise pollution in the EU*

[18] European Environment Agency (2018) *Population Exposure to environmental noise*

[19] World Health Organization (2012) *Burden of disease from environmental noise.*

[20] O. Hunaidi (2000) *Traffic Vibrations in Buildings*. Construction Technology Update No. 39.

[21] Mercier, H., Ammann, W.J., Deischl, F., Eisenmann, J., Floegl, I., Hirsch, G.H., Klein, G.K., Lande, G.J., Mahrenholtz, O., Natke H.G, Nussbaumer, H., Pretlove, A.J., Rainer, J.H., Saemann E.U., Steinbeisser, L. (1995) *Vibration Problems in Structures: Practical Guidelines.* Birkhauser.

[22] Swedish Geotechnical Society (2012) *SGF Informationsskrift 1:2012 - Markvibrationer*. SGF:s markvibrationskommitté.

[23] Ingemansson (2008) *Vibrationsutredning för detaljplan av handel vid Torpavallen.*

[24] Swedish Geotechnical Institute (2001) - *Jords Egenskaper*. SGI.

[25] N. Ural (2018) *The Importance of Clay in Geotechnical Engineering.*

[26] M. Olsson (2010) *Calculating long-term settlement in soft clays - with special focus on the Gothenburg region*. Swedish Geotechnical Institute.

[27] Scania Specification (n.d.) *Specifications - P 250 DB4x2HNZ Euro 6 Two Axle Tipper* URL: https://www.scania.com/content/dam/scanianoe/market/uk/brochures/truck/spec-sheets/p-series/spec-sheet-scania-p250db4x2hnz.PDF (Visited on 2019-03-12)

[28] Ramudden (n.d.) *FARTHINDER, 2,0 m "Wakeup"* URL: http://www.ramudden.se/produkter/farthinder/farthinder-3 (Visited on 2019-03-12)

[29] M. Agostinacchio, D. Ciampa, S.Olita (2014) *Quarter Car Model, M. Agostinacchio et. al, The vibrations induced by surface irregularities in road pavements – a Matlab® approach* European Transport Research Review.

[30] Tompkins, Eric (1981) *9: The Beginnings of Tyre Science"*

[31] Daniel S. Stutts (2000) *Vibration Analysis of Discrete One and Two Degree of Freedom Systems.*

[32] J. Hajek, C. Blaney, D. Hein (2006) *Mitigation of Highway Traffic-Induced Vibration*

[33] G. Lombaert, G. Degrande (2003) *The experimental validation of a numerical model for the prediction of the vibrations in the free field produced by road traffic.* Journal of Sound and Vibration.

[34] Michael G. Smith (2017) *The impact of railway vibration and noise on sleep* University of Gothenburg.

[35] Wikimedia Commons (n.d) Rayleigh Wave. URL: https://commons.wikimedia.org/wiki/File:Rayleigh_wave.jpg (Visited on 2019-05-08)

[36] Wikimedia Commons (n.d) Love wave. URL: https://nl.wikipedia.org/wiki/Lovegolf/media/File:Love_wave.jpg (Visited on 2015-05-08)

[37] M. Davoodi, A. Pourdeilami, H. Jahankhah, M.K. Jafari (2018) *Application of perfectly matched layer to soil-foundation interaction analysis.* Journal of Rock Mechanics and Geotechnical Engineering.

[38] Lejia Jiao (2013) *Vehicle model for tyre-ground contact force evaluation.* Department of Aeronautical and Vehicle Engineering KTH Royal Institute of Technology.

[39] MathWorks (n.d) *Solver.* URL: https://se.mathworks.com/help/simulink/gui/solver.html (Visited on 2019-05-12)

[40] M. Tomlinson & J. Woodward (2008) *Pile Design and Construction Practice*. Taylor & Francis, Oxon.

[41] M.E. Haque (n.d) *Types of Foundations*. North Seattle Community Collage.

[42] Michael Valley, S.E. (n.d) *Foundation Analysis and Design*. FEMA.

A
Appendix 1

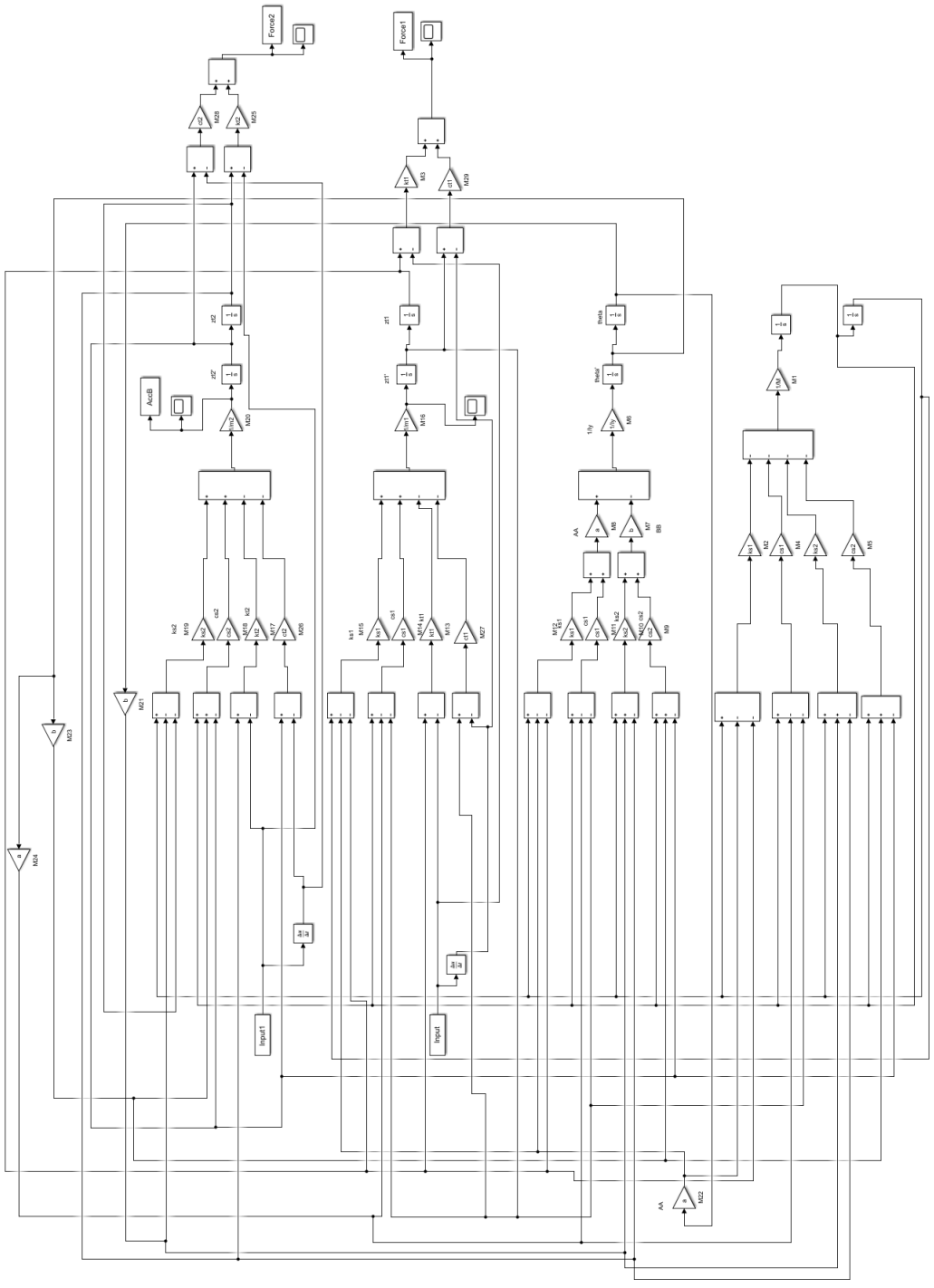

Figure A.1: The SIMULINK model used to generate the results presented in Section 3.2